Summer 2010

Modeling and its numerical method for micro-scaled diffusion -reaction systems in the neuromuscular junction

Abdul Khaliq

NOTE TO USERS

This reproduction is the best copy available.

UMI®

MODELING AND ITS NUMERICAL METHOD FOR MICRO-SCALED DIFFUSION-REACTION SYSTEMS IN THE NEUROMUSCULAR JUNCTION

by

Abdul Khaliq, B.S., M.S.

A Dissertation Presented in Partial Fulfillment
of the Requirements for the Degree of
Ph.D. in Engineering

COLLEGE OF ENGINEERING AND SCIENCE
LOUISIANA TECH UNIVERSITY

August 2010

UMI Number: 3429513

UMI®

Dissertation Publishing

ProQuest®

LOUISIANA TECH UNIVERSITY

THE GRADUATE SCHOOL

05/12/2010

Date

We hereby recommend that the dissertation prepared under our supervision

by ABDUL KHALIQ

entitled

MODELING AND ITS NUMERICAL METHOD FOR MICRO-SCALED

DIFFUSION-REACTION SYSTEMS IN THE NEUROMUSCULAR

JUNCTION

be accepted in partial fulfillment of the requirements for the Degree of

Ph.D. in Engineering

Supervisor of Dissertation Research

Head of Department

Department

Recommendation concurred in:

Advisory Committee

Approved:

Director of Graduate Studies

Dean of the College

Approved:

Dean of the Graduate School

ABSTRACT

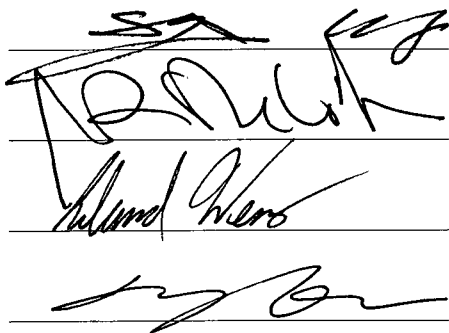The main subject of this research is the neuromuscular junction (NMJ). The NMJ is a biological structure composed of the interface between a neuron and a muscle cell. Currently, there is not a fully three dimensional model of diffusion-reaction processes occurring in the NMJ. Developing a useful predictive model of this structure will assist in the therapeutic efforts to restore and rehabilitate NMJ function to humans and in developing strategies to prevent damage to the NMJ. This research work developed 1D mass transport and full 3D reaction diffusion models. A new finite difference scheme is presented for solving 1D mass diffusion with Neumann boundary condition in cylindrical coordinates, which can be applied in neuromuscular junction processes. This new scheme is obtained based on the Crank-Nicholson method, together with a non-traditional second-order finite difference approximation for the boundary condition. The scheme is proved to be unconditionally stable, and the solution system is a tri-diagonal linear system which can be easily solved by the Thomas algorithm. The scheme is tested by several examples. Results show that our scheme is promising. Finally, the scheme can be readily generalized to the multi-dimensional cases.

A three-dimensional model of the reaction-diffusion processes of a neurotransmitter and its ligand receptor in a disk-shaped volume is established which represents the transmission process of acetylcholine in the synaptic cleft in the neuromuscular junction. The behavior of the reaction-diffusion system is described by a

three-dimensional diffusion equation with nonlinear reaction terms due to the rate processes of acetylcholine with the receptor. A new stable and accurate numerical method is used to solve the equations with Neumann boundaries in cylindrical coordinates. The simulation analysis agrees with experimental measurements of end-plate current and agrees well with the results of the conformational state of the acetylcholine receptor as a function of time and acetylcholine concentration of earlier investigations with a smaller error compared to experiments. An asymmetric emission of acetylcholine in the synaptic cleft and the subsequent effects on open receptor population is simulated. Sensitivity of the open receptor dynamics to the changes in the diffusion parameters and neuromuscular junction volume is investigated. The effects of anisotropic diffusion and non-symmetric emission of transmitter at the pre-synaptic membrane is simulated.

APPROVAL FOR SCHOLARLY DISSEMINATION

The author grants to the Prescott Memorial Library of Louisiana Tech University the right to reproduce, by appropriate methods, upon request, any or all portions of this Thesis. It is understood that "proper request" consists of the agreement, on the part of the requesting party, that said reproduction is for his personal use and that subsequent reproduction will not occur without written approval of the author of this Thesis. Further, any portions of the Thesis used in books, papers, and other works must be appropriately referenced to this Thesis.

Finally, the author of this Thesis reserves the right to publish freely, in the literature, at any time, any or all portions of this Thesis.

Author _Abdul Khaliq_

Date _07/26/2010_

TABLE OF CONTENTS

LIST OF TABLES

LIST OF FIGURES

NOMENCLATURE

A	acetylcholine concentration
A_0	acetylcholine initial concentration
AR	single bound acetylcholine receptors
AR_0	initial single bound acetylcholine receptors
A_2R	double bound closed acetylcholine receptors
A_2R^{open}	double bound open acetylcholine receptors
D_r	diffusion coefficient along R
D_φ	diffusion coefficient along φ
D_z	diffusion coefficient along Z
E	potential across end-plate
k_R	forward kinetic reaction constant related to A
k_{-R}	reverse kinetic reaction constant related to A
k_{AR}	forward kinetic reaction constant related to AR
k_{-AR}	reverse kinetic reaction constant related to AR
k_{open}	forward kinetic reaction constant related to open R
k_{close}	reverse kinetic reaction constant related to close R
L	length of the cleft
r_{max}	radius of the cleft

R	unbound acetylcholine receptors
R_0	initial unbound acetylcholine receptors
r	radial coordinate
z	transverse coordinate

Greek Symbols

Δr	special grid size along radius
Δt	time increment
$\Delta \varphi$	special grid size along angular direction
φ	angular coordinate
Δz	special grid size along transverse coordinate

ACKNOWLEDGEMENTS

This dissertation owes many thanks to a number of people for their support and encouragement. I express my deepest gratitude to my advisor, Dr. Weizhong Dai, for his guidance, generous help, and many hours he spent with me to discuss the numerical strategies to solve the problems presented in this dissertation. Sincere acknowledgement is also extended to my advisory committee members Dr. Long Que, Dr. Leland Weiss, Dr. Mark DeCoster and Dr. Shengnian Wang for teaching and directing me.

Furthermore, I owe a lot of thanks to my friend Dr. Frank Jenkins for his unconditional, sincere help to complete this dissertation. Finally, I want to express my appreciation to my family who always inspired me to complete this research. This dissertation is dedicated to all those named here.

CHAPTER 1

INTRODUCTION

1.1 General Overview

The main subject of this research is the neuromuscular junction (NMJ). The NMJ is a biological structure composed of the interface between a neuron and a myocyte (muscle cell). The NMJ is a type of synapse: a region between two cells through which they signal each other. The synapse is a biological structure common to animals and is a core feature of intercellular signaling and communication. Neurons play a central role in cognition and movement (the two defining behaviors of animals), and the synapse is the primary mode of neuron function. The NMJ is the site where all animal movement initiates; consequently, it has long been a subject of intense biological study [1]-[8].

The NMJ is small and delicate, and its structure and function are both highly complex. These characteristics make the NMJ a difficult system to investigate quantitatively. The present mechanical probes used to quantify NMJ behavior are extremely invasive at the scale of interest [9], [10]. When used naively, these tools can perturb NMJ behavior beyond normal, or even disrupt it into nonfunctionality. Some chemical methods exist as well; however, it is very difficult to isolate specific reactions in a chemical network (almost by definition, because an isolated entity is *not* part of

1

a network). A change in one reaction tends to propagate throughout the entire network. Two other important issues are: (1) technology has produced instruments which can be so sensitive that it is nearly impossible to isolate them from environmental disturbances, and (2) under certain conditions it can be difficult to discriminate between "signal" and "noise"; at the molecular scale data is inherently noisy.

There are two principle types of neuro probes to perform electro-physiological measurement:

   a. Shank type (metal or silicon)

   The shank type are usually arranged in arrays and used for single cell culture or brain slices. These electrodes have diameters between 10-30 μm.

   b. Glass micro-pipette

   The glass micro-pipettes are used in voltage and current clamped experiments. The micro-pipettes have an inner diameter on the order of 0.5 μm.

A voltage clamp experiment makes it possible to measure the magnitude of the ionic current crossing a cell's membrane at any given voltage. Conversely, a current clamp experiment records the potential of a cell membrane for some constant current injected into the cell. A voltage clamp experiment is commonly used to measure current flowing through the end plate membrane. This is crucial because the current is directly proportional to the number of ions crossing the membrane. The ions cross the membrane through voltage gated channels, which open only when the membrane voltage within a particular range

Historically, many of the genius-level creative insights which led to fundamental explanations of universal processes were possible because the analyst's ability to

recognize symmetries in the system, and to reduce these symmetries to equations and theorems [11]. However, in complex systems, it can be difficult to determine at what scale symmetries might be recognized, even if they exist. The complexity of biological systems, in particular, tends to resist creative insight applied in the traditional way.

To address these difficulties, mathematical models of the NMJ have been developed to assist in the analysis and explanation of experimental results and provide a systematic approach which can be used by analysts who need not have traditional genius abilities [11], [12]-[15].

A mathematical model of a system is much easier to manipulate than the real system. For example, the components of a mathematical model can be defined as controls or variables in any combination. The system behavior can be simulated with different combinations, and the results can be analyzed. In this way, artificial experiments can be calculated before committing the resources to accomplish actual experiments [16]-[19]. Many biological processes consist of a long series of coupled events of which only a few can be directly measured experimentally. The event of interest may not be directly measureable or might be the termination of a series of imperfectly known steps. With a mathematical model, one can hypothesize various mechanistic events and iteratively compare the results of the model with experiment. Models can be used to quantify the connectivity of processes which are coupled through several degrees of separation [12], [13].

As with all components of every biological system, the NMJ is subject to injury, disease, and senescence. Developing a useful analytical and predictive model of this

structure will assist in the therapeutic efforts to restore and rehabilitate NMJ function to humans and in developing strategies to prevent damage to the NMJ.

1.2 Research Objectives

The objective of this research is to develop a model of neuromuscular junction processes in three dimensions. The model should describe and explain observed behavior and predict results of new experiments and observations. Our coordinates of reference will be the cylindrical coordinate system, since the NMJ can be considered as a cylinder. To achieve our objective, several steps will be pursued as follows:

(1) Develop a stable 1D mass transport model for Neumann boundary conditions.

(2) Test the 1D model with known analytical solution and experimental data.

(3) Extend the 1D model to a full 3D reaction-diffusion model for the core acetylcholine and cholinergic receptor processes in the neuromuscular junction.

(4) Develop a numerical scheme for solving the 3D model.

(5) Analyze the stability of the 3D numerical scheme.

(6) Test the 3D scheme by comparing the existing experimental and numerical results.

(7) Apply the numerical scheme to investigate the acetylcholine distribution and open receptor population in the NMJ during an action potential under simulated absence of enzyme activity.

1.3 Organization of the Dissertation

In Chapter 1, a general review of the main idea of the work is given; the objective of this dissertation is proposed; and the organization of this research is described.

Chapter 2 describes the fundamentals of neuromuscular junction and reviews the related previous work done by other researchers.

Chapter 3 specifies the problem description for 1D mass transport and 3D reaction-diffusion models including governing equation with associated initial and boundary conditions.

Chapter 4 describes the numerical schemes for solving 1D diffusion and 3D reaction-diffusion models. A novel numerical method to implement the Neumann boundary conditions in cylindrical coordinates is delineated. The 3D reaction-diffusion scheme including algorithm is discussed in detail. The stability analysis for the obtained finite difference schemes is included in this chapter.

In Chapter 5, results and discussion are described. The first section explains the results of 1D mass transport model while the second section considers 3D reaction-diffusion solutions.

In Chapter 6, we give the conclusions of our work and suggest future research work.

CHAPTER 2

BACKGROUND AND PREVIOUS WORK

2.1 Reaction-Diffusion in Neuromuscular Junction

2.1.1 Synapse Structure

It has been stated that the region where activity is transmitted between cells which share a physical interface is called a synapse, and the synapse is an important mode used for intercellular communication. Three general synapse classes exist: chemical, electrical, and immunological; and there are several types of chemical synapses. The fundamental structure of all synapses can be separated into three components: (1) the presynaptic membrane, (2) the postsynaptic membrane, and (3) the synaptic gap (cleft), which separates the membranes. The basic structure of a chemical synapse is especially well described by these three components, while electrical and immunological synapses have additional features which distinguish them as individual types. Note that because all synapses share structural characteristics, the study (experimental and simulation) of any one type can lead to insights about the similarities and differences of the others [1]-[3].

2.1.2 Neuromuscular Junction

Nerve cells can be a part of two types of synapses; in one case, a neuron connects to another neuron; and in the other case, a neuron connects to a myocyte. This work

concerns the case of a neuron connecting to a myocyte, identified as the NMJ, and it is in this region that a neuron signals a muscle fiber to contract. The NMJ is a chemical synapse, and therefore, consists of three main portions: the neuron (presynaptic membrane), the region where the neuron connects to the myocyte, called the motor end-plate (postsynaptic membrane), and the cleft separating these portions where the chemistry of muscle movement is initiated. An important feature specific to the NMJ is the junctional folds which are embed in the postsynaptic membrane [1]-[5], [20].

A global illustration of the NMJ is shown in Figure 2.1, where a neuron is attached to a muscle fiber at the motor end-plate. At the neuromuscular junction, the motor-nerve fiber loses its fatty myelin sheath and branches into fine terminals, and each terminal lies in a shallow gutter-like depression on the surface of the muscle cell [2], [4].
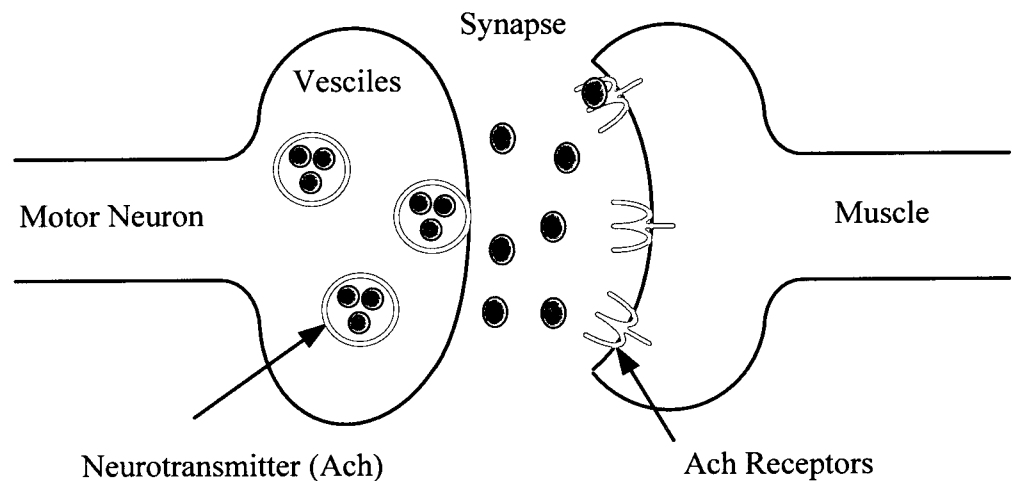
Figure 2.1 A global illustration of the NMJ.

At the nerve-muscle interface, the membranes of the neuron and the myocyte are separated by a fluid-filled cleft approximately 50 nanometers (nm) wide. About every micrometer along the nerve presynaptic membrane there are specialized areas which are

associated with clusters of tiny vesicles, each containing on the order of 10,000 molecules of the neurotransmitter acetylcholine (Ach). In the muscle membrane, directly opposite from the vesicle clusters, are the junctional folds (not shown in Figure 2.1). At the crests of these folds and part of the way down into them, are structures known as acetylcholine receptors. These receptors are specialized protein molecules embedded in the membrane of the motor-end-plate and can be found anywhere on the surface of a muscle cell [2], [5]-[8]. The receptors are tightly packed in these regions. Qualitatively, the receptors are densely packed and concentrated along the ridges of the motor end-plate surface and are very sparse in the junctional fold troughs. That placement makes sense because the acetylcholine receptors are localized in the regions of periodic high acetylcholine concentration.

2.1.3 A Basic Neuromuscular Junction Processes

A voltage impulse arriving at the presynaptic nerve terminal causes an influx of calcium (Ca^{+2}) ions across its membrane. This influx induces several hundred of the synaptic vesicles to fuse with the presynaptic membrane at specialized regions called active zones as shown in Figure 2.2. As can be seen in Figure 2.2, this influx of Calcium ions free the vesicles' content of acetylcholine molecules into the synaptic cleft [2]. The transmitter diffuses rapidly across the cleft to the muscle cell membrane where it combines with the embedded receptor molecules as shown in Figure 2.3. Each receptor can bind two acetylcholine molecules, and the acetylcholine molecules stay attached for about 1 millisecond (ms) [2], [6].
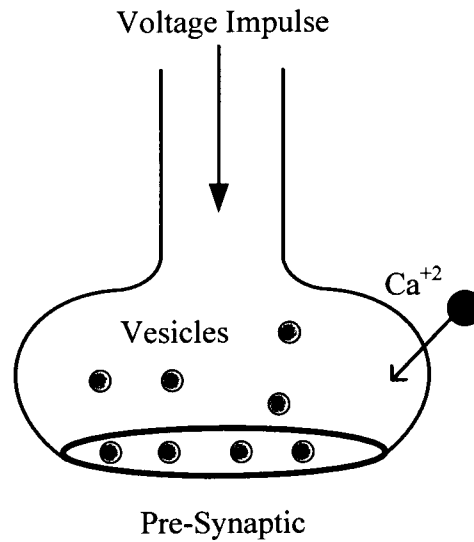
Figure 2.2 Normal reaction initialization.

Within 0.3 milliseconds after each acetylcholine packet or vesicle load is released, it causes approximately 2,000 receptors in the muscle-cell membrane to change their conformation into an open state. In this open state, the receptors are channels which can pass both sodium (Na^+) and potassium (K^+) ions through the membrane. Each individual channel has a specific conductance known as "Single Channel Conductance". This conductance changes with the exchange of ions through the post-synaptic membrane. The measured value of a single channel conductance is approximately 42 pS (pico Siemens). This value is a crucial parameter to estimate the number of open receptors extracted from experimentally measured data. This flow of ions (Na^+ into the muscle, and K^+ out) gives rise to a net electric current that short-circuits the normal potential of -90 millivolts (mV) across the resting cell membrane [3].
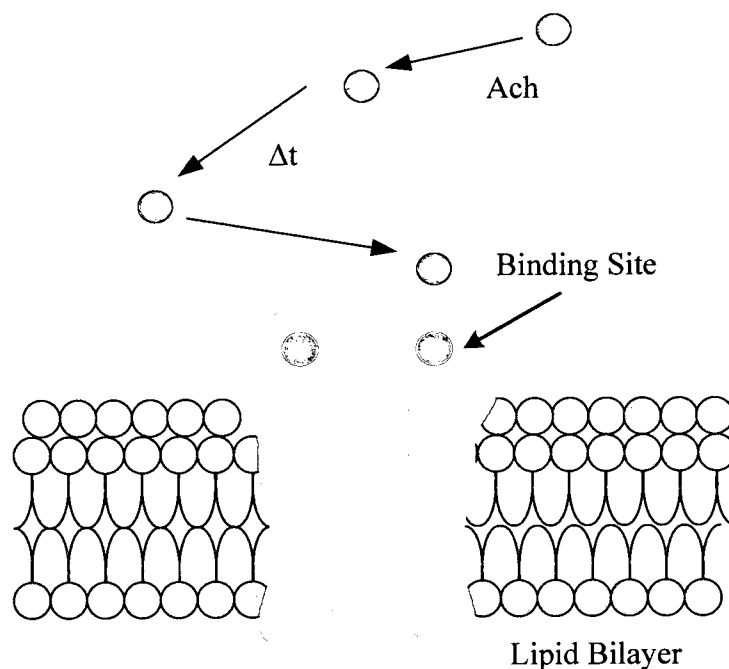
Figure 2.3 Acetylcholine diffusion in the neuromuscular junction.

This brief depolarization is known as the "end-plate potential" or the "excitatory postsynaptic potential". Under normal conditions, the end-plate potential exceeds the threshold value for initiating an impulse that spreads through the entire muscle-cell membrane and causes the muscle-cell to contract. Other protein structures in the membrane powered by adenosine triphosphate (ATP), called protein pumps, actively transport Na^+ and K^+ ions continuously through the membrane in their opposite directions, respectively. This simultaneous process consumes energy and restores the depolarized membrane back to its normal resting potential when the open receptors return to their closed state [5]. Acetylcholine molecules would linger in the synaptic cleft, diffusing from one receptor to another on the post-synaptic membrane and opening additional channels, if it were not for the enzyme acetylcholinesterase, which catalytically breaks acetylcholine down into acetate and choline molecules as Figure 2.4 illustrates.
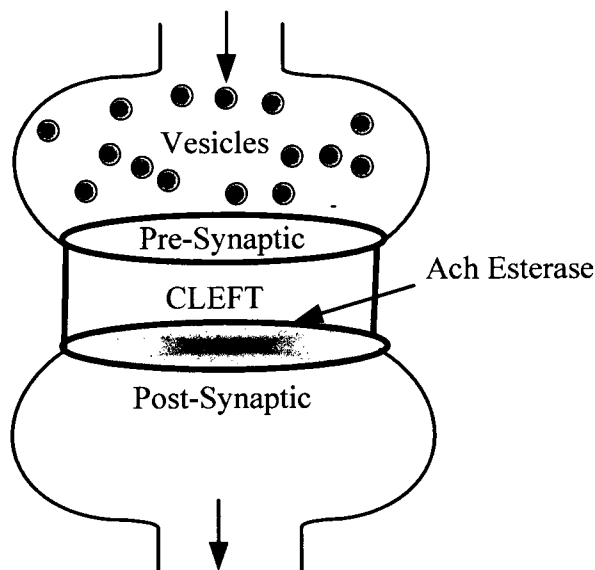
Figure 2.4 Ach Esterase in the neuromuscular junction.

The molecules of this enzyme are not embedded in the muscle cell membrane like the acetylcholine receptors; instead, they are immobilized within a loose matrix of collagen and mucopolysaccaride fibers that extend throughout the synaptic cleft and deep into the junctional folds [2]-[8].

Acetylcholinesterase destroys about a third of the acetylcholine molecules before they even reach the receptors and then rapidly cleaves those remaining as they detach from the receptors. The speed with which acetylcholine is bound to the receptors and inactivated makes it possible for the entire process of neuromuscular transmission to be repeated up to several hundred times per second [2]-[5].

The acetylcholine receptor is comprised of five subunits; three are designated as β, δ, and γ; and two with identical structure designated as α. Each α-unit can bind one acetylcholine molecule at a special acetylcholine binding site. These receptors are normally closed in the absence of ligand binding, and can open within approximately 20

microseconds of an appropriate ligand binding event. The receptor subsequently closes after dissociation of at least one ligand from the receptor [1], [4].

The response of the acetylcholine receptor can be separated into two steps. Each receptor, which is normally in the closed state, binds two acetylcholine molecules, one to each subunit *a*, to form what is called a *ligand*-receptor complex. After binding, this complex undergoes a conformation transition which opens a pore into the muscle membrane that is permeable to Na^+, K^+, and Ca^{+2}. The binding and unbinding steps are relatively slow; transitions to and from the open state of the pore are, in contrast, relatively rapid. Thus, channel openings occur in short bursts which can last several milliseconds, and which represent the lifetime of the ligand-receptor complex. During the burst, the channel flickers open and shut [21]-[27].

The rapid depolarization and re-polarization events which constitute the many-times-per-second neuromuscular transmission process are possible, in part, because of the activity of the cholinesterase protein. There are at least two kinds of cholinesterase found in humans: acetylcholinesterase and butyrylcholinesterase. The difference between them is that each has a preference to react with its root-named effector molecule (the substrate), acetylcholine and butyrylcholine, respectively [27],[28]. Acetylcholine and butyrylcholine are both transmitter-type molecules with similar chemistry, and each cholinesterase can react with the other's substrate as well, though not preferentially. Acetylcholinesterase is found primarily in the blood and neural synapses, while butyrylcholinesterase is located primarily in the liver [27].

As stated earlier, the function of acetylcholinesterase is to deactivate acetylcholine. Like most enzymes, acetylcholinesterase is a large polymer where the

conformation and inter-molecular and intra-molecular forces of its structure play important roles in its function. Because of these conditions, the portion of this molecule where its chemical activity is located may be significantly smaller than the body of the entire molecule (in other cases, the entire molecular body may be used to build the active region). In addition, the molecule could have multiple active regions. Consequently, descriptions of the chemical kinetics of enzymes usually focus on their active sites: their characterization and number; rather than quantifying the properties of individual enzyme molecules [29].

The activity of acetylcholinesterase is extremely high. Each active site of this enzyme is able to hydrolyze approximately 14,000 acetylcholine molecules per second at normal body temperature [30], which is also close to the theoretical number of molecular collisions at that same temperature [28]. Typical chemical reactions depend on the number of collisions between molecules and their orientation relative to each other. Some orientations result in a reaction and some do not. For acetylcholinesterase, this high activity means that essentially every collision between acetylcholinesterase and acetylcholine molecules results in a reaction and enzymes with that property are termed "diffusion limited". Qualitatively, this "diffusion limited" means the reaction speed of acetylcholinesterase is controlled only by how quickly acetylcholine molecules can reach the active sites. Some enzymes are thought to accelerate catalysis to this limit by using dipolar electric fields to pre-orient their substrate to the optimal position as it is drawn in to the enzyme's active site [31]-[34]. The ability to catalyze a reaction with every substrate collision also makes acetylcholine a very reliable enzyme, and reliability is a

useful and important attribute for an enzyme whose function is such an integral part of movement and cognition.

2.2 Normal Chemical Kinetics in the Neuromuscular Junction

The chemical reactions associated with the NMJ which occur in the synaptic cleft can be described by the following chemical stoichiometric Equations (2.1) through (2.6):
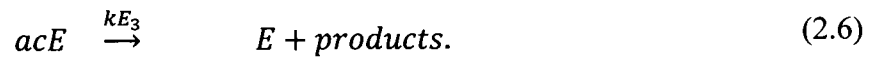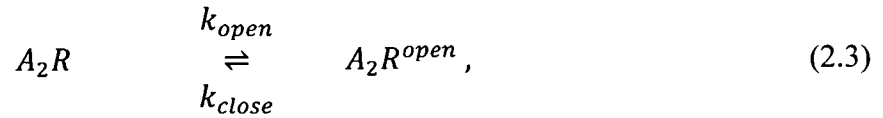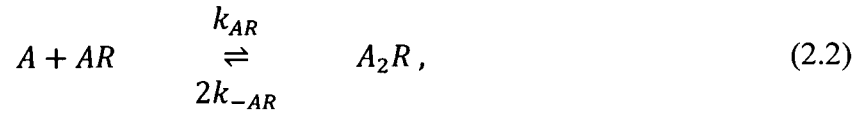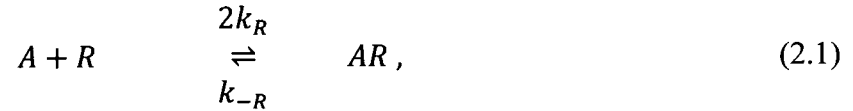
$$A + R \underset{k_{-R}}{\overset{2k_R}{\rightleftharpoons}} AR, \tag{2.1}$$

$$A + AR \underset{2k_{-AR}}{\overset{k_{AR}}{\rightleftharpoons}} A_2R, \tag{2.2}$$

$$A_2R \underset{k_{close}}{\overset{k_{open}}{\rightleftharpoons}} A_2R^{open}, \tag{2.3}$$

$$A + E \underset{kE_{-1}}{\overset{kE_1}{\rightleftharpoons}} AE, \tag{2.4}$$

$$AE \overset{kE_2}{\longrightarrow} acE, \tag{2.5}$$

$$acE \overset{kE_3}{\longrightarrow} E + products. \tag{2.6}$$

where A, R, AR, A_2R, A_2R^{open} are the molar concentration of the acetylcholine, unbound receptors, single bound acetylcholine receptors, double bound closed acetylcholine receptors, and double bound open acetylcholine receptors, respectively; E, AE, and acE are the acetylcholinesterase, Michaelis ligand-substrate complex, and acylate enzyme respectively; k_R, k_{-R}, k_{AR}, k_{-AR}, k_{close}, k_{open}, kE_1, kE_{-1}, kE_2, and kE_3 are the reaction rate constants [2], [6].

Equations (2.1) through (2.6) represent the full kinetic cycle of acetylcholine initially reacting with acetylcholinesterase and proceeding to the final renewal of the

enzyme. The first step shows acetylcholine, A, reacting with acetylcholinesterase, E, reversibly to form the Michaelis complex of AE. The forward reaction, controlled by the rate constant kE_1, is several orders of magnitude faster than the reverse reaction controlled by kE_{-1}. In the next step, species AE then irreversibly reacts to form the acylated enzyme intermediate acE, where the reaction rate is controlled by the constant kE_2. The final step shows how acE then decomposes back to acetylcholinesterase and reaction products, where the rate is controlled by the rate constant kE_3 and one of the reaction products is choline. This final step regenerates the enzyme and is the major resource for acetylcholine replacement because choline is a precursor of acetylcholine. Water is also a reactant in this last step, but in this case, water is treated as an excess solvent, and as such, its concentration does not change and so is not included in the reaction kinetics [9], [10], [26], [28].

Equation (2.1) represents the first acetylcholine molecule reversibly binding to the closed receptor. Because there are two sites available for docking, a numerical factor of two is included with the kinetic rate constant $2k_R$, which controls the forward binding reaction. Because only one acetylcholine molecule can dissociate from the receptor in the reverse reaction, the kinetic rate constant k_{-R} does not require an additional multiplicative factor.

The two-step process kinetics of acetylcholine receptor function is represented by Equation (2.1). Just as in Equation (2.2), the first step of this equation shows a second acetylcholine molecule binding reversibly to the ligand-receptor complex AR. Only one position for binding exists on the receptor in this case, so the forward kinetic rate constant, k_{AR}, does not require a multiplicative factor. In the reverse reaction, either of the

two acetylcholine molecules could dissociate from the closed ligand-receptor complex A_2R so the numerical factor of two is included with the kinetic rate constant $2k_{-AR}$. The second step of Equation (2.3) shows the closed, double-bound, ligand-receptor complex reversibly changing from the closed conformation to the open conformation, A_2R^{open} (forward reaction), and back to the closed conformation (reverse reaction). The forward and backward reactions are controlled by the kinetic rate constants k_{open} and k_{close}, respectively. It is at this step where the redistribution of sodium and potassium ions through this open channel leads to the eventual contraction of the muscle cell. Several experiments and kinetic-thermodynamic analyses [31], [35]-[38] have shown that the conformational change from A_2R to A_2R^{open} is energetically favored, so that a channel which has two molecules of acetylcholine bound to it will spend most of its time of existence in the open condition. Figure 2.5 depicts the normal receptor kinetics. This process does not include a complete set of the normal chemical reactions in a NMJ. A complete inhibition of the enzyme is assumed in the current model. This research is focused to develop a numerical scheme that can capture the dynamics of the diffusion-reaction in a NMJ in a simple case. The future work may include a more comprehensive set of chemical reactions including enzyme and diffusion of a toxic inhibitor.

Pre-Synaptic

$$A + R \leftrightarrow AR$$
$$A + AR \leftrightarrow A_2R$$
$$A_2R^{Close} \leftrightarrow A_2R^{Open}$$

Post Synaptic
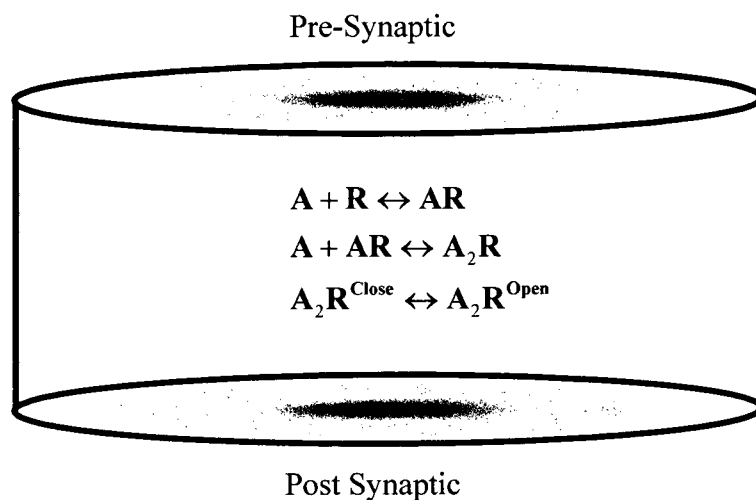
Figure 2.5 Normal receptor chemical kinetics.

2.3 Previous Works

The synaptic chemical transmission is an important part of the transport of neuronal signals, and investigation of the molecular events was instrumental in creating neurotransmitter theory. Analysis of such behavior can be best accomplished with the transmission process represented as a reaction-diffusion simulation for the neurotransmitter because comprehensive analysis that is exclusively experimental is impractical for the molecular processes in the cleft. Unless great care is taken, the tools used to collect the data can disrupt the physical system so badly that it ceases natural function.

In response, mathematical models of NMJ processes have been developed [39]-[57]. The fundamental NMJ transmission process involves the dynamic behavior of Ach in diffusion through the synaptic gap and its reactions with the receptors at the end-plate. This transmission process is essentially diffusion coupled with chemical reactions, and

the analysis of this process is best approached mathematically with diffusion-reaction kinetics [58], [59].

Diffusion-reaction kinetic systems are analyzed with systems of coupled nonlinear partial differential equations (PDEs). Nonlinear PDE systems usually do not have analytic solutions and need to be solved with numerical methods [60]-[63]. A few analytical models of NMJ processes have been developed in spite of the complexity associated with this system [47], [50], [51]. However, these analytical models either do not incorporate the complete reaction kinetics or use assumptions which simplify the geometry or spatial dimensions. The bulk of the published researches which achieve a more complete description of the NMJ diffusion-reaction processes are based on numerical solutions [39]-[46], [47]-[49], [52]-[57]. Finite difference discretization is one numerical technique commonly chosen to solve coupled nonlinear PDEs. Applying this method results in transforming a system of nonlinear PDEs into a system of coupled nonlinear algebraic equations [62].

A brief summary of several published mathematical investigations of the dynamic behavior of the NMJ which were especially pertinent to the research presented here, follows in the next section.

2.3.1 Magleby Model

One of the first investigations is the work done by K. L. Magleby and C. F. Stevens in 1972 [64]. Their work coupled the chemical reactions in the cleft to the voltage and current behavior at the junction end-plate and focused on deriving expressions for the end-plate current and receptor state/conformation. The assumptions

and definitions used to build their model reflect the available computational resources and what was then known about NMJ chemistry:

- The NMJ volume was assumed to be well mixed.

- One Ach molecule reacted with a single receptor.

- The receptors behaved independently of each other.

- Only three receptor states exist: unbound, bound-closed, and bound-open.

- The end-plate conductance was proportional to the number of bound-open receptors

The study covered the reactions of Ach and the receptor.

$$A + R \quad \underset{k_{-R}}{\overset{k_R}{\rightleftharpoons}} \quad AR, \tag{2.7}$$

$$AR \quad \underset{k_{close}}{\overset{k_{open}}{\rightleftharpoons}} \quad AR^{open}. \tag{2.8}$$
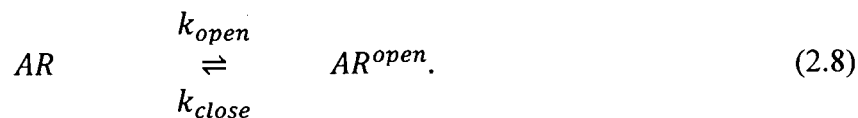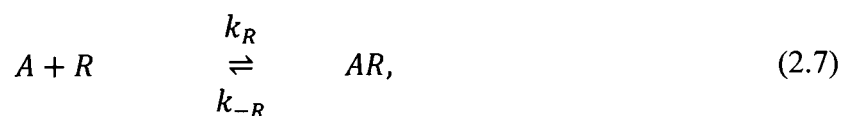
This assumption of a well-mixed volume avoided the need for partial differential equations or a space coordinate [64]. The nomenclature used by Magleby is listed in Table 2.1. The resulting governing Equations (2.9) through (2.12):

Table 2.1 The nomenclature used by Magleby [64]

Nomenclature	Definition
$\bar{V}$	volume of cleft
$f(t)$	time course of Ach emittance from presynaptic membrane
g	end-plate conductance
γ	single receptor conductance

$G(t - \tau)$	kernel characterizing diffusion out of the cleft volume

$$g = \gamma(AR^{open}), \tag{2.9}$$

$$\frac{d(AR^{open})}{dt} = -k_{open}(AR^{open}) + k_{close}(AR), \tag{2.10}$$

$$\frac{d(AR)}{dt} = k_{open}(AR^{open}) + k_R(A)[R_0 - (AR^{open}) - (AR)], \tag{2.11}$$

$$-(k_{close} + k_{-R})(AR),$$

$$\bar{V}\frac{d(A)}{dt} = f(t) - \int_0^t G(t - \tau)(A_\tau)\, d\tau. \tag{2.12}$$

The initial conditions are assumed to be:

$$(A)(0) = (A_0), \qquad (AR^{open})(0) = 0, \qquad (AR)(0) = 0 \tag{2.13}$$

The integro-differential equation is eliminated through appropriate use of simplification, substitution, and conservation relations. This study demonstrated that the observed exponential decay of end-plate currents could be coupled to a rate of receptor conformational change and not by the decay of Ach concentration in the cleft [39].

2.3.2 Rosenberry Model

Rosenberry, in 1979 [65], developed a model using homogeneous reaction spaces. Simulations using one-space and two-spaces were applied, each using the full normal NMJ chemistry:

$$A + R \quad \underset{k_{-R}}{\overset{2k_R}{\rightleftharpoons}} \quad AR, \tag{2.14}$$

$$A + AR \quad \underset{k_{close}}{\overset{k_{open}}{\rightleftharpoons}} \quad A_2R^{open}, \tag{2.15}$$

$$A + E + \overset{kE_1}{\underset{kE_{-1}}{\rightleftharpoons}} AE, \qquad (2.16)$$

$$AE \overset{kE_2}{\longrightarrow} acE, \qquad (2.17)$$

$$acE \overset{kE_3}{\longrightarrow} E + products. \qquad (2.18)$$
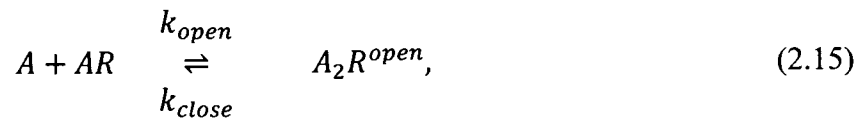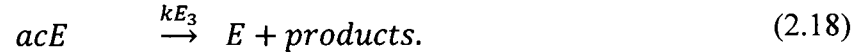
The two-space model was found to match more of the experimental results. Sophisticated mass (chemical species) conservation relations and dimensional scaling methods were used to (1) extend the one-space homogeneous reaction into the two-space homogeneous reaction model, and (2) reduce the number of independent variables in the system. Because of the choice of homogeneous reaction space, no location coordinates were needed. Loss of Ach from diffusion was compensated for by a reactive term which was proportional to the amount of Ach in the cleft. The nomenclature used by Rosenberry is listed in Table 2.2. The resulting governing Equations (2.19) through (2.22) :

Table 2.2 The nomenclature used by Rosenberry [65]

Nomenclature	Definition
t	Time
K_M	equilibrium constant
K_i	equilibrium constant
k_D	diffusional loss constant

$$\frac{d(AR)}{dt} = k_R(A)(R) - k_{-R}(AR) \qquad (2.19)$$

$$\frac{d(A)}{dt} = \left(1 + \frac{(E)}{K_M}\right)^{-1} \{-[k_R(R) + kE_1(E) + k_D](A) + k_{-R}(AR)\} \qquad (2.20)$$

$$\frac{d(A_2R^{open})}{dt} = k_R(A)(A_2R) - 2k_{-R}(A_2R^{open}) \tag{2.21}$$

$$\frac{d(acE)}{dt} = \left(1 + \frac{(A)}{K_i}\right)^{-1} \{kE_1(E)(A) - kE_3(acE)\} \tag{2.22}$$

The initial conditions assumed to be:

$$(AR)(0) = 0, \quad (A)(0) = (A_0), \quad (A_2R^{open})(0) = 0, \quad (acE)(0) = 0 \tag{2.23}$$

An analog computer was used to generate solutions for the equations. The two-space model predicted current amplitudes and time constants within a factor of two of those observed experimentally. This result indicated that the current time courses and amplitudes were determined primarily by the receptor behavior with Ach, and indirectly, Ach with the enzyme esterase [65].

2.3.3 Wathey Model

The Wathey [66] model treated the NMJ as the space between two circular planes where Ach diffused radially and symmetrically from the center towards the boundary. The full normal cleft reaction chemistry was simulated, depicted by Equations (2.25) through (2.28).

$$A + R \quad \overset{2k_R}{\underset{k_{-R}}{\rightleftharpoons}} \quad AR, \tag{2.24}$$

$$A + AR \quad \overset{k_{open}}{\underset{k_{close}}{\rightleftharpoons}} \quad A_2R^{open}, \tag{2.25}$$

$$A + E + H_2O \quad \overset{kE_1}{\longrightarrow} \quad AE, \tag{2.26}$$

$$AE \quad \overset{kE_2}{\longrightarrow} \quad E + products. \tag{2.27}$$
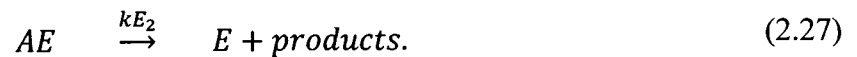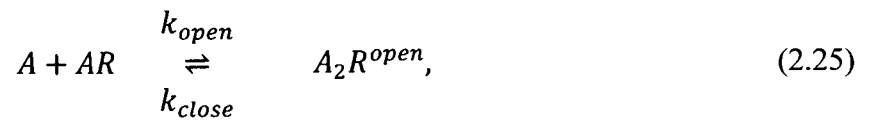
The geometry and coordinate system were chosen to be a thin disk and cylindrical, respectively, as shown in Figure 2.6. Ach was assumed to instantaneously appear in the cleft as a radially symmetric distribution, and subsequently diffusing, while simultaneously reacting with receptor and enzyme species uniformly distributed throughout the volume. The diffusion occurs along the radial direction. The diffusion along the transverse direction is assumed instantaneous. The radial direction is about 10 times larger than transverse which makes this instantaneous diffusion a valid assumption. A pulse of Ach appears in the center of the disk and diffuses out radially.
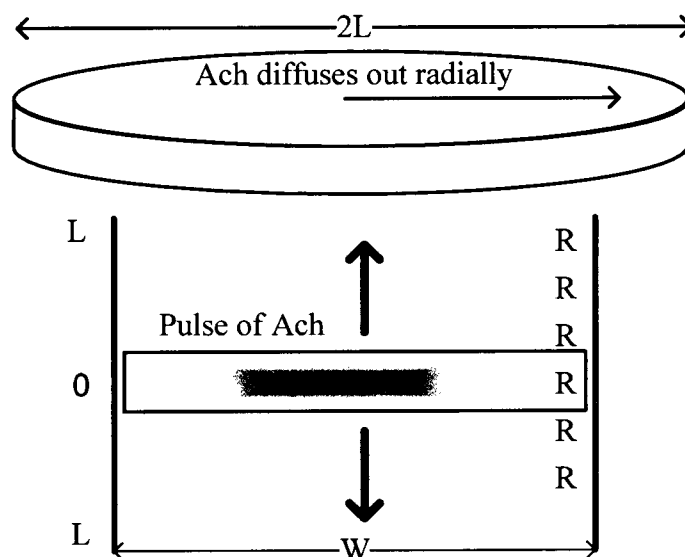
Figure 2.6 Schematic of the model where L is the radius, w the width, Ach is released at center of disk and diffuse out radially out of the cleft and instantaneously reach receptors (R) concentrated at the opposite edge.

Conservation relations were used to reduce the number of independent variables in the system. The nomenclature used by Wathey is listed in Table 2.3. The resulting governing Equations (2.28) through (2.31):

Table 2.3 The nomenclature used by Wathey [66]

Nomenclature	Definition
r	radial coordinate
t	Time
V	vesicle radius
α	Ach molecules emitted
r_{max}	radius of cleft
(E_0)	initial amount of esterase
(R_0)	initial amount of receptor
D_A	diffusion coefficient

$$\frac{\partial(A)}{\partial t} = D_A \left[\frac{\partial^2(A)}{\partial r^2} + \frac{1}{r}\frac{\partial(A)}{\partial r} \right] - kE_1(A)[(E_0) - (AE)]$$

$$-2k_R(A)[(R_0) - (AR) - (A_2R^{open})] - k_{open}(A)(AR)$$

$$+ k_{-R}(AR) + 2k_{close}(A_2R^{open}) \tag{2.28}$$

$$\frac{\partial(AR)}{\partial t} = 2k_R(A)[(R_0) - (AR) - (A_2R^{open})] + 2k_{close}(A_2R^{open})$$

$$- k_{open}(A)(AR) - k_{-R}(AR) \tag{2.29}$$

$$\frac{\partial(A_2R^{open})}{\partial t} = k_{open}(A)(AR) - 2k_{close}(A_2R^{open}) \tag{2.30}$$

$$\frac{\partial(AE)}{\partial t} = kE_1(A)[(E_0) - (AE)] - kE_2(A) \tag{2.31}$$

The initial conditions were assumed to be:

$$(A)(r,0) = \begin{cases} \alpha\left[\left(\frac{r}{V}\right)^4 - 2\left(\frac{r}{V}\right)^2 + 1\right] & if \ \ 0 \le r \le V \\ 0 & if \ \ r > V \end{cases} \qquad (2.32)$$

The boundary conditions for A were assumed to be:

$$(A)(r_{max}, t) = 0, \quad \frac{\partial(A)}{\partial r}\Big|_{r=0} = 0 \qquad (2.33)$$

2.3.4 Friboulet Model

Friboulet and Thomas [67] presented a model with disk geometry where the Ach diffused transversely across the cleft, reacting with uniformly distributed enzyme, and subsequently reacted with receptors at the post-synaptic membrane as illustrated in Figure 2.7.

(a)

(b)
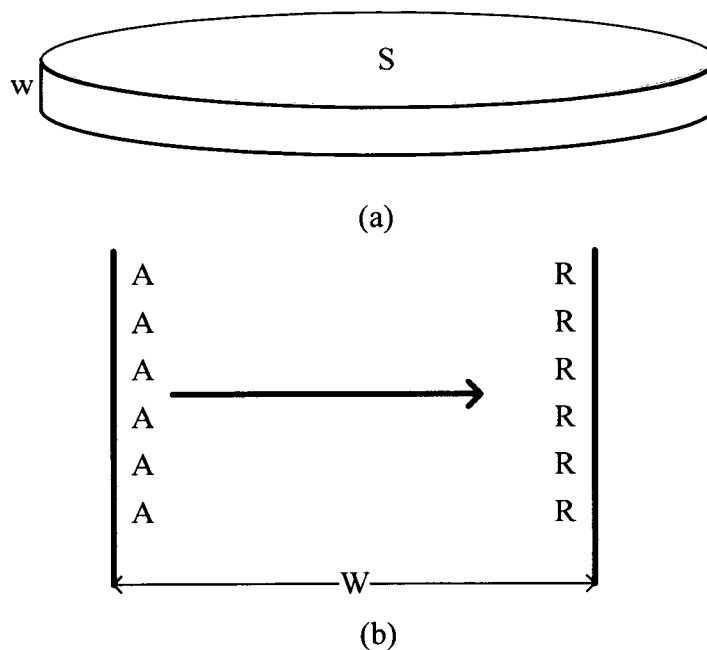
Figure 2.7 Schematic of the model (a) Critical area, where s is the surface area, w the width; (b) width of the disk where Ach (A) is homogenously distributed, Ach is released at one edge and diffuse through the width to reach receptors (R) concentrated at the opposite edge.

The reactions of normal NMJ chemistry were considered, as shown in the Equations (2.34) through (2.35):

$$A + R \quad \overset{2k_R}{\underset{k_{-R}}{\rightleftharpoons}} \quad AR, \tag{2.34}$$

$$A + AR \quad \overset{k_R}{\underset{2k_{-R}}{\rightleftharpoons}} \quad A_2R, \tag{2.35}$$

$$A_2R \quad \overset{k_{open}}{\underset{k_{close}}{\rightleftharpoons}} \quad A_2R^{open}, \tag{2.36}$$

$$A + E \quad \overset{kE_1}{\underset{kE_{-1}}{\rightleftharpoons}} \quad AE, \tag{2.37}$$

$$AE \quad \overset{kE_2}{\longrightarrow} \quad acE, \tag{2.38}$$

$$acE \quad \overset{kE_3}{\longrightarrow} \quad E + products. \tag{2.39}$$
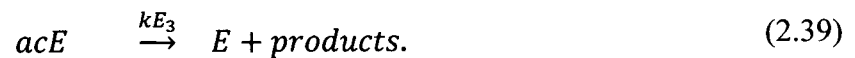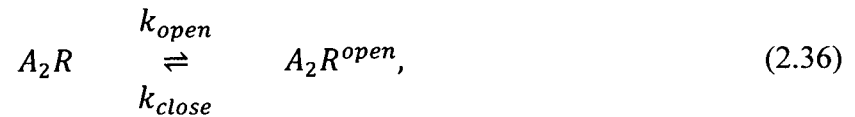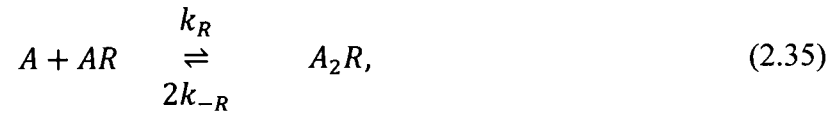
The NMJ geometry was modeled as a thin disk. Ach was assumed to form a uniform distribution at the presynaptic membrane, then diffuse transversely across the cleft to the receptors at the post synaptic membrane, while reacting with esterase enzyme distributed uniformly in the cleft volume.

The loss of Ach from the gap was modeled mathematically as a reactive "sink" term. Several independent variables were removed from the system with the use of conservation relations among the chemical species. The Table 2.4 shows the nomenclature used by Friboulet. The resulting Equations are (2.40) through (2.45):

Table 2.4 The nomenclature used by Friboulet [67]

Nomenclature	Definition

z	transverse coordinate
t	Time
D_A	diffusion coefficient
(A_0)	initial amount of Ach
(E_0)	initial amount of esterase
(R_0)	initial amount of receptor
z_{max}	Width of the cleft

$$\frac{\partial(A)}{\partial t} = D_A \frac{\partial^2(A)}{\partial z^2} - k_R(A)\{2[(R_0) - (AR) - (A_2R) - (A_2R^{open})] + (AR)\}$$

$$+k_{-R}[(AR) + 2(A_2R)] + kE_{-1}(AE)$$

$$-kE_{-1}(A)[(E_0) - (AE) - (acE)] \tag{2.40}$$

$$\frac{\partial(AR)}{\partial t} = k_R(A)\{2[(R_0) - (AR) - (A_2R) - (A_2R^{open})] - (AR)\}$$

$$+k_{-R}[2(A_2R) - (AR)] \tag{2.41}$$

$$\frac{\partial(A_2R)}{\partial t} = k_R(A)(AR) + k_{close}(A_2R^{open}) - 2k_{-R}(A_2R) - k_{open}(A_2R) \tag{2.42}$$

$$\frac{\partial(A_2R^{open})}{\partial t} = k_{open}(A_2R) - k_{close}(A_2R^{open}) \tag{2.43}$$

$$\frac{\partial(AE)}{\partial t} = kE_1(A)[(E_0) - (AE) - (acE)] - (kE_2 + kE_{-1})(AE) \tag{2.44}$$

$$\frac{\partial(acE)}{\partial t} = kE_2(AE) - kE_3(acE) \tag{2.45}$$

The initial conditions for ODE's are assumed to be:

$$(AR)(0) = 0, (AE)(0) = 0, (A_2R)(0) = 0, (A_2R^{open})(0) = 0, (acE)(0) = 0 \tag{2.46}$$

The initial conditions for PDE assumed to be:

$$(A)(z, 0) = (A_0) \tag{2.47}$$

The boundary conditions for A are assumed to be:

$$(A)(z_{max}, t) = 0, \quad \frac{\partial (A)}{\partial x}\bigg|_{z=0} = 0 \tag{2.48}$$

2.3.5 Naka Model

Naka and Shiba [68] extended the work of Rosenberry, Wathey, and Friboulet into a two dimensional space geometrically modeled as an axis-symmetrical thin disk. Full normal NMJ chemistry was included.

The reactions of normal NMJ chemistry were considered as shown in the Equations (2.49) through (2.54):

$$A + R \underset{k_{-R}}{\overset{2k_R}{\rightleftharpoons}} AR, \tag{2.49}$$

$$A + AR \underset{2k_{-AR}}{\overset{k_{AR}}{\rightleftharpoons}} A_2R, \tag{2.50}$$

$$A_2R \underset{k_{close}}{\overset{k_{open}}{\rightleftharpoons}} A_2R^{open}, \tag{2.51}$$

$$A + E \underset{kE_{-1}}{\overset{kE_1}{\rightleftharpoons}} AE, \tag{2.52}$$

$$AE \overset{kE_2}{\longrightarrow} acE, \tag{2.53}$$

$$acE \overset{kE_3}{\longrightarrow} E + products. \tag{2.54}$$
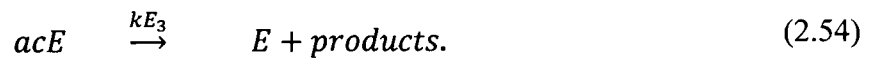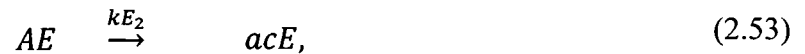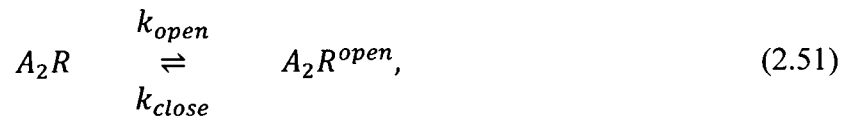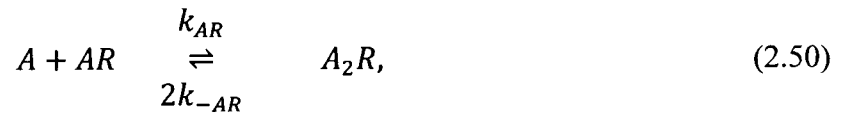
Acetylcholine simultaneously diffused transversely across the gap from the presynaptic membrane to the post-synaptic membrane, radially out of the gap, and reacted with receptors and enzyme. The extension into two dimensions enabled an

examination of anisotropic effects in the NMJ processes. All chemical species in the normal reactions were computed directly in the simulation as independent variables except for unbound receptor. Cylindrical coordinates were chosen, as shown in Figure 2.8:
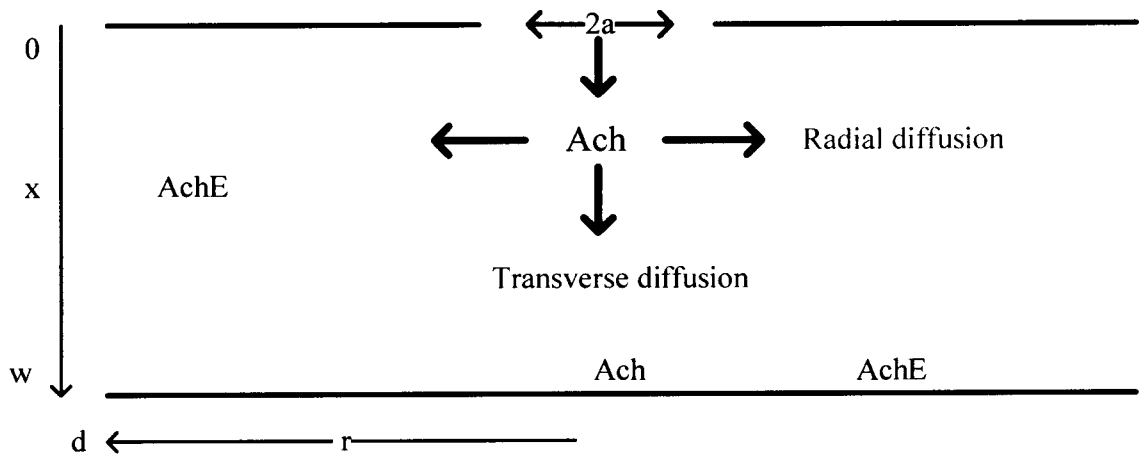
Figure 2.8 Reaction-diffusion system for Ach in a two dimensional square space of axis-symmetrical disc of the synaptic cleft. A quantum of Ach molecules are released from the release area indicated as a pore on the presynaptic membrane. The radius of the release area is denoted by a [68].

Table 2.5 provides the nomenclature used by Naka. The chemistry and the model assumptions lead to Equations (2.55) through (2.60) :

Table 2.5 The nomenclature used by Naka [68]

Nomenclature	Definition
z	transverse coordinate
r	radial coordinate
t	Time
D_z	transverse diffusion coefficient

D_r	radial diffusion coefficient
(A_0)	initial amount of Ach
(E_0)	initial amount of esterase
(R_0)	initial amount of receptor
r_{max}	radius of cleft
z_{max}	width of the cleft

$$\frac{\partial(A)}{\partial t} = D_z \frac{\partial^2(A)}{\partial z^2} + D_r \left[\frac{\partial^2(A)}{\partial r^2} + \frac{1}{r} \frac{\partial(A)}{\partial r} \right] - kE_1(A)[(E_0) - (AE) - (acE)]$$

$$+kE_{-1}(AE) - 2k_R(A)[(R_0) - (AR) - (A_2R) - (A_2R^{open})]$$

$$+k_{-R}(AR) - k_R(A)(AR) + 2k_{-R}(A_2R) \tag{2.55}$$

$$\frac{\partial(AR)}{\partial t} = -2k_R(A)[(R_0) - (AR) - (A_2R) - (A_2R^{open})] + k_{-R}(AR)$$

$$+k_R(A)(AR) - 2k_{-R}(A_2R) \tag{2.56}$$

$$\frac{\partial(A_2R)}{\partial t} = -k_R(A)(AR) + 2k_{-R}(A_2R) - k_{open}(A_2R) + k_{close}(A_2R^{open}) \tag{2.57}$$

$$\frac{\partial(A_2R^{open})}{\partial t} = k_{open}(A_2R) - k_{close}(A_2R^{open}) \tag{2.58}$$

$$\frac{\partial(AE)}{\partial t} = kE_1(A)[(E_0) - (AE) - (acE)] - kE_{-1}(AE) - kE_2(AE) \tag{2.59}$$

$$\frac{\partial(acE)}{\partial t} = kE_2(AE) - kE_3(acE) \tag{2.60}$$

The initial conditions for ODE's are assumed to be:

$$(AR)(0) = 0, (A_2R)(0) = 0, (AE)(0) = 0, (A_2R^{open})(0) = 0, (acE)(0) = 0 \tag{2.61}$$

The initial conditions for PDE assumed to be:

$$(A)(r, 0) = (A_0) \tag{2.62}$$

The boundary conditions for A are assumed to be:

$$(A)(r_{max}, t) = 0, \quad \frac{\partial(A)}{\partial r}\bigg|_{r=0} = 0, \quad \frac{\partial(A)}{\partial z}\bigg|_{z=0} = 0, \frac{\partial(A)}{\partial z}\bigg|_{z=z_{max}} = 0 \tag{2.63}$$

This work analyzed anisotropic effects in the NMJ. The ability to study anisotropy is a fundamental advantage of multi-dimensional simulations.

2.3.6 Other Work

The simulations of NMJ reaction-diffusion activity done after year 2000 have concentrated on using the numerical method of finite element analysis. This method is well suited to handle complex geometries, such as the structure of the receptors and junctional folds found in the NMJ [69]-[71].

An investigation by Kuzenetsov and Hooman [72] modeled aspects of intracellular mass transport in axons. In this case, the nonlinear PDEs contained terms representing active transport as well as diffusion and reaction, and the boundary conditions differed from those in the NMJ. However, it is interesting to note that those PDEs were also solved with finite difference approximation.

Currently, there is not a fully three dimensional model of diffusion-reaction processes occurring in the NMJ, wherein the system is modeled as a disk using the cylindrical coordinate system. Development of such a 3D model will allow us to investigate how the spatial distribution of physical properties in the NMJ affects the behavior of processes in the NMJ, in particular, how nonsymmetrical emission of Ach affects the diffusion-reaction process. Thus, the aim of this dissertation research is to develop such a fully 3D model which will include normal chemical kinetics.

CHAPTER 3

MATHEMATICAL MODELS

In Chapter 3, we consider 1D mass diffusion, 3D reaction-diffusion, and propose mathematical models for 1D mass diffusion and 3D reaction-diffusion models, respectively [73]-[80].

3.1 Modeling for 1D Mass Diffusion

Three dimensional mass transport in the neuromuscular junction using cylindrical coordinates may be reduced to the one dimensional problem shown in Figure 3.1 under the following conditions:

a. Uniformly distributed release of Ach in the pre-synaptic membrane at t=0.

b. An instantaneous transport of Ach from pre-synaptic membrane to post-synaptic membrane occurs.

c. Ach only diffuses symmetrically out of the cleft along the radial coordinate.

d. Pre-synaptic and post-synaptic membranes are impermeable to Ach. These membranes are treated as insulated boundaries for Ach diffusion. Ach can only diffuse out of the cleft through radial diffusion.

e. The concentration of Ach out of the cleft is assumed to be zero.
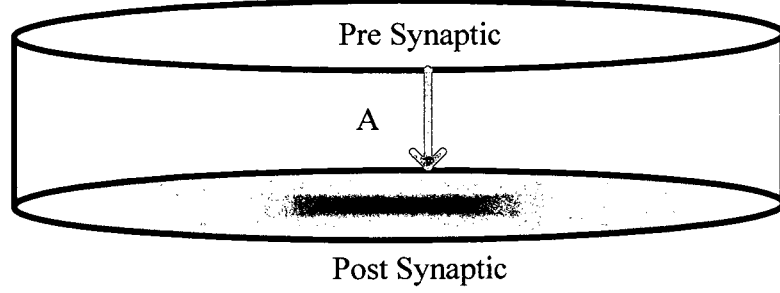
Figure 3.1 1D mass transport in the neuromuscular junction.

As such, a one-dimensional mass transport equation with initial and boundary conditions discussed above in cylindrical coordinates is given by the following Equations (3.1) through (3.3):

$$\frac{\partial A(r,t)}{\partial t} = \frac{D_A}{r}\frac{\partial}{\partial r}\left(r\frac{\partial A(r,t)}{\partial r}\right) + S(r,t), \quad 0 < r < R, t > 0, \tag{3.1}$$

$$A(r,0) = A_0(r), \tag{3.2}$$

$$\frac{\partial A(0,t)}{\partial r} = \frac{\partial A(R,t)}{\partial r} = 0, \tag{3.3}$$

where $A(r,t)$ is the mass concentration, D_A is the diffusion coefficient, $S(r,t)$ is the source term and R is the radius [66], [73].

3.2 Modeling for 3D Reaction-Diffusion

The NMJ is a three dimensional reaction-diffusion system. Ach is released in the presynaptic membrane, and receptors are located on the post-synaptic membrane. Ach transports across the cleft and reacts with receptors. It also diffuses out of the cleft along the radial direction. A three dimensional model is crucial to capture the fine scale dynamics of this reaction-diffusion system. 3D modeling is essential to study (a)

anisotropic diffusion along radial, transverse and angular direction and (b) asymmetric Ach injection at different location in the pre-synaptic membrane.

The six major chemical reactions occurring in the cleft which are included in the model are listed as follows:
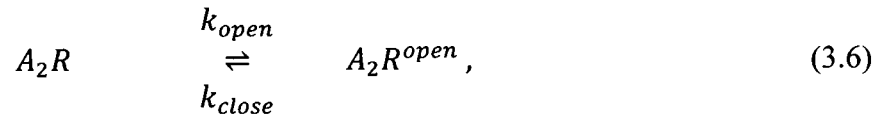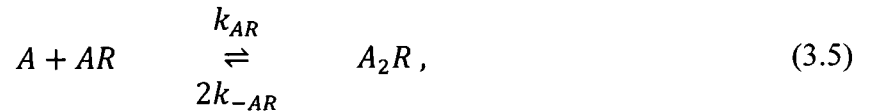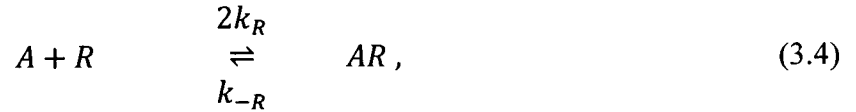
$$A + R \quad \overset{2k_R}{\underset{k_{-R}}{\rightleftharpoons}} \quad AR, \tag{3.4}$$

$$A + AR \quad \overset{k_{AR}}{\underset{2k_{-AR}}{\rightleftharpoons}} \quad A_2R, \tag{3.5}$$

$$A_2R \quad \overset{k_{open}}{\underset{k_{close}}{\rightleftharpoons}} \quad A_2R^{open}, \tag{3.6}$$

where A, R, AR, A_2R, A_2R^{open} are the molar concentration of the acetylcholine, unbound receptors, single-bound acetylcholine receptors, double-bound closed acetylcholine receptors, and double-bound open acetylcholine receptors respectively, and k_R, k_{-R}, k_{AR}, k_{-AR}, k_{close}, k_{open} are the forward and backward reaction constants for R, AR, A_2R, A_2R^{open}, respectively. These reactions involve free acetylcholine and the immobilized four receptor species, all of which are imbedded on the surface of the post-synaptic membrane [2]-[5], [68].

The NMJ is considered to be a three-dimensional molecular transport-reaction system, in which its geometry is the space between two circular planes of equal area. The volume is bounded at the top by the pre-synaptic membrane and at the bottom by the post synaptic membrane, and open to the external environment at the edge, as shown in Figure 3.2
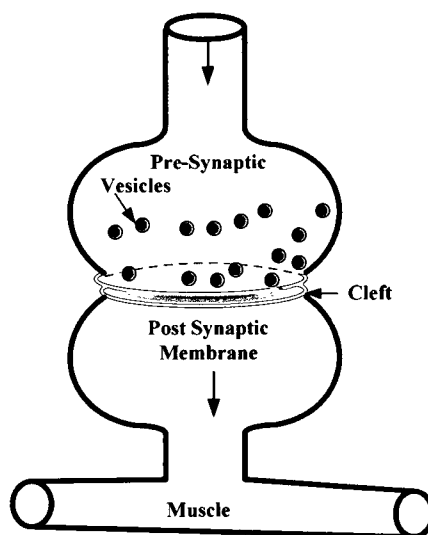
Figure 3.2 Schematic diagram of the neuromuscular junction.

To develop a 3D model, we first position the cylindrical coordinates into the considered volume as shown in Figures 3.3 and 3.4, together which illustrate how the cylindrical coordinates are superimposed over the chosen geometry and related terms. Table 3.1 shows the magnitude of geometric dimensions, reaction rate constants, diffusion coefficients, and other parameters.

(a)   (b)
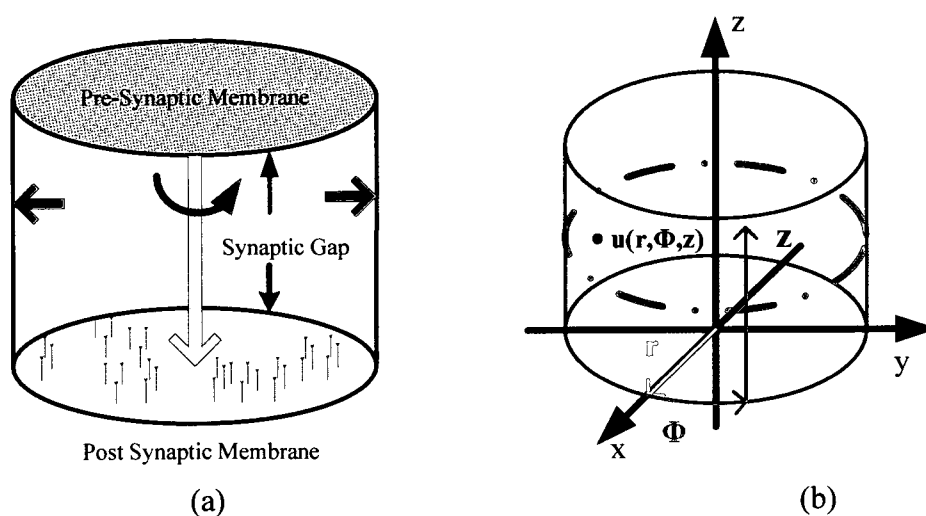
Figure 3.3 (a) Schematic diagram of the neuromuscular junction synaptic gap and (b) cylindrical coordinate system.
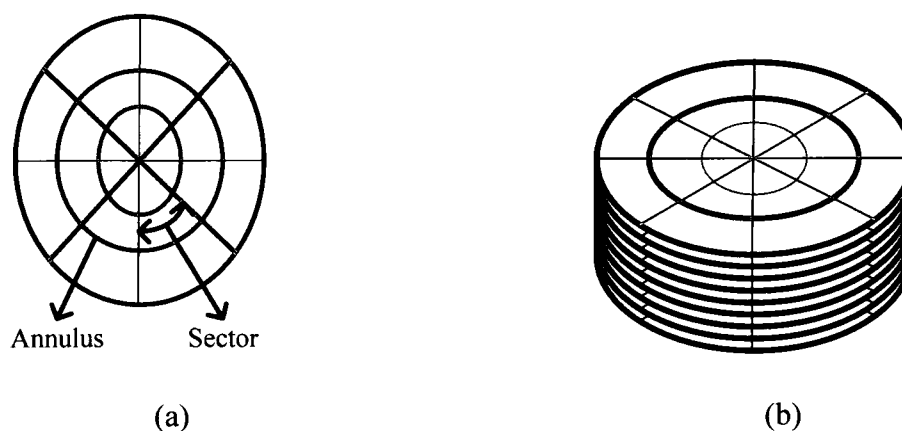
Figure 3.4 (a) Annulus, sector and disk modeled in a cylindrical coordinate system; (b) The arrangement of the annuli, sectors, and disks as modeled in the synaptic gap.

Table 3.1 Magnitude of geometric dimensions, reaction rate constants, diffusion coefficients, and other parameters as used in the model [64]-[69]

Name	Value (units)	Units/Constant
k_R	3.0×10^7 $M^{-1}S^{-1}$	3.0×10^7 $M^{-1}S^{-1}$
k_{-R}	1.0×10^4 S^{-1}	1.0×10^4 S^{-1}
k_{AR}	3.0×10^7 $M^{-1}S^{-1}$	3.0×10^7 $M^{-1}S^{-1}$
k_{-AR}	1.0×10^4 S^{-1}	1.0×10^4 S^{-1}
k_{open}	2.0×10^4 $M^{-1}S^{-1}$	2.0×10^4 $M^{-1}S^{-1}$
k_{close}	0.7×10^3 S^{-1}	0.75×10^3 S^{-1}
D_r	0.7×10^{-6} cm^{-2}/s	2.0×10^{-6} cm^{-2}/s
D_ϕ	0.7×10^{-6} cm^{-2}/s	2.0×10^{-6} cm^{-2}/s
D_z	0.7×10^{-6} cm^{-2}/s	2.0×10^{-6} cm^{-2}/s
r_{max}	5.0×10^{-5} cm	5.0×10^{-5} cm=0.5um
L	5.0×10^{-6} cm	5.0×10^{-6} cm=0.05 um
V_R	1.5611×10^{-15} cm^3	0.75×10^3 S^{-1}
N_{AV}	6.022×10^{23} mol^{-1}	

The reaction rates of the chemical equations given above can be expressed by the following Equations (3.7) through (3.10) :

$$\frac{\partial(R)}{\partial t} = -2k_R(A)(R) + k_{-R}(AR),$$

(3.7)

$$\frac{\partial(AR)}{\partial t} = 2k_R(A)(R) - k_{-R}(AR) - k_{AR}(A)(AR) + 2k_{-AR}(A_2R),$$

(3.8)

$$\frac{\partial(A_2R)}{\partial t} = k_{AR}(A)(AR) - 2k_{-AR}(A_2R) - k_{open}(A_2R) + k_{close}(A_2R^{open}),$$

(3.9)

$$\frac{\partial((A_2R^{open})}{\partial t} = k_{open}(A_2R) - k_{close}(A_2R^{open}).$$

(3.10)

The acetylcholine is transported across the cleft and reacts with the receptors located on the postsynaptic membrane. The reaction rate for diffusing acetylcholine must be written as a diffusion-reaction equation in cylindrical coordinates:

$$\frac{\partial(A)}{\partial t} = \frac{D_r}{r}\frac{\partial}{\partial r}\left(r\frac{\partial(A)}{\partial r}\right) + \frac{D_\phi}{r^2}\frac{\partial^2(A)}{\partial \phi^2} + D_z\frac{\partial^2(A)}{\partial z^2} - 2k_R(A)(R) + k_{-R}(AR)$$

$$-k_{AR}(A)(AR) + 2k_{-AR}(A_2R) ,$$

(3.11)

where D_r, D_ϕ, D_ϕ , are diffusion coefficients along radial, angular and transverse direction, and $0 < r < r_{max}, 0 < z < L, 0 < \phi < 2\pi$. Here, r_{max} and L are radius and length of the cleft, respectively.

The boundary conditions for A are assumed to be:

$$\frac{\partial(A)\ (r,\phi,0,t)}{\partial z} = 0\ , \qquad \frac{\partial(A)\ (r,\phi,L,t)}{\partial z} = 0\ ,$$

(3.12)

$$(A)(r,\phi + 2\pi, z, t) = A(r,\phi,z,t),$$

(3.13)

$$(A)(0,\phi,z,t) = A_0\ (r_{max},\phi,z,t) = 0.$$

(3.14)

The initial conditions for $(A),(R),(AR),(A_2R),(A_2R^{open})$ are assumed to be:

$$(A)(r,\phi,z,0) = (A)_0\ ,(R)(r,\phi,z,0) = (R)_0,$$

(3.15)

$$(AR)(r,\phi,z,0) = (A_2R)(r,\phi,z,0) = (A_2R^{open})(r,\phi,z,0) = 0.$$

(3.16)

Here, A_0 is given by Equation (4.49), $(A)_0 = 1.4 \times 10^{14}$ and $(R)_0 = 15,700$ ([2], [64]-[69]).

The above 3D model includes several nonlinear terms, which make it very difficult to find an analytic solution. Therefore, it is indispensable to develop a numerical method for solving the above 3D model.

CHAPTER 4

NUMERICAL METHOD

In this chapter, we will develop finite difference schemes for solving 1D mass diffusion model and 3D reaction-diffusion model proposed in Chapter 3.

4.1 Finite Difference Scheme for 1D Mass Diffusion Model

To obtain a second-order accurate finite difference scheme for solving the 1D mass diffusion model, we first design a mesh, where the distance between the actual left boundary and r_1 is assumed to be $\theta_1 \Delta r$, and the distance between the actual right boundary and r_M is $\theta_2 \Delta r$, as shown in Figure 4.1.
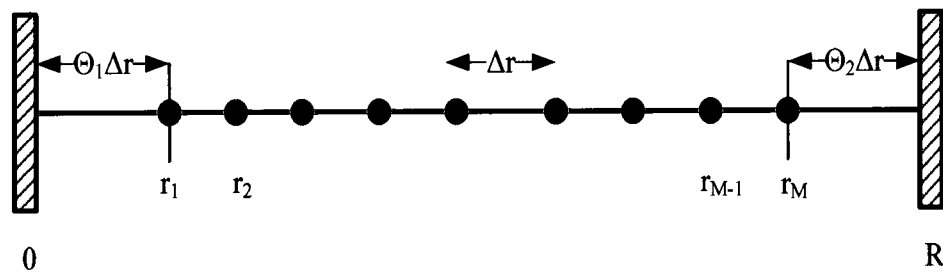
Figure 4.1: Grid points and nomenclature for the present numerical scheme.

We assume that the number of interior grid points is M. As such, the grid size and the coordinates of the grid points can be determined as follows:

$$\Delta r = \frac{R}{N + \theta - 1}, \tag{4.1}$$

$$r_i = (i - 1 + \theta_1)\Delta r, \qquad i = 1, \dots, M. \tag{4.2}$$

We denote A_i^n to be the approximation of $A(r_i, t_n)$, where $t_n = n\Delta t$ and Δt is the time increment. At the interior points r_i ($2 \leq i \leq M - 1$), we employ a weighted Crank-Nicolson scheme for the diffusion equation as follows:

$$\frac{A_i^{n+1} - A_i^n}{\Delta t} = (1 + \omega)\frac{1}{2r_i\Delta r}\left[r_{i+\frac{1}{2}}\frac{A_{i+1}^{n+1} - A_i^{n+1}}{\Delta r} - r_{i-\frac{1}{2}}\frac{A_i^{n+1} - A_{i-1}^{n+1}}{\Delta r}\right]$$

$$+ (1 - \omega)\frac{1}{2r_i\Delta r}\left[r_{i+\frac{1}{2}}\frac{A_{i+1}^n - A_i^n}{\Delta r} - r_{i-\frac{1}{2}}\frac{A_i^n - A_{i-1}^n}{\Delta r}\right] + S_i^{n+\frac{1}{2}} \tag{4.3}$$

where ω is a relaxation factor with $0 \leq \omega \leq 1$. Note that the insulated boundary consider is usually discretized using the first order finite difference approximation or the second order approximation with a ghost point. However, the ghost point method cannot be applied to multi-dimensional case such as $\frac{\partial A(r,\phi,t)}{\partial t} = \frac{D_A}{r}\frac{\partial}{\partial r}\left(r\frac{\partial A(r,\phi,t)}{\partial r}\right) + \frac{D_\phi}{r^2}\frac{\partial^2(A)}{\partial \phi^2}$ where

$0 < r < R, 0 \leq \phi \leq 2\pi$. Because $\lim_{r\to 0}\left[\frac{1}{r^2}\frac{\partial^2(A)}{\partial \phi^2}\right]$ is difficult to find. In this dissertation, we propose a novel numerical approximation dealing with the insulated boundary condition.

To this end, first, we express the finite difference approximation for $\frac{\partial}{\partial r}\left(r\frac{\partial A}{\partial r}\right)$ at r_1, which is the point next to the left boundary, as follows:

$$b\frac{\partial}{\partial r}\left(r\frac{\partial A(r,t)}{\partial r}\right)_1 = \frac{a}{\Delta r^2}r_{\frac{3}{2}}[A(r_2,t) - A(r_1,t)] - \frac{1}{\Delta r}r_1\frac{\partial A}{\partial r}(r_1 - \theta_1\Delta r, t), \tag{4.4}$$

where a, b, θ_1 are constants to be determined and $r_{\frac{3}{2}} = r_1 + \frac{\Delta r}{2}$. It should be pointed out that

Equation (4.4) is an improvement of the combined compact finite difference methods [81]-[83], by introducing the parameter θ_1 in order to increase the order of accuracy. If each term of Equation (4.4) is expanded into Taylor series at r_1, we will obtain the left-hand-side (LHS) and right-hand-side (RHS) results of Equation (4.4) as follows:

$$LHS = br_1 A_{rr}(r_1, t) + bA_r(r_1, t), \tag{4.5}$$

$$RHS = \frac{a}{\Delta r^2} r_{\frac{3}{2}} \left[\Delta r A_r(r_1, t) + \frac{\Delta r^2}{2} A_{rr}(r_1, t) + \frac{\Delta r^3}{6} A_{r^3}(r_1, t) \right]$$

$$- \frac{1}{\Delta r} r_1 \left[A_r(r_1, t) - \theta_1 \Delta r A_{rr}(r_1, t) + \frac{\theta_1^2 \Delta r^2}{2} A_{r^3}(r_1, t) \right] + O(\Delta r^2)$$

$$= \frac{1}{\Delta r} r_1 \left[a r_{\frac{3}{2}} - r_1 \right] A_r(r_1, t) + \left[\frac{a}{2} r_{\frac{3}{2}} + r_1 \theta_1 \right] A_{rr}(r_1, t)$$

$$+ \frac{\Delta r}{2} \left[\frac{a}{3} r_{\frac{3}{2}} - r_1 \theta_1^2 \right] A_{r^3}(r_1, t) + O(\Delta r^2). \tag{4.6}$$

Matching both sides give:

$$\left[a r_{\frac{3}{2}} - r_1 \right] = b, \tag{4.7}$$

$$\left[\frac{a}{2} r_{\frac{3}{2}} + r_1 r_1 \right] = br_1, \tag{4.8}$$

$$\left[\frac{a}{3} r_{\frac{3}{2}} - r_1 \theta_1^2 \right] = 0. \tag{4.9}$$

Dividing Equation (4.7) by Equation (4.8), replacing $a r_{\frac{3}{2}}$ by $r_1 \theta_1^2$ from Equation (4.9) and then using the fact that $r_1 = \theta_1 \Delta r$, we obtain a quadratic equation with respect to θ_1 as:

$$\theta_1^2 - 3\theta_1 - 4 = 0. \tag{4.10}$$

Solving the above equation for θ_1 with $\theta_1 \geq 0$, one may obtain:

$$\theta_1 = \frac{3 + \sqrt{105}}{12}, \tag{4.11}$$

$$a = r_1\,\theta_1, \qquad b = r_{\frac{3}{2}}\left(\frac{\theta_1}{2}+\frac{1}{3}\right), \qquad \frac{a}{b} = \frac{r_1\,\theta_1}{r_{\frac{3}{2}}\left(\frac{\theta_1}{2}+\frac{1}{3}\right)}. \tag{4.12}$$

Thus, a second-order finite difference approximation at r_1 can be obtained by dropping the truncation error $O(\Delta r^2)$:

$$\frac{\partial}{\partial r}\left(r\frac{\partial A(r,t)}{\partial r}\right)_1 \cong \frac{a}{b\,\Delta r^2}\,r_{\frac{3}{2}}\,[A(r_2,t)-A(r_1,t)] - \frac{1}{b\,\Delta r}\,r_1\,\frac{\partial A}{\partial r}(r_1-\theta_1\,\Delta r,t). \tag{4.13}$$

Symmetrically, we can express the finite difference approximation of $\frac{\partial}{\partial r}\left(r\frac{\partial A}{\partial r}\right)$ at r_M, which is the point next to the right boundary, as:

$$b^*\frac{\partial}{\partial r}\left(r\frac{\partial A(r,t)}{\partial r}\right)_M = \frac{1}{\Delta r}\,r_M\,\frac{\partial A}{\partial r}(r_M+\theta_2\,\Delta r,t)$$

$$-\frac{a^*}{\Delta r^2}\,r_{M-\frac{1}{2}}\,[A(r_M,t)-A(r_{M-1},t)], \tag{4.14}$$

where a^*, b^*, θ_2 are constants to be determined and $r_{M-1} = r_M - \Delta r$. Again, matching both sides in Taylor series gives:

$$\frac{1}{\Delta r}\left(r_M - a^*r_{M-\frac{1}{2}}\right) = b^*, \tag{4.15}$$

$$r_M\theta_2 + \frac{a^*}{2}\,r_{M-\frac{1}{2}} = b^*\,r_M, \tag{4.16}$$

$$r_M(\theta_2)^2 - \frac{a^*}{3}\,r_{M-\frac{1}{2}} = 0. \tag{4.17}$$

Dividing Equation (4.15) by Equation (4.16) and then replacing $a^*r_{M-\frac{1}{2}}$ by $3r_M(\theta_2)^2$ from Equation (4.17), we obtain a quadratic equation with respect to θ_2 as:

$$(6r_M + 3\,\Delta r)\theta_2^2 + 2\Delta r\theta_2 - 2r_M = 0 \tag{4.18}$$

Substituting $r_M = (M-1+\theta_1)\,\Delta r$ from Equation (4.2) into Equation (4.18) and then solving for θ_2 with $\theta_2 \geq 0$, one may obtain:

$$\theta_2 = \frac{\sqrt{1 + 6(2\theta_1 + 2M - 1)(\theta_1 + M - 1)} - 1}{3(2\theta_1 + 2M - 1)},$$ (4.19)

and hence,

$$\frac{a^*}{b^*} = \frac{r_M\,\theta_2}{r_{M-\frac{1}{2}}(\frac{\theta_2}{2} + \frac{1}{3})}.$$ (4.20)

As such a second-order finite difference approximation at r_M can be obtained:

$$\frac{\partial}{\partial r}\left(r\frac{\partial A(r,t)}{\partial r}\right)_M \cong \frac{1}{b^*\,\Delta r}\,r_M\,\frac{\partial A}{\partial r}(r_M - \theta_2\,\Delta r, t),$$

$$-\frac{a^*}{b^*\,\Delta r^2}\,r_{M-\frac{1}{2}}\,[A(r_M, t) - A(r_{M-1}, t)].$$ (4.21)

Using the Neumann boundary condition, Equation (3.3), one may simplify Equations (4.13) and (4.21) to

$$\frac{\partial}{\partial r}\left(r\frac{\partial A(r,t)}{\partial r}\right)_1 \cong \frac{a}{b\,\Delta r^2}\,r_{\frac{3}{2}}\,[A(r_2, t) - A(r_1, t)],$$ (4.22)

$$\frac{\partial}{\partial r}\left(r\frac{\partial A(r,t)}{\partial r}\right)_M \cong -\frac{a^*}{b^*\,\Delta r^2}\,r_{M-\frac{1}{2}}\,[A(r_M, t) - A(r_{M-1}, t)].$$ (4.23)

Thus, we develop a weighted Crank- Nicolson scheme for the diffusion equation at r_1 and r_M together with Equation (4.3) can be written as follows:

$$\frac{A_1^{n+1} - A_1^n}{\Delta t} = (1 + \omega)\frac{aD_A}{b\,r_1}\,r_{\frac{3}{2}}\,\frac{A_2^{n+1} - A_1^{n+1}}{2\Delta r^2}$$

$$+ (1 - \omega)\frac{aD_A}{b\,r_1}\,r_{\frac{3}{2}}\frac{A_2^n - A_1^n}{2\Delta r^2} + S_i^{n+\frac{1}{2}},$$ (4.24)

$$\frac{A_i^{n+1} - A_i^n}{\Delta t} = (1 + \omega)\frac{D_A}{2r_i\,\Delta r}\left[r_{i+\frac{1}{2}}\frac{A_{i+1}^{n+1} - A_i^{n+1}}{\Delta r} - r_{i-\frac{1}{2}}\frac{A_i^{n+1} - A_{i-1}^{n+1}}{\Delta r}\right]$$

$$+ (1 - \omega)\frac{D_A}{2r_i\,\Delta r}\left[r_{i+\frac{1}{2}}\frac{A_{i+1}^n - A_i^n}{\Delta r} - r_{i-\frac{1}{2}}\frac{A_i^n - A_{i-1}^n}{\Delta r}\right] + S_i^{n+\frac{1}{2}},$$ (4.25)

$$\frac{A_M^{n+1} - A_M^n}{\Delta t} = -(1 + \omega)\frac{a^*D_A}{b^* \, r_1} \, r_{M-\frac{1}{2}} \, \frac{A_M^{n+1} - A_{M-1}^{n+1}}{2\Delta r^2}$$

$$- (1 - \omega)\frac{a^*D_A}{b^* \, r_M} \, r_{M-\frac{1}{2}} \frac{A_M^n - A_{M-1}^n}{2\Delta r^2} + S_i^{n+\frac{1}{2}}, \tag{4.26}$$

where ω is a parameter with $0 \le \omega \le 1$. It can be seen that the truncation error of the new

scheme when $\omega = 0$ (which is a Crank-Nicolson type of scheme) has an order of Δt^2

$+ \Delta r^2$ at all grid points $(r_i, t_{n+\frac{1}{2}})$, $j = 1, \cdots$, M. It should be pointed out that if the present

scheme is written in matrix form, one may see that the system for obtaining

$\{A_i^{n+1}\}_{i=1,\ldots,M}$ is a tridiagonal linear system,

$$\begin{bmatrix} b_1 & c_1 & 0 & \cdots & \cdots & 0 \\ a_2 & b_2 & c_2 & 0 & \cdots & 0 \\ 0 & a_3 & b_3 & c_3 & \cdots & 0 \\ \vdots & \vdots & \ddots & \ddots & \ddots & \vdots \\ 0 & \cdots & 0 & a_{M-1} & b_{M-1} & c_{M-1} \\ 0 & \cdots & \cdots & 0 & a_M & b_M \end{bmatrix} \begin{bmatrix} A_1^{n+1} \\ A_2^{n+1} \\ A_3^{n+1} \\ \vdots \\ A_{M-1}^{n+1} \\ A_M^{n+1} \end{bmatrix} = \begin{bmatrix} d_1^{n+1} \\ d_2^{n+1} \\ d_3^{n+1} \\ \vdots \\ d_{M-1}^{n+1} \\ d_M^{n+1} \end{bmatrix}$$

which can be easily solved by the Thomas algorithm [62].

4.2 Finite Difference Scheme for 3D Mass Diffusion – Reaction Model

To develop an accurate finite difference scheme for the above problem, we first

designed a mesh, where the grids along the radial (r), angular (ϕ), and transverse (z)

directions are shown in Figure 4.2. In particular, the distance between the actual left

boundary (z = 0) and (z = 1) is assumed to be $\theta_1\Delta z$, and the distance between the actual

right boundary (z = L) and (z = k) is assumed to be $\theta_2\Delta z$, as shown in Figure 4.2 (c), in

order to develop an accurate finite difference scheme incorporating with the Neumann

boundary condition along the z-direction.

(a)

(b)

(c)
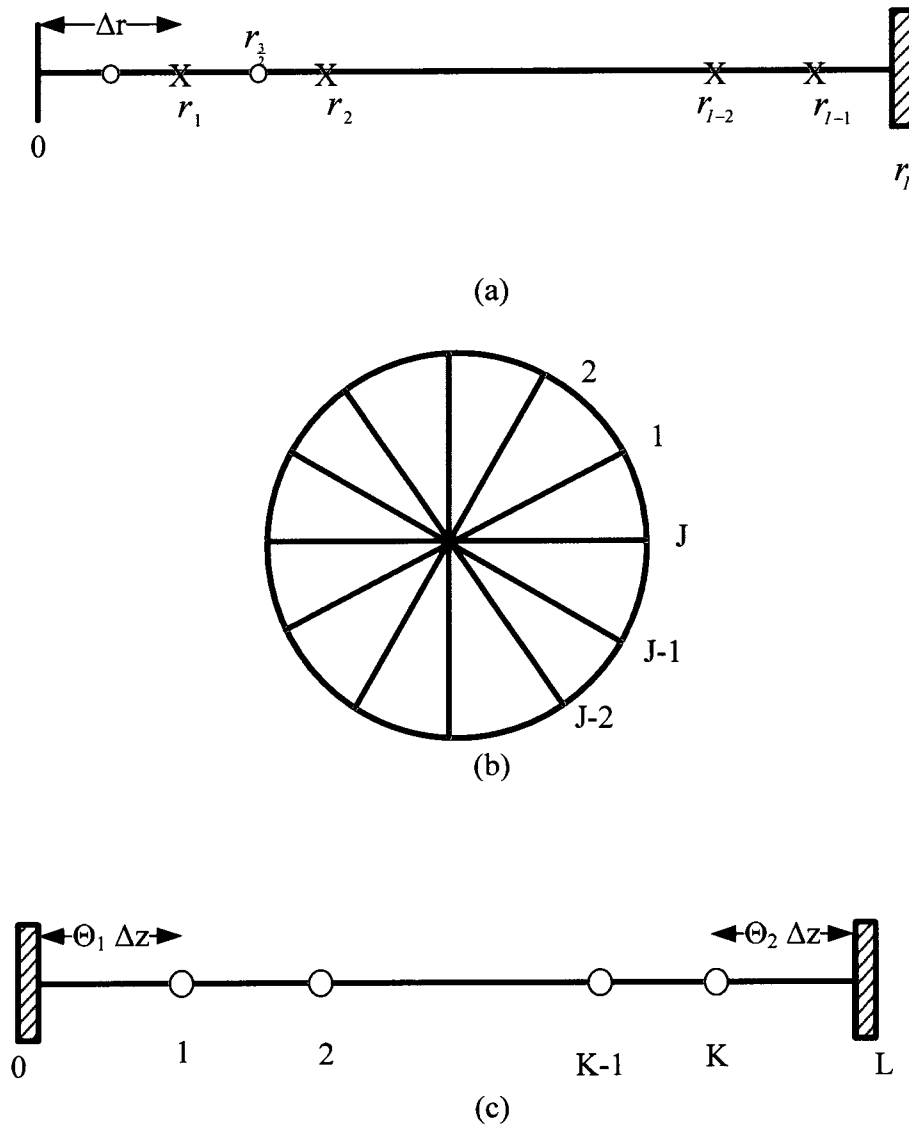
Figure 4.2 (a) Grid points along r-direction; (b) Grid points along φ-direction for the numerical scheme; (c) Grid points along z-direction for the numerical scheme.

We denote $r_i = i\Delta r, \phi_j = j\Delta\phi, z_k = (j - 1 + \theta_1)\Delta z$, where $\Delta r = \frac{R}{I}, \Delta\phi =$

$\frac{2\pi}{J}$ and $\Delta z = \frac{K}{K+\theta_1+\theta_2-1}$ are grid sizes along the r, φ, and z-direction, respectively; and

$1 \leq i \leq I$, $1 \leq j \leq J$, $1 \leq k \leq K$. Here, we obtain $\theta_1 = \theta_2 = \frac{\sqrt{3}}{3}$, as seen in the

derivation later. We denote $A_{i,j,k}^n$ is the approximation of $A(i\Delta r, j\Delta\phi, k\Delta z, n\Delta t)$, where n

is time level and Δt is time increment. Similar notations are used for A, R, AR, A_2R, A_2R^{open}.

We employ a standard fourth-order Runge-Kutta (RK) method to solve Equations (3.7) through (3.10). For simplicity, species (R) is presented as follows:

$$R_{i,j,k}^{n+1} = R_{i,j,k}^n + \frac{1}{6.0}(rk1 + 2rk2 + 2rk3 + rk4), \tag{4.27}$$

where coefficients for the Runge-Kutta method $(rk1, rk2, rk3, rk4)$ are determined as:

$$rk1 = \Delta t \left(-2k_R \left(\frac{A_{i,j,k}^{n+1} + A_{i,j,k}^n}{2} \right) \left(R_{i,j,k}^n \right) + k_{-R} AR_{i,j,k}^n \right), \tag{4.28}$$

$$rk2 = \Delta t \left(-2k_R \left(\frac{A_{i,j,k}^{n+1} + A_{i,j,k}^n}{2} \right) \left(R_{i,j,k}^n + rk1/2.0 \right) - k_{-R} \left(AR_{i,j,k}^n + \frac{rk1}{2.0} \right) \right), \tag{4.29}$$

$$rk3 = \Delta t \left(-2k_R \left(\frac{A_{i,j,k}^{n+1} + A_{i,j,k}^n}{2} \right) \left(R_{i,j,k}^n + rk2R/2.0 \right) - k_{-R} \left(AR_{i,j,k}^n + \frac{rk2}{2.0} \right) \right), \tag{4.30}$$

$$rk4 = \Delta t \left(-2k_R \left(\frac{A_{i,j,k}^{n+1} + A_{i,j,k}^n}{2} \right) \left(R_{i,j,k}^n + rk3 \right) + k_{-R} \left(AR_{i,j,k}^n + rk3 \right) \right), \tag{4.31}$$

where $1 \le i \le I - 1$, $1 \le j \le J - 1$, $1 \le k \le K$. Similarly, values for species R, AR, A_2R, A_2R^{open} are computed.

To solve Equation (3.11), we employ a Crank- Nicolson finite difference scheme at interior points, k=2 ,...,K-1, as follows:

$$\frac{A_{i,j,k}^{n+1} - A_{i,j,k}^n}{\Delta t} = \frac{D_r}{2r_i \Delta r} \left[r_{i+\frac{1}{2}} \frac{A_{i+1,j,k}^{n+1} - A_{i,j,k}^{n+1}}{\Delta r} - r_{i-\frac{1}{2}} \frac{A_{i,j,k}^{n+1} - A_{i-1,j,k}^{n+1}}{\Delta r} \right]$$

$$+ \frac{D_r}{2r_i \Delta r} \left[r_{i+\frac{1}{2}} \frac{A_{i+1,j,k}^n - A_{i,j,k}^n}{\Delta r} - r_{i-\frac{1}{2}} \frac{A_{i,j,k}^n - A_{i-1,j,k}^n}{\Delta r} \right]$$

$$+ \frac{D_\phi}{2 r_i^2} \left[\frac{A_{i,j+1,k}^{n+1} - 2A_{i,j,k}^{n+1} + A_{i,j-1,k}^{n+1}}{\Delta\phi^2} + \frac{A_{i,j+1,k}^n - 2A_{i,j,k}^n + A_{i,j-1,k}^n}{\Delta\phi^2} \right]$$

$$+ \frac{D_z}{2} \left[\frac{A_{i,j,k+1}^{n+1} - 2A_{i,j,k}^{n+1} + A_{i,j,k-1}^{n+1}}{\Delta z^2} + \frac{A_{i,j,k+1}^n - 2A_{i,j,k}^n + A_{i,j,k-1}^n}{\Delta z^2} \right]$$

$$-2k_R \left(\frac{A_{i,j,k}^{n+1} + A_{i,j,k}^n}{2}\right)\left(\frac{R_{i,j,k}^{n+1} + R_{i,j,k}^n}{2}\right) + k_{-R}\frac{AR_{i,j,k}^{n+1} + AR_{i,j,k}^n}{2}$$

$$-k_{AR}\left(\frac{A_{i,j,k}^{n+1} + A_{i,j,k}^n}{2}\right)\left(\frac{A_2 R_{i,j,k}^{n+1} + A_2 R_{i,j,k}^n}{2}\right)$$

$$+ 2k_{-AR}\frac{(A_2 R^{open})_{i,j,k}^{n+1} + (A_2 R^{open})_{i,j,k}^n}{2}. \tag{4.32}$$

To obtain a new finite difference scheme for the Neumann boundary condition, Equation (3.12), we first design a mesh, where the distance between the actual left boundary and z_1 is assumed to be $\theta_1 \Delta z$, and the distance between the actual right boundary and z_K is $\theta_2 \Delta z$, as shown in Figure 4.2 (c). For simplicity, we denote $(A)(r, \phi, z, t)$ and Δz as $A(z, t)$, and h, respectively, and then express the finite difference approximation of $\frac{\partial^2 A(z,t)}{\partial z^2}$ at z_1, which is the grid point next to the left boundary, as follows:

$$b\frac{\partial^2 A(z_1, t)}{\partial z^2} = \frac{a}{h^2}[A(z_2, t) - A(z_1, t)] - \frac{1}{h}\frac{\partial A(z_1 - \theta_1 h, t)}{\partial z}, \tag{4.33}$$

where a, b, θ_1 are are constants to be determined. If Equation (4.33) is rewritten as follows:

$$b\frac{\partial^2 A(z_1, t)}{\partial z^2} + \frac{1}{h}\frac{\partial A(z_1 - \theta_1 h, t)}{\partial z} = \frac{a}{h^2}[A(z_2, t) - A(z_1, t)], \tag{4.34}$$

we may see that the above equation is an improvement of the combined compact finite difference method (where the first and second-order derivatives are included [76]-[78]) by introducing the parameter θ_1 in order to raise the order of accuracy. The first-order derivative is kept in Equation (4.33) so that the Neumann boundary condition can be applied directly without discretizing. Expanding each term of Equation (4.33) into Taylor series at z_1, we obtain the right-hand-side (RHS) result of Equation (4.33) as follows:

$$RHS = \frac{a}{h^2} \left[hA_z(z_1,t) + \frac{h^2}{2} A_{zz}(z_1,t) + \frac{h^3}{6} A_{z^3}(z_1,t) \right]$$

$$- \frac{1}{h} \left[A_z(z_1,t) - \theta_1 h A_{zz}(z_1,t) + \frac{\theta_1^2 h^2}{2} A_{z^3}(z_1,t) \right] + O(h^2)$$

$$= \frac{1}{h} [a-1] A_z(z_1,t) + \left[\frac{a}{2} + \theta_1 \right] A_{zz}(z_1,t) + \frac{h}{2} \left[\frac{a}{3} - \theta_1^2 \right] A_{z^3}(z_1,t)$$

$$+ O(h^2) \tag{4.35}$$

Matching both sides gives:

$$a = 1, \qquad b = \frac{1}{2} + \frac{\sqrt{3}}{3}, \qquad \theta_1 = \frac{\sqrt{3}}{3} \tag{4.36}$$

Thus, substituting the values of a, b, θ_1 in Equation (4.36) into Equation (4.33) and dropping the truncation error $O(h^2)$, we obtain a second-order finite difference approximation at z_1 as

$$\frac{\partial^2 A(z_1,t)}{\partial z^2} \approx \frac{a}{bh^2} [A(z_2,t) - A(z_1,t)] - \frac{1}{bh} \frac{\partial A(z_1 - \theta_1 h, t)}{\partial z} \tag{4.37}$$

Symmetrically, we can express the finite difference approximation of $\frac{\partial^2 A(z,t)}{\partial z^2}$ at z_K, which is the grid point next to the right boundary, as

$$b^* \frac{\partial^2 A(z_K,t)}{\partial z^2} = \frac{1}{h} \frac{\partial A(z_K + \theta_2 h, t)}{\partial z} - \frac{a^*}{h^2} [A(z_K,t) - A(z_{K-1},t)] \tag{4.38}$$

where a^*, b^*, θ_2 are are constants to be determined. Again, matching both sides in Taylor series gives

$$a^* = 1, \qquad b^* = \frac{1}{2} + \frac{\sqrt{3}}{3}, \qquad \theta_2 = \frac{\sqrt{3}}{3} \tag{4.39}$$

and hence a second-order finite difference approximation at z_K for the right boundary can be obtained as

$$\frac{\partial^2 A(z_K, t)}{\partial z^2} \approx \frac{1}{b^* h} \frac{\partial A(z_K + \theta_2 h, t)}{\partial z} - \frac{a^*}{b^* h^2} [A(z_K, t) - A(z_{K-1}, t)] \qquad (4.40)$$

If the number of interior grid points K is given, then the grid size and the coordinates of the grid points can be determined as follows:

$$h = \frac{L}{K + \theta_1 + \theta_2 - 1}, \qquad z_k = (k - 1 + \theta_1)h, \qquad k = 1, \dots, K. \qquad (4.41)$$

Using the Neumann boundary condition, Equation (3.12), one may simplify Equations (4.37) and (4.40) to

$$\frac{\partial^2 A(z_1, t)}{\partial z^2} \approx \frac{a}{bh^2} [A(z_2, t) - A(z_1, t)], \qquad (4.42)$$

$$\frac{\partial^2 A(z_K, t)}{\partial z^2} \approx -\frac{a^*}{b^* h^2} [A(z_K, t) - A(z_{K-1}, t)]. \qquad (4.43)$$

Thus for the location z_1, we apply the second-order finite difference approximation obtained in the above for $\frac{\partial^2 (A)}{\partial z^2}$ to Equation (3.12) and obtain a finite difference scheme as follows:

$$\frac{A_{i,j,1}^{n+1} - A_{i,j,1}^{n}}{\Delta t} = \frac{D_r}{2r_i \Delta r} \left[r_{i+\frac{1}{2}} \frac{A_{i+1,j,1}^{n+1} - A_{i,j,1}^{n+1}}{\Delta r} - r_{i-\frac{1}{2}} \frac{A_{i,j,1}^{n+1} - A_{i-1,j,1}^{n+1}}{\Delta r} \right]$$

$$+ \frac{D_r}{2r_i \Delta r} \left[r_{i+\frac{1}{2}} \frac{A_{i+1,j,1}^{n} - A_{i,j,1}^{n}}{\Delta r} - r_{i-\frac{1}{2}} \frac{A_{i,j,k}^{n} - A_{i-1,j,1}^{n}}{\Delta r} \right]$$

$$+ \frac{D_\phi}{2 r_i^2} \left[\frac{A_{i,j+1,1}^{n+1} - 2A_{i,j,1}^{n+1} + A_{i,j-1,1}^{n+1}}{\Delta \phi^2} + \frac{A_{i,j+1,1}^{n} - 2A_{i,j,1}^{n} + A_{i,j-1,1}^{n}}{\Delta \phi^2} \right]$$

$$+ \frac{D_z}{2} \frac{a}{b} \left[\frac{A_{i,j,2}^{n+1} - A_{i,j,2}^{n+1}}{\Delta z^2} + \frac{A_{i,j,2}^{n} - A_{i,j,1}^{n}}{\Delta z^2} \right]$$

$$- 2k_R \left(\frac{A_{i,j,1}^{n+1} + A_{i,j,1}^{n}}{2} \right) \left(\frac{R_{i,j,1}^{n+1} + R_{i,j,1}^{n}}{2} \right) + k_{-R} \frac{AR_{i,j,1}^{n+1} + AR_{i,j,1}^{n}}{2}$$

$$-k_{AR}\left(\frac{A_{i,j,1}^{n+1}+A_{i,j,1}^{n}}{2}\right)\left(\frac{A_2R_{i,j,1}^{n+1}+A_2R_{i,j,1}^{n}}{2}\right)$$

$$+2k_{-AR}\frac{(A_2R^{open})_{i,j,1}^{n+1}+(A_2R^{open})_{i,j,1}^{n}}{2}, \tag{4.44}$$

where $a=1$, $b=\frac{1}{2}+\frac{\sqrt{3}}{3}$ and $1\le i \le I-1$, $0\le j \le J-1$.

Similarly, for the location z_K, we apply the second-order finite difference approximation obtained in the above for $\frac{\partial^2 (A)}{\partial z^2}$ to Equation (3.11) and obtain a finite difference scheme as follows:

$$\frac{A_{i,j,K}^{n+1}-A_{i,j,K}^{n}}{\Delta t}=\frac{D_r}{2r_i\Delta r}\left[r_{i+\frac{1}{2}}\frac{A_{i+1,j,K}^{n+1}-A_{i,j,K}^{n+1}}{\Delta r}-r_{i-\frac{1}{2}}\frac{A_{i,j,K}^{n+1}-A_{i-1,j,K}^{n+1}}{\Delta r}\right]$$

$$+\frac{D_r}{2r_i\Delta r}\left[r_{i+\frac{1}{2}}\frac{A_{i+1,j,K}^{n}-A_{i,j,K}^{n}}{\Delta r}-r_{i-\frac{1}{2}}\frac{A_{i,j,k}^{n}-A_{i-1,j,K}^{n}}{\Delta r}\right]$$

$$+\frac{D_\phi}{2\,r_i^2}\left[\frac{A_{i,j+1,K}^{n+1}-2A_{i,j,K}^{n+1}+A_{i,j-1,K}^{n+1}}{\Delta\phi^2}+\frac{A_{i,j+1,K}^{n}-2A_{i,j,K}^{n}+A_{i,j-1,K}^{n}}{\Delta\phi^2}\right]$$

$$+\frac{D_z}{2}\frac{a^*}{b^*}\left[\frac{A_{i,j,K}^{n+1}-A_{i,j,K-1}^{n+1}}{\Delta z^2}+\frac{A_{i,j,K}^{n}-A_{i,j,K-1}^{n}}{\Delta z^2}\right]$$

$$-2k_R\left(\frac{A_{i,j,K}^{n+1}+A_{i,j,K}^{n}}{2}\right)\left(\frac{R_{i,j,K}^{n+1}+R_{i,j,K}^{n}}{2}\right)+k_{-R}\frac{AR_{i,j,K}^{n+1}+AR_{i,j,K}^{n}}{2}$$

$$-k_{AR}\left(\frac{A_{i,j,K}^{n+1}+A_{i,j,K}^{n}}{2}\right)\left(\frac{A_2R_{i,j,K}^{n+1}+A_2R_{i,j,K}^{n}}{2}\right)$$

$$+2k_{-AR}\frac{(A_2R^{open})_{i,j,K}^{n+1}+(A_2R^{open})_{i,j,K}^{n}}{2}, \tag{4.45}$$

where $a^*=1$, $b^*=\frac{1}{2}+\frac{\sqrt{3}}{3}$ and $1\le i \le I-1$, $0\le j \le J-1$.

Initial conditions are discretized as

$$A_{i,j,k}^{0}=(A_0)_{i,j,k}\;,\;R_{i,j,k}^{0}=(R_0)_{i,j,k}\,, \tag{4.46}$$

$$AR^0_{i,j,k} = \left(A_2 R^0_{i,j,k}\right)_{i,j,k} = (A_2 R^{opoen})^0_{i,j,k} = 0 \ , \tag{4.47}$$

where $1 \le i \ \le I - 1 , 1 \le j \ \le J - 1, 1 \le k \ \le K$. The discrete boundary condition for $A^n_{i,j,K}$ is

$$A^n_{i,J,K} = A^n_{i,0,k}, A^n_{i,-1,k} = A^n_{i,J-1,k}, A^n_{I,j,k} = (A_0)_{I,j,k} \tag{4.48}$$

It is noted that when $i=1$, Equation (4.32) needs the value of $A^0_{i,j,k}$. Here, we evaluate it using an average of the nearest J points in the neighborhood surrounding the grid point at $r=0$ as follows:

$$A^n_{0,j,k} = \frac{\Delta\phi}{2\pi} \sum_{j=0}^{J-1} A^n_{1,j,k} \tag{4.49}$$

It should be pointed out that the finite difference scheme, Equation (3.11), is unconditionally stable, and the proof can be seen in the next section.

Thus, an **Algorithm** for obtaining the values of species *(A, R, AR, A_2R, A_2R^{open})* at time level n+1 from time level n can be described as follows:

- Guess the values of species *(A, R, AR, A_2R, A_2R^{open})* at time level n+1.

- Obtain the values of species *(A,R, AR, A_2R, A_2R^{open})* at time level n+1 by using the Runge-Kutta method, as seen in Equations (11)-(12).

- Substitute those updated values of species *(A, R, AR, A_2R, A_2R^{open})* at time level n+1 into Equation (13). As such, Equation (13) becomes a linear system for unknown variable (A). Solve the obtained linear system by using an iterative method until a criterion for convergence $\max (i,j,k) \left| A^{n+1(new)}_{i,j,k} - A^{n+1(old)}_{i,j,k} \right| \le \varepsilon$ is satisfied.

Repeat steps 2 and 3 until a criterion for overall convergence is satisfied.

4.3 Stability for 1D Finite Difference Scheme

We now show that our present scheme, Equations (4.24) through (4.26), is unconditionally stable. For the simplicity, we first introduce two finite difference operators:

$$\nabla_{\bar{r}} A_j^q = \frac{1}{\Delta r}[A_j^q - A_{j-1}^q]$$

$$P_r[A_j^q] = r_{j+\frac{1}{2}}\frac{A_{j+1}^q - A_j^q}{\Delta r^2} - r_{j-\frac{1}{2}}\frac{A_j^n - A_{j-1}^q}{\Delta r^2}, q = n, n+1. \tag{4.50}$$

We then multiply Equation (4.24) by $2r_1\Delta r\frac{b}{a}[A_1^{n+1} + A_1^n]$, Equation (4.25) by

$2r_j\Delta r[A_j^{n+1} + A_j^n], 2 \leq j \leq M - 1$, Equation (16c) by $2r_M\Delta r\frac{b^*}{a^*}[A_M^{n+1} + A_M^n]$, and add

all of them together. This gives

$$\frac{2\Delta r}{\Delta t}\frac{b}{a}r_1([A_1^{n+1}]^2 - [A_1^n]^2) + \frac{2\Delta r}{\Delta t}\sum_{j=2}^{M-1} r_j\left([A_j^{n+1}]^2 - [A_j^n]^2\right)$$

$$+\frac{2\Delta r}{\Delta t}\frac{b^*}{a^*}r_M([A_M^{n+1}]^2 - [A_M^n]^2)$$

$$= \Delta r D_A \sum_{j=2}^{M-1} P_r\left[A_j^{n+1} + A_j^n\right] \cdot \left[A_j^{n+1} + A_j^n\right]$$

$$+D_A r_{\frac{3}{2}}\nabla_{\bar{r}}[A_2^{n+1} + A_2^n] \cdot [A_1^{n+1} + A_1^n]$$

$$-D_A r_{M-\frac{1}{2}}\nabla_{\bar{r}}[A_M^{n+1} + A_M^n] \cdot [A_M^{n+1} + A_M^n]$$

$$+\omega D_A \Delta r \sum_{j=2}^{M-1} P_r\left[A_j^{n+1} - A_j^n\right] \cdot \left[A_j^{n+1} + A_j^n\right]$$

$$+\omega D_A r_{\frac{3}{2}} \nabla_{\bar{r}} [A_2^{n+1} - A_2^n] \cdot [A_1^{n+1} + A_1^n]$$

$$-\omega D_A r_{M-\frac{1}{2}} \nabla_{\bar{r}} [A_M^{n+1} - A_M^n] \cdot [A_M^{n+1} + A_M^n]$$

$$+\Delta r \left\{ 2\frac{b}{a} r_1 S_1^{n+\frac{1}{2}} \cdot [A_1^{n+1} + A_1^n] + \sum_{j=2}^{M-1} 2 r_j S_j^{n+\frac{1}{2}} \cdot [A_j^{n+1} + A_j^n] + 2\frac{b^*}{a^*} r_M S_M^{n+\frac{1}{2}} \right.$$

$$\left. \cdot [A_M^{n+1} + A_M^n] \right\}. \tag{4.51}$$

Denoting $U_j = A_j^{n+1} + A_j^n$ for the purpose of simple notation, the first three terms

(FTT) on the right-hand-side can be simplified to

$$FTT = \frac{D_A}{\Delta r} \sum_{j=2}^{M-1} \{ r_{j+\frac{1}{2}} [U_{j+1} - U_j] - r_{j-\frac{1}{2}} [U_j - U_{j-1}] \} \cdot U_j + D_A r_{\frac{3}{2}} \nabla_{\bar{r}} U_2 \cdot U_1$$

$$-D_A r_{M-\frac{1}{2}} \nabla_{\bar{r}} U_M \cdot U_M$$

$$= D_A \sum_{j=3}^{M} r_{j-\frac{1}{2}} \nabla_{\bar{r}} U_j \cdot U_{j-1} - D_A \sum_{j=2}^{M-1} r_{j-\frac{1}{2}} \nabla_{\bar{r}} U_j \cdot U_j + D_A r_{\frac{3}{2}} \nabla_{\bar{r}} U_2 \cdot U_1$$

$$-D_A r_{M-\frac{1}{2}} \nabla_{\bar{r}} U_M \cdot U_M$$

$$= D_A \sum_{j=2}^{M} r_{j-\frac{1}{2}} \nabla_{\bar{r}} U_j \cdot U_{j-1} - D_A \sum_{j=2}^{M} r_{j-\frac{1}{2}} \nabla_{\bar{r}} U_j \cdot U_j$$

$$= -D_A \Delta r \sum_{j=2}^{M} r_{j-\frac{1}{2}} \nabla_{\bar{r}} U_j \cdot \nabla_{\bar{r}} U_j$$

$$= -D_A \Delta r \sum_{j=2}^{M} r_{j-\frac{1}{2}} (\nabla_{\bar{r}} [A_j^{n+1} + A_j^n])^2. \tag{4.52}$$

Similarly, letting $V_j = A_j^{n+1} - A_j^n$, the next three terms (NTT) on the right-hand-side can

be simplified to

$$NTT = \omega \frac{D_A}{\Delta r} \sum_{j=2}^{M-1} \{r_{j+\frac{1}{2}}[V_{j+1} - V] - r_{j-\frac{1}{2}}[V_j - V_{j-1}]\} \cdot U_j + \omega D_A r_{\frac{3}{2}} \nabla_{\bar{r}} V_2 \cdot U_1$$

$$-\omega D_A r_{M-\frac{1}{2}} \nabla_{\bar{r}} V_M \cdot U_M$$

$$= \omega D_A \sum_{j=3}^{M} r_{j-\frac{1}{2}} \nabla_{\bar{r}} V_j \cdot U_{j-1} - \omega D_A \sum_{j=2}^{M-1} r_{j-\frac{1}{2}} \nabla_{\bar{r}} V_j \cdot U_j + \omega D_A r_{\frac{3}{2}} \nabla_{\bar{r}} V_2 \cdot U_1$$

$$-\omega D_A r_{M-\frac{1}{2}} \nabla_{\bar{r}} V_M \cdot U_M$$

$$= \omega D_A \sum_{j=2}^{M} r_{j-\frac{1}{2}} \nabla_{\bar{r}} V_j \cdot U_{j-1} - \omega D_A \sum_{j=2}^{M} r_{j-\frac{1}{2}} \nabla_{\bar{r}} V_j \cdot U_j$$

$$= -\omega D_A \Delta r \sum_{j=2}^{M} r_{j-\frac{1}{2}} \nabla_{\bar{r}} V_j \cdot \nabla_{\bar{r}} U_j$$

$$= -\omega D_A \Delta r \sum_{j=2}^{M} r_{j-\frac{1}{2}} ((\nabla_{\bar{r}} A_j^{n+1})^2 - (\nabla_{\bar{r}} A_j^n)^2). \tag{4.53}$$

By Cauchy-Schwartz's inequality $(2ab \leq \varepsilon a^2 + \frac{1}{\varepsilon} b^2)$, $\varepsilon > 0$, we have

$$2S_j^{n+\frac{1}{2}} \cdot [A_j^{n+1} + A_j^n] \leq [A_j^{n+1} + A_j^n]^2 + [S_j^{n+\frac{1}{2}}]^2$$

$$\leq 2\left([A_j^{n+1}]^2 + [A_j^n]^2\right) + [S_j^{n+\frac{1}{2}}]^2, \tag{4.54}$$

for any j. Substituting Equations (4.41) through (4.43) into Equation (4.40) and dropping the negative term $-D_A \Delta r \sum_{j=2}^{M} r_{j-\frac{1}{2}} (\nabla_{\bar{r}} [A_j^{n+1} + A_j^n])^2$ on the RHS, we can simplify Equation (4.40) to

$$\frac{2\Delta r}{\Delta t} \frac{b}{a} r_1 ([A_1^{n+1}]^2 - [A_1^n]^2) + \frac{2\Delta r}{\Delta t} \sum_{j=2}^{M-1} r_j \left([A_j^{n+1}]^2 - [A_j^n]^2\right)$$

$$+\frac{2\Delta r}{\Delta t}\frac{b^*}{a^*}r_M([A_M^{n+1}]^2 - [A_M^n]^2) + \omega D_A \Delta r \sum_{j=2}^{M} r_{j-\frac{1}{2}}((\nabla_{\bar{r}}A_j^{n+1})^2 - (\nabla_{\bar{r}}A_j^n)^2)$$

$$\leq 2\Delta r \frac{b}{a} r_1([A_1^{n+1}]^2 + [A_1^n]^2) + 2\Delta r \sum_{j=2}^{M-1} r_j\left([A_j^{n+1}]^2 + [A_j^n]^2\right)$$

$$+2\Delta r \frac{b^*}{a^*}r_M([A_M^{n+1}]^2 + [A_M^n]^2) + \Delta r(\frac{b}{a}r_1\left[S_1^{n+\frac{1}{2}}\right]^2 + \sum_{j=2}^{M-1} r_j\left[S_j^{n+\frac{1}{2}}\right]^2$$

$$+\frac{b^*}{a^*}r_M\left[S_M^{n+\frac{1}{2}}\right]^2). \tag{4.55}$$

Multiplying Equation (4.44) by Δt and letting

$$F(n) \equiv 2\Delta r(\frac{b}{a}r_1\left([A_1^n]^2 + \sum_{j=2}^{M-1} r_j\left[A_j^n\right]^2 + \frac{b^*}{a^*}r_M[A_M^n]^2\right)$$

$$+\omega D_A \Delta r \Delta t \sum_{j=2}^{M} r_{j-\frac{1}{2}}(\nabla_{\bar{r}}A_j^n)^2, \tag{4.56}$$

$$\Phi(n) \equiv \Delta r\left(\frac{b}{a}r_1\left[S_1^{n+\frac{1}{2}}\right]^2 + \sum_{j=2}^{M-1} r_j\left[S_j^{n+\frac{1}{2}}\right]^2 + \frac{b^*}{a^*}r_M\left[S_M^{n+\frac{1}{2}}\right]^2\right). \tag{4.57}$$

Equation (4.44) can be further simplified to

$$F(n+1) \leq \frac{1+\Delta t}{1-\Delta t} \cdot F(n) + \frac{\Delta t}{1-\Delta t} \cdot \Phi(n)$$

$$\leq \frac{1+\Delta t}{1-\Delta t} \cdot [\frac{1+\Delta t}{1-\Delta t}F(n-1) + \frac{\Delta t}{1-\Delta t}\Phi(n-1)] + \frac{\Delta t}{1-\Delta t}\Phi(n)$$

$$\leq \cdots$$

$$\leq \left(\frac{1+\Delta t}{1-\Delta t}\right)^{n+1} F(0) + \frac{\Delta t}{1-\Delta t}$$

$$\left[1 + \frac{1+\Delta t}{1-\Delta t} + \left(\frac{1+\Delta t}{1-\Delta t}\right)^2 + \cdots + \left(\frac{1+\Delta t}{1-\Delta t}\right)^n\right] \max_{0 \le k \le n} \Phi(k)$$

$$\le \left(\frac{1+\Delta t}{1-\Delta t}\right)^{n+1} \left[F(0) + \max_{0 \le k \le n} \Phi(k)\right]. \tag{4.58}$$

Using the inequalities $(1+\varepsilon)^n \le e^{n\varepsilon}$ for $\varepsilon > 0$ and $(1-\varepsilon)^{-1} \le e^{2\varepsilon}$ for $0 < \varepsilon \le \frac{1}{2}$, we

obtain $(1+\Delta t)^{n+1} \le e^{(n+1)\Delta t}$ and $(1-\Delta t)^{-1} \le e^{2\Delta t}$, and hence, when Δt is

sufficiently small, the solution to the present scheme satisfies

$$F(n+1) \le e^{3(n+1)\Delta t}\left[F(0) + \max_{0 \le k \le n} \Phi(k)\right] \le e^{3t_0}\left[F(0) + \max_{0 \le k \le n} \Phi(k)\right], \tag{4.59}$$

for any $0 \le (n+1)\Delta t \le t_0$. Hence, for any $0 \le n\Delta t \le t_0$, we obtain

$$2\left(\frac{b}{a}r_1[A_1^n]^2 + \sum_{j=2}^{M-1} r_j[A_j^n]^2 + \frac{b^*}{a^*}r_M[A_M^n]^2 + \omega D_A \Delta r \Delta t \sum_{j=2}^{M} r_{j-\frac{1}{2}}(\nabla_{\bar{r}}A_j^n)^2\right.$$

$$\le e^{3t_0}\left\{2\left(\frac{b}{a}r_1[A_1^0]^2 + \sum_{j=2}^{M-1} r_j[A_j^0]^2 + \frac{b^*}{a^*}r_M[A_M^0]^2\right)\right.$$

$$\left. + \omega D_A \Delta r \Delta t \sum_{j=2}^{M} r_{j-\frac{1}{2}}(\nabla_{\bar{r}}A_j^0)^2\right\}$$

$$+ e^{3t_0}\max_{0 \le k \le n-1}\Phi\left(\frac{b}{a}r_1\left[S_1^{k+\frac{1}{2}}\right]^2 + \sum_{j=2}^{M-1} r_j\left[S_j^{k+\frac{1}{2}}\right]^2 + \frac{b^*}{a^*}r_M\left[S_M^{k+\frac{1}{2}}\right]^2\right), \tag{4.60}$$

implying that the scheme is unconditionally stable with respect to the initial condition

and source term.

4.4 Stability for 3D Finite Difference Scheme

To analyze the stability of the finite difference scheme, Equation (4.32), with the

initial and boundary conditions, Equations (4.46) through (4.49), we first define the

following difference operators:

$$P_r[A_{i,j,k}^n] \equiv \left[r_{i+\frac{1}{2}} \frac{A_{i+1,j,k}^n - A_{i,j,k}^n}{(\Delta r)^2} - r_{i-\frac{1}{2}} \frac{A_{i,j,k}^n - A_{i-1,j,k}^n}{(\Delta r)^2} \right],$$

(4.61)

$$P_\phi[A_{i,j,k}^n] \equiv \frac{A_{i,j+1,k}^n - 2A_{i,j,k}^n + A_{i,j-1,k}^n}{(\Delta \phi)^2},$$

(4.62)

$$P_z[A_{i,j,k}^n] \equiv \frac{A_{i,j,k+1}^n - 2A_{i,j,k}^n + A_{i,j,k-1}^n}{(\Delta z)^2},$$

(4.63)

$$\nabla_{\bar{r}} A_{i,j,k}^n \equiv \frac{A_{i,j,k}^n - A_{i-1,j,k}^n}{\Delta r},$$

(4.64)

$$\nabla_{\bar{\phi}} A_{i,j,k}^n \equiv \frac{A_{i,j,k}^n - A_{i,j-1,k}^n}{\Delta \phi},$$

(4.65)

$$\nabla_{\bar{z}} A_{i,j,k}^n \equiv \frac{A_{i,j,k}^n - A_{i,j,k-1}^n}{\Delta z},$$

(4.66)

$$W_t[A_{i,j,k}^n] \equiv \frac{A_{i,j,k}^{n+1} + A_{i,j,k}^n}{2}.$$

(4.67)

We assume that the values of species *(A,R, AR, A_2R, A_2R^{open})* at time level n+1 have already been known since they are calculated ahead based on the Runge-Kutta method. As such, Equation (4-32) can be simplified to, at interior points, $k=2,...,K-1$,

$$\frac{A_{i,j,k}^{n+1} - A_{i,j,k}^n}{\Delta t} = \frac{D_r}{r_i} P_r\{W_t[A_{i,j,k}^n]\} + \frac{D_\phi}{r_i^2} P_\phi\{W_t[A_{i,j,k}^n]\} + D_z P_z\{W_t[A_{i,j,k}^n]\}$$

$$- C_{i,j,k}^{n+\frac{1}{2}} \left(\frac{A_{i,j,k}^{n+1} + A_{i,j,k}^n}{2} \right) + f_{i,j,k}^{n+\frac{1}{2}}$$

(4.68)

where $1 \le i \le I-1$, $1 \le j \le J-1$; at the location z_1,

$$\frac{A_{i,j,1}^{n+1} - A_{i,j,1}^n}{\Delta t} = \frac{D_r}{r_i} P_r\{W_t[A_{i,j,1}^n]\} + \frac{D_\phi}{r_i^2} P_\phi\{W_t[A_{i,j,1}^n]\} + \frac{a D_z}{b \Delta_z} \nabla_{\bar{z}}\{W_t[A_{i,j,1}^n]\}$$

$$- C_{i,j,1}^{n+\frac{1}{2}} \left(\frac{A_{i,j,1}^{n+1} + A_{i,j,1}^n}{2} \right) + f_{i,j,1}^{n+\frac{1}{2}}$$

(4.69)

where $a = 1$, $b = \frac{1}{2} + \frac{\sqrt{3}}{3}$ and $1 \le i \le I-1$, $0 \le j \le J-1$; and at the location z_K,

$$\frac{A_{i,j,K}^{n+1} - A_{i,j,K}^{n}}{\Delta t} = \frac{D_r}{r_i} P_r\{W_t[A_{i,j,K}^n]\} + \frac{D_\phi}{r_i^2} P_\phi\{W_t[A_{i,j,K}^n]\} - \frac{a^* D_z}{b^* \Delta_z} \nabla_{\bar{z}}\{W_t[A_{i,j,K}^n]\}$$

$$-C_{i,j,K}^{n+\frac{1}{2}}\left(\frac{A_{i,j,K}^{n+1} + A_{i,j,K}^n}{2}\right) + f_{i,j,K}^{n+\frac{1}{2}} \qquad (4.70)$$

where $a^* = 1$, $b^* = \frac{1}{2} + \frac{\sqrt{3}}{3}$ and $1 \le i \le I - 1$, $0 \le j \le J - 1$. Here, $C_{i,j,k}^{n+\frac{1}{2}}$ and $f_{i,j,k}^{n+\frac{1}{2}}$,

which are from the values of species $(A, R, AR, A_2R, A_2R^{open})$, are considered to be

positive coefficient and a source term respectively.

Theorem. The finite difference scheme Equations (4.68) through (4.70), with initial and

boundary conditions, Equations (4.46) through (4.49), is unconditionally stable with

respect to the initial condition and source term.

Proof. Assume that A_1 and A_2 are two solutions obtained based on Equations (4.68)

through (4.70) with same boundary conditions but different initial conditions and source

terms f_1 and f_2 respectively. Letting $A = A_1 - A_2$ and $f = f_1 - f_2$, then A and f satisfy

Equations (4.68, 4.69, 4.70) with the boundary conditions

$$A_{i,J,k}^n = A_{i,0,k}^n, \qquad A_{i,-1,k}^n = A_{i,J-1,k}^n, \qquad A_{I,j,k}^n = 0, \qquad A_{0,j,k}^n = \frac{\Delta\phi}{2\pi}\sum_{j=0}^{J-1} A_{1,j,k}^n \qquad (4.71)$$

for $1 \le j \le J - 1$, $0 \le k \le K$.

We then multiply Equation (4.68) by $2r_i\Delta z\,\Delta t[A_{i,j,k}^{n+1} + A_{i,j,k}^n]$ for interior points, $k=2,\ldots,$

$K\text{-}1$; multiply Equation (4.69) by $2\frac{a}{b}r_i\Delta z\,\Delta t[A_{i,j,1}^{n+1} + A_{i,j,1}^n]$; multiply Equation (4.70) by

$2\frac{b^*}{a^*}r_i\Delta z\,\Delta t[A_{i,j,K}^{n+1} + A_{i,j,K}^n]$. This gives

$$2\Delta z r_i\{\frac{b}{a}\left([A_{i,j,1}^{n+1}]^2 - [A_{i,j,1}^n]^2\right)$$

$$+ \sum_{k=2}^{K-1} \left([A_{i,j,k}^{n+1}]^2 - [A_{i,j,k}^n]^2 \right) + \frac{b^*}{a^*} \left([A_{i,j,K}^{n+1}]^2 - [A_{i,j,K}^n]^2 \right) \}$$

$$= 2\Delta z \Delta t \Delta D_r \{ \frac{b}{a} P_r\{W_t[A_{i,j,1}^n]\}[A_{i,j,1}^{n+1} + A_{i,j,1}^n]$$

$$+ \sum_{k=2}^{K-1} P_r\{W_t[A_{i,j,k}^n]\}[A_{i,j,k}^{n+1} + A_{i,j,k}^n] + \frac{b^*}{a^*} P_r\{W_t[A_{i,j,K}^n]\}[A_{i,j,K}^{n+1} + A_{i,j,K}^n]\}$$

$$+ 2\Delta z \Delta t \frac{D_\phi}{r_i} \{ \frac{b}{a} P_\phi\{W_t[A_{i,j,1}^n]\}[A_{i,j,1}^{n+1} + A_{i,j,1}^n]$$

$$+ \sum_{k=2}^{K-1} P_\phi\{W_t[A_{i,j,k}^n]\}[A_{i,j,k}^{n+1} + A_{i,j,k}^n] + \frac{b^*}{a^*} P_\phi\{W_t[A_{i,j,K}^n]\}[A_{i,j,K}^{n+1} + A_{i,j,K}^n]\}$$

$$+ \Delta t r_i D_z \{ \nabla_{\bar{z}}[A_{i,j,2}^{n+1} + A_{i,j,2}^n][A_{i,j,1}^{n+1} + A_{i,j,1}^n]$$

$$+ 2\Delta z \sum_{k=2}^{K-1} P_z\{W_t[A_{i,j,k}^n]\}[A_{i,j,k}^{n+1} + A_{i,j,k}^n] - \nabla_{\bar{z}}[A_{i,j,K}^{n+1} + A_{i,j,K}^n][A_{i,j,K}^{n+1} + A_{i,j,K}^n]\}$$

$$- \Delta z \Delta t r_i \{ \frac{b}{a} C_{i,j,1}^{n+\frac{1}{2}}[A_{i,j,1}^{n+1} + A_{i,j,1}^n]^2 + \sum_{k=2}^{K-1} C_{i,j,k}^{n+\frac{1}{2}}[A_{i,j,k}^{n+1} + A_{i,j,k}^n]^2$$

$$+ \frac{b^*}{a^*} C_{i,j,K}^{n+\frac{1}{2}}[A_{i,j,K}^{n+1} + A_{i,j,K}^n]^2 \} + 2\Delta z \Delta t r_i \{ \frac{b}{a} f_{i,j,1}^{n+\frac{1}{2}}[A_{i,j,1}^{n+1} + A_{i,j,1}^n]$$

$$+ \sum_{k=2}^{K-1} f_{i,j,k}^{n+\frac{1}{2}}[A_{i,j,k}^{n+1} + A_{i,j,k}^n] + \frac{b^*}{a^*} f_{i,j,K}^{n+\frac{1}{2}}[A_{i,j,K}^{n+1} + A_{i,j,K}^n]\} \tag{4.72}$$

Since the third term on the RHS of Equation (4.72) can be simplified to

$$2\Delta z \sum_{k=2}^{K-1} P_z\{W_t[A_{i,j,k}^n]\}[A_{i,j,k}^{n+1} + A_{i,j,k}^n] + \nabla_{\bar{z}}[A_{i,j,2}^{n+1} + A_{i,j,2}^n][A_{i,j,1}^{n+1} + A_{i,j,1}^n]$$

$$- \nabla_{\bar{z}}[A_{i,j,K}^{n+1} + A_{i,j,K}^n][A_{i,j,K}^{n+1} + A_{i,j,K}^n],$$

$$= \sum_{k=2}^{K-1} \{ \nabla_{\bar{z}}[A_{i,j,k+1}^{n+1} + A_{i,j,k+1}^{n}] - \nabla_{\bar{z}}[A_{i,j,k}^{n+1} + A_{i,j,k}^{n}] \} [A_{i,j,k}^{n+1} + A_{i,j,k}^{n}]$$

$$+ \nabla_{\bar{z}}[A_{i,j,2}^{n+1} + A_{i,j,2}^{n}][A_{i,j,1}^{n+1} + A_{i,j,1}^{n}] - \nabla_{\bar{z}}[A_{i,j,K}^{n+1} + A_{i,j,K}^{n}][A_{i,j,K}^{n+1} + A_{i,j,K}^{n}]$$

$$= \sum_{k=3}^{K} \nabla_{\bar{z}}[A_{i,j,k}^{n+1} + A_{i,j,k}^{n}][A_{i,j,k-1}^{n+1} + A_{i,j,k-1}^{n}].$$

$$- \sum_{k=2}^{K-1} \nabla_{\bar{z}}[A_{i,j,k}^{n+1} + A_{i,j,k}^{n}][A_{i,j,k}^{n+1} + A_{i,j,k}^{n}] + \nabla_{\bar{z}}[A_{i,j,2}^{n+1} + A_{i,j,2}^{n}][A_{i,j,1}^{n+1} + A_{i,j,1}^{n}]$$

$$- \nabla_{\bar{z}}[A_{i,j,K}^{n+1} + A_{i,j,K}^{n}][A_{i,j,K}^{n+1} + A_{i,j,K}^{n}]$$

$$= -\Delta z \sum_{k=2}^{K} \nabla_{\bar{z}}[A_{i,j,k}^{n+1} + A_{i,j,k}^{n}]^{2} \tag{4.73}$$

and $C_{i,j,1}^{n++\frac{1}{2}}[A_{i,j,1}^{n+1} + A_{i,j,1}^{n}] \geq 0$, one may drop the third and fourth terms on the RHS of

Equation (4.71) and simplify it to

$$2\Delta z r_i \{ \frac{b}{a} \left([A_{i,j,1}^{n+1}]^2 - [A_{i,j,1}^{n}]^2 \right)$$

$$+ \sum_{k=2}^{K-1} \left([A_{i,j,k}^{n+1}]^2 - [A_{i,j,k}^{n}]^2 \right) + \frac{b^*}{a^*} \left([A_{i,j,K}^{n+1}]^2 - [A_{i,j,K}^{n}]^2 \right) \}$$

$$\leq 2\Delta z \Delta t \Delta D_r \{ \frac{b}{a} P_r \{ W_t[A_{i,j,1}^{n}] \} [A_{i,j,1}^{n+1} + A_{i,j,1}^{n}]$$

$$+ \sum_{k=2}^{K-1} P_r \{ W_t[A_{i,j,k}^{n}] \} [A_{i,j,k}^{n+1} + A_{i,j,k}^{n}] + \frac{b^*}{a^*} P_r \{ W_t[A_{i,j,K}^{n}] \} [A_{i,j,K}^{n+1} + A_{i,j,K}^{n}] \}$$

$$+ 2\Delta z \Delta t \frac{D_\phi}{r_i} \{ \frac{b}{a} P_\phi \{ W_t[A_{i,j,1}^{n}] \} [A_{i,j,1}^{n+1} + A_{i,j,1}^{n}]$$

$$+ \sum_{k=2}^{K-1} P_\phi \{ W_t[A_{i,j,k}^{n}] \} [A_{i,j,k}^{n+1} + A_{i,j,k}^{n}] + \frac{b^*}{a^*} P_\phi \{ W_t[A_{i,j,K}^{n}] \} [A_{i,j,K}^{n+1} + A_{i,j,K}^{n}] \}$$

$$+2\Delta z \Delta t r_i \{\frac{b}{a} f_{i,j,1}^{n+\frac{1}{2}}[A_{i,j,1}^{n+1} + A_{i,j,1}^{n}]$$

$$+ \sum_{k=2}^{K-1} f_{i,j,k}^{n+\frac{1}{2}}[A_{i,j,k}^{n+1} + A_{i,j,k}^{n}] + \frac{b^*}{a^*} f_{i,j,K}^{n+\frac{1}{2}}[A_{i,j,K}^{n+1} + A_{i,j,K}^{n}]\} \tag{4.74}$$

Summing Equation (4.74) over i and j, where $1 \leq i \leq I - 1$, $0 \leq j \leq J - 1$, and multiplying the result by $\Delta r \Delta \phi$, we obtain

$$2\Delta r \Delta \phi \Delta z \sum_{i=1}^{I-1} \sum_{j=0}^{J-1} r_i \{\frac{b}{a}\left([A_{i,j,1}^{n+1}]^2 - [A_{i,j,1}^{n}]^2\right)$$

$$+ \sum_{k=2}^{K-1} \left([A_{i,j,k}^{n+1}]^2 - [A_{i,j,k}^{n}]^2\right) + \frac{b^*}{a^*}\left([A_{i,j,K}^{n+1}]^2 - [A_{i,j,K}^{n}]^2\right)\}$$

$$\leq 2\Delta r \Delta \phi \Delta z \Delta t D_r \sum_{i=1}^{I-1} \sum_{j=0}^{J-1} \{\frac{b}{a} P_r\{W_t[A_{i,j,1}^{n}]\}[A_{i,j,1}^{n+1} + A_{i,j,1}^{n}]$$

$$+ \sum_{k=2}^{K-1} P_r\{W_t[A_{i,j,k}^{n}]\}[A_{i,j,k}^{n+1} + A_{i,j,k}^{n}] + \frac{b^*}{a^*} P_r\{W_t[A_{i,j,K}^{n}]\}[A_{i,j,K}^{n+1} + A_{i,j,K}^{n}]\}$$

$$+ 2\Delta r \Delta \phi \Delta z \Delta t \sum_{i=1}^{I-1} \sum_{j=0}^{J-1} \frac{D_\phi}{r_i} \{\frac{b}{a} P_\phi\{W_t[A_{i,j,1}^{n}]\}[A_{i,j,1}^{n+1} + A_{i,j,1}^{n}]$$

$$+ \sum_{k=2}^{K-1} P_\phi\{W_t[A_{i,j,k}^{n}]\}[A_{i,j,k}^{n+1} + A_{i,j,k}^{n}] + \frac{b^*}{a^*} P_\phi\{W_t[A_{i,j,K}^{n}]\}[A_{i,j,K}^{n+1} + A_{i,j,K}^{n}]\}$$

$$+ 2\Delta r \Delta \phi \Delta z \Delta t \sum_{i=1}^{I-1} \sum_{j=0}^{J-1} r_i \{\frac{b}{a} f_{i,j,1}^{n+\frac{1}{2}}[A_{i,j,1}^{n+1} + A_{i,j,1}^{n}]$$

$$+ \sum_{k=2}^{K-1} f_{i,j,k}^{n+\frac{1}{2}}[A_{i,j,k}^{n+1} + A_{i,j,k}^{n}] + \frac{b^*}{a^*} f_{i,j,K}^{n+\frac{1}{2}}[A_{i,j,K}^{n+1} + A_{i,j,K}^{n}]\}. \tag{4.75}$$

Using the similar argument in Equation (4.72) together with Equation (4.71), we have

$$2\Delta r \sum_{j=0}^{J-1}\sum_{i=1}^{I-1} P_r\{W_t[A_{i,j,k}^n]\}[A_{i,j,k}^{n+1}+A_{i,j,k}^n] = -\Delta r\sum_{j=0}^{J-1}\sum_{i=1}^{I} r_{i-\frac{1}{2}}\nabla_{\bar{r}}[A_{i,j,k}^{n+1}+A_{i,j,k}^n]^2 \quad (4.76)$$

$$2\Delta\phi \sum_{j=0}^{J-1} P_\phi\{W_t[A_{i,j,k}^n]\}[A_{i,j,k}^{n+1}+A_{i,j,k}^n] = -\Delta\phi\sum_{j=0}^{J-1}\nabla_{\bar{\phi}}[A_{i,j,k}^{n+1}+A_{i,j,k}^n]^2 \quad (4.77)$$

for any $1 \le j \le J-1$, $0 \le k \le K$. Substituting Equations (4.76) through (4.77) into Equation (4.75), we may drop the first two terms on the RHS of Equation (4.75) and simplify it to

$$2\Delta r\Delta\phi\Delta z \sum_{i=1}^{I-1}\sum_{j=0}^{J-1} r_i\{\frac{b}{a}\left([A_{i,j,1}^{n+1}]^2 - [A_{i,j,1}^n]^2\right)$$

$$+ \sum_{k=2}^{K-1}\left([A_{i,j,k}^{n+1}]^2 - [A_{i,j,k}^n]^2\right) + \frac{b^*}{a^*}\left([A_{i,j,K}^{n+1}]^2 - [A_{i,j,K}^n]^2\right)\}$$

$$\le 2\Delta r\Delta\phi\Delta z\Delta t \sum_{i=1}^{I-1}\sum_{j=0}^{J-1}\{\frac{b}{a}f_{i,j,1}^{n+\frac{1}{2}}[A_{i,j,1}^{n+1}+A_{i,j,1}^n]$$

$$+ \sum_{k=2}^{K-1} f_{i,j,k}^{n+\frac{1}{2}}[A_{i,j,k}^{n+1}+A_{i,j,k}^n] + \frac{b^*}{a^*}f_{i,j,K}^{n+\frac{1}{2}}[A_{i,j,K}^{n+1}+A_{i,j,K}^n]\}. \quad (4.78)$$

Using the Cauchy-Schwartz's inequality $\left(2xy \le \varepsilon x^2 + \frac{1}{\varepsilon}y^2\right)$ and $(x + y)^2 \le 2x^2 + 2y^2$, we have

$$2f_{i,j,1}^{n+\frac{1}{2}}[A_{i,j,1}^{n+1}+A_{i,j,1}^n] \le \frac{a}{b}\left[f_{i,j,1}^{n+\frac{1}{2}}\right]^2 + 2\frac{b}{a}\{[A_{i,j,1}^{n+1}]^2 + [A_{i,j,1}^n]^2\}, \quad (4.79)$$

$$2f_{i,j,K}^{n+\frac{1}{2}}[A_{i,j,K}^{n+1}+A_{i,j,K}^n] \le \frac{a^*}{b^*}\left[f_{i,j,K}^{n+\frac{1}{2}}\right]^2 + 2\frac{b^*}{a^*}\{[A_{i,j,K}^{n+1}]^2 + [A_{i,j,K}^n]^2\}, \quad (4.80)$$

$$2f_{i,j,k}^{n+\frac{1}{2}}[A_{i,j,k}^{n+1}+A_{i,j,k}^n] \le \left[f_{i,j,k}^{n+\frac{1}{2}}\right]^2 + 2\left\{[A_{i,j,k}^{n+1}]^2 + [A_{i,j,k}^n]^2\right\} \quad (4.81)$$

for any $2 \leq k \leq K - 1$. Substituting Equation (4.79)-(4.81) into Equation (4.78) and then denoting

$$A(n) = 2\Delta r \Delta \phi \Delta z \sum_{i=1}^{I-1} \sum_{j=0}^{J-1} r_i \{ \frac{b}{a} [A_{i,j,1}^{n+1}]^2 + \sum_{k=2}^{K-1} [A_{i,j,k}^{n+1}]^2 + \frac{b^*}{a^*} [A_{i,j,K}^{n+1}]^2 \} \qquad (4.82)$$

$$F(n) = \Delta r \Delta \phi \Delta z \sum_{i=1}^{I-1} \sum_{j=0}^{J-1} r_i \{ \frac{b}{a} [f_{i,j,1}^{n+1}]^2 + \sum_{k=2}^{K-1} [f_{i,j,k}^{n+1}]^2 + \frac{b^*}{a^*} [f_{i,j,K}^{n+\frac{1}{2}}]^2 \}, \qquad (4.83)$$

we can further simplify Equation (4.78) to

$$A(n + 1) \leq \frac{1 + \Delta t}{1 - \Delta t} A(n) + \frac{\Delta t}{1 - \Delta t} F(n)$$

$$\leq \frac{1 + \Delta t}{1 - \Delta t} \left[\frac{1 + \Delta t}{1 - \Delta t} A(n - 1) + \frac{\Delta t}{1 - \Delta t} F(n - 1) \right] + \frac{\Delta t}{1 - \Delta t} F(n)$$

$$\leq \left(\frac{1 + \Delta t}{1 - \Delta t} \right)^{n+1} A(0)$$

$$+ \frac{\Delta t}{1 - \Delta t} \left[1 + \frac{1 + \Delta t}{1 - \Delta t} + \cdots + \left(\frac{1 + \Delta t}{1 - \Delta t} \right)^n \right] \max_{0 \leq n_1 \leq n} F(n_1)$$

$$\leq \max_{0 \leq n_1 \leq n} F(n_1)$$

$$\leq \left(\frac{1 + \Delta t}{1 - \Delta t} \right)^{n+1} [A(0) + \max_{0 \leq n_1 \leq n} F(n_1)]. \qquad (4.84)$$

Using the inequalities $(1 + \varepsilon)^n \leq e^{n\varepsilon}$ for $\varepsilon > 0$ and $(1 - \varepsilon)^{-1} \leq e^{2\varepsilon}$ for $0 < \varepsilon \leq \frac{1}{2}$, we obtain

$$A(n + 1) \leq e^{3n\Delta t} [A(0) + \max_{0 \leq n_1 \leq n} F(n_1)] \qquad (4.85)$$

$$\leq e^{3t_0} [A(0) + \max_{0 \leq n_1 \leq n} F(n_1)].$$

For any $(1 + n)\Delta t \leq t_0$, implying the scheme is unconditionally stable with respect to the initial condition and source term.

CHAPTER 5

RESULTS AND DISCUSSIONS

5.1 1D Example

To test the accuracy of our present scheme, we first consider a simple 1D diffusion problem in cylindrical coordinates as follows:

$$\frac{\partial A}{\partial t} = \frac{D_A}{r}\frac{\partial}{\partial r}\left(r\frac{\partial A}{\partial r}\right) + \frac{\pi}{r}e^{-\pi^2 t}\sin(\pi r) \tag{5.1}$$

where $A(r, t)$ is the mass concentration, D_A is the diffusion coefficient, and R is the radius. The initial condition assumed to be

$$A(r, 0) = \cos(\pi r) \tag{5.2}$$

and the boundary condition is

$$\frac{\partial A(0, t)}{\partial r} = \frac{\partial A(1, t)}{\partial r} = 0 \tag{5.3}$$

It can be seen that the exact solution to this problem is

$$A(r, t) = e^{-\pi^2 t}\cos(\pi r). \tag{5.4}$$

The schematic diagram showing the description of the problem is shown in Figure 5.1.

Outer Surface is insulated = Neumann BC
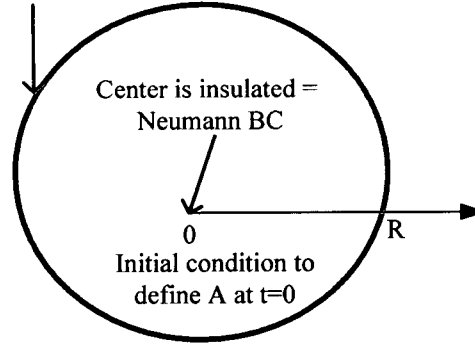
Figure 5.1: Schematic for numerical example 1.

Convergence rates of the scheme can be obtained by calculating the l_2 - norm error of the numerical solution compared with the exact solution as follows:

$$E(M, \Delta t) = \max_{0 \le n \Delta t \le 1.0} \sqrt{\Delta r \sum_{i=1}^{M} [A_i^n - A^{Exact}(r_i, t_n)]^2}$$
(5.5)

Suppose that $E(M, \Delta t) = O(\Delta t^p + \Delta t^q)$. If Δt is small enough, then $E(M, \Delta t) \approx O(\Delta t^p + \Delta t^q)$. Consequently, $\frac{E(M, \Delta t)}{E(2M, \Delta t)} \approx 2^q$ and $q \approx log_2 \left[\frac{E(M, \Delta t)}{E(2M, \Delta t)}\right]$ for the convergence rate with respect to variable r. On the other hand, if Δr is small enough, we have $p \approx log_2 \left[\frac{E(M, \Delta t)}{E(M, \Delta t/2)}\right]$ for the convergence rate with respect to variable t.

To compare our numerical result with other methods, we also employ the current popular ghost point method [62] for solving the above problem, where a mesh is shown in Figure 5.2 and is given by Equation (5.6) and $i = 1, \cdots, N$.

$$\frac{A_i^{n+1} - A_i^n}{\Delta t} = \frac{1}{2 \Delta r} \left[\frac{A_{i+1}^{n+1} - 2A_i^{n+1} + A_{i-1}^{n+1}}{\Delta r} + \frac{A_{i+1}^n - 2A_i^n + A_{i-1}^n}{\Delta r} \right]$$

$$+ \frac{1}{2r_i} \left[\frac{A_{i+1}^{n+1} - A_{i-1}^{n+1}}{2 \Delta r} + \frac{A_{i+1}^n - A_{i-1}^n}{2 \Delta r} \right] + \frac{\pi}{r_i} e^{-\pi^2 \left(n + \frac{1}{2}\right) \Delta t} \sin(\pi r_i)$$
(5.6)
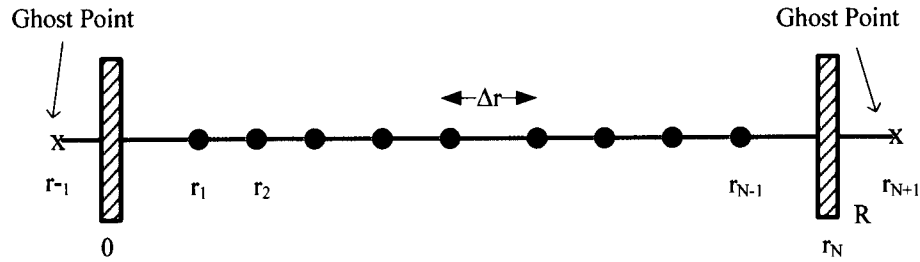
Figure 5.2 Grid points and nomenclature for the ghost point numerical scheme.

Here, r_{N+1} is a ghost point outside the right boundary of the system. In the ghost point method, it is assumed that $A_{N+1}^n = A_{N-1}^n$ for any time level n. Thus, when i = N, one may substitute $A_{N+1}^n = A_{N-1}^n$ in Equation (5.6) to eliminate the fictitious value A_{N+1}^n. On the other hand, at the boundary point r_0, one may obtain from the boundary condition shown in Equation (5.7).

$$\lim_{r \to 0} \left[\frac{\partial^2 A(r,t)}{\partial r^2} + \frac{1}{r} \frac{\partial A(r,t)}{\partial r} \right] = 2 \frac{\partial^2 A(0,t)}{\partial r^2} \tag{5.7}$$

and
$$\lim_{r \to 0} \frac{\pi}{r} e^{-\pi^2 t} \sin(\pi r) = \pi^2 e^{-\pi^2 t} \tag{5.8}$$

Thus, Equation (5.6) at r = 0 can be discretized as:

$$\frac{A_0^{n+1} - A_0^n}{\Delta t} = \frac{1}{\Delta r} \left[\frac{A_1^{n+1} - 2A_0^{n+1} + A_{-1}^{n+1}}{\Delta r} + \frac{A_1^n - 2A_0^n + A_{-1}^n}{\Delta r} \right]$$

$$+ \pi^2 e^{-\pi^2 \left(n + \frac{1}{2} \right) \Delta t} \tag{5.9}$$

Table 5.1 shows the l_2 − norm errors and convergence rates with respect to variable r when $\Delta t = 10^{-5}$ and the number of grid points M = N = 51, 101, and 201 for the present scheme, Equations (4.24) through (4.26), and the ghost point scheme, Equations (5.7) through (5.8). From the Table 5.1, one may see that the errors and convergence rates for

both schemes are about the same, which is expected because both of them are second-order accurate in truncation error.

Table 5.1 l_2 - *norm* error and convergences rates when $\Delta t = 10^{-5}$ and $0 \leq t \leq 1.0$

GRIDS	Equation (4.24-4.26) l_2 - *norm* error	Equation(4.24)-(4.26) *Rate*	Equation (5.6)-(5.9) l_2 - *norm* error	Equation (5.6)-(5.9) *Rate*
51	2.11×10^{-4}	-	2.11×10^{-4}	-
101	5.25×10^{-5}	2.01	5.00×10^{-5}	2.08
201	1.31×10^{-5}	2.01	1.28×10^{-5}	1.97

Figure 5.3 shows the numerical solution obtained by the present scheme using 201 grid points as compared with the exact solution at t = 0.1, 0.2 and 1.0. It can be seen from Figure 5.3 that there are no significant differences between these two solutions. The straigt lines represent the numerical and the solid circles show the analytical solution. The solutions approach to thermal equalibilrium with increasing the duration of the simulation.
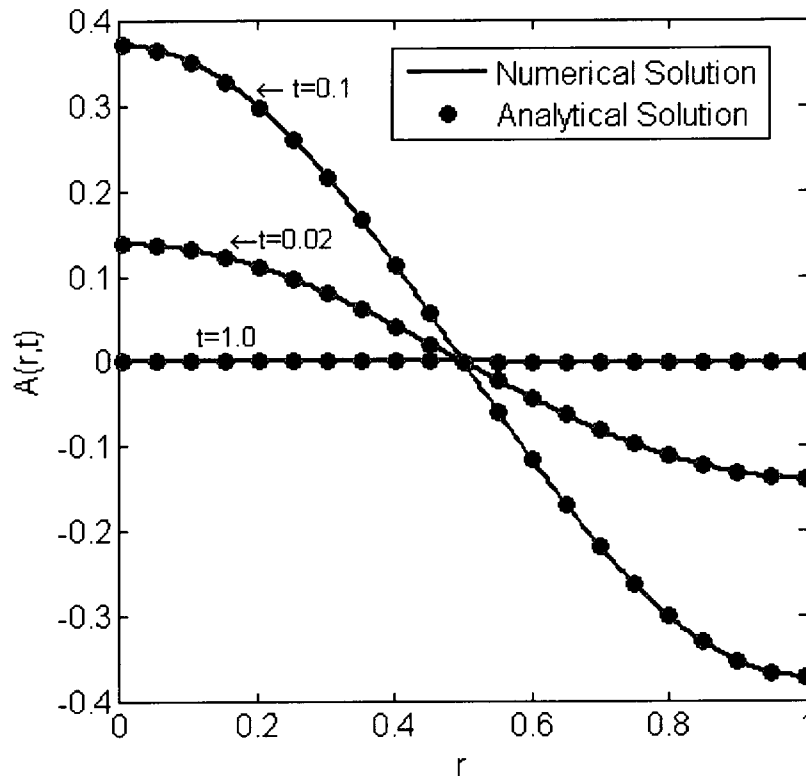
Figure 5.3 Numerical solution obtained by the present method versus the
analytical solution with M = 201, $\Delta t = 10^{-6}$ and t = 0.1,0.2,1.0.

In order to evaluate the stability of both numerical schemes, we consider the
initial condition to be a step function, where M = N = 51, and at the first 20 grid points
the value of the function is 10 and at other points the function is zero, as shown in Figure
5.4. Results at t = 0.024, 0.06, 0.12 when Δt = 0.001, 0.0025, 0.005, respectively, are
plotted in Figure 5.5. It can be seen that at Δt = 0.001 and 0.0025 both numerical schemes
produce a smooth solution; however, at Δt = 0.005, the ghost point method produces an
oscillatory solution around x = 0.4. This solution indicates that our scheme can handle
extreme gradients better than the standard approach when applied to solve similar
problems.
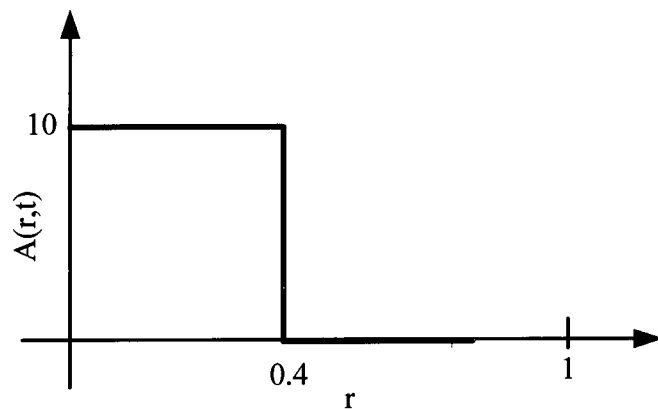
Figure 5.4 Step function for the initial condition.
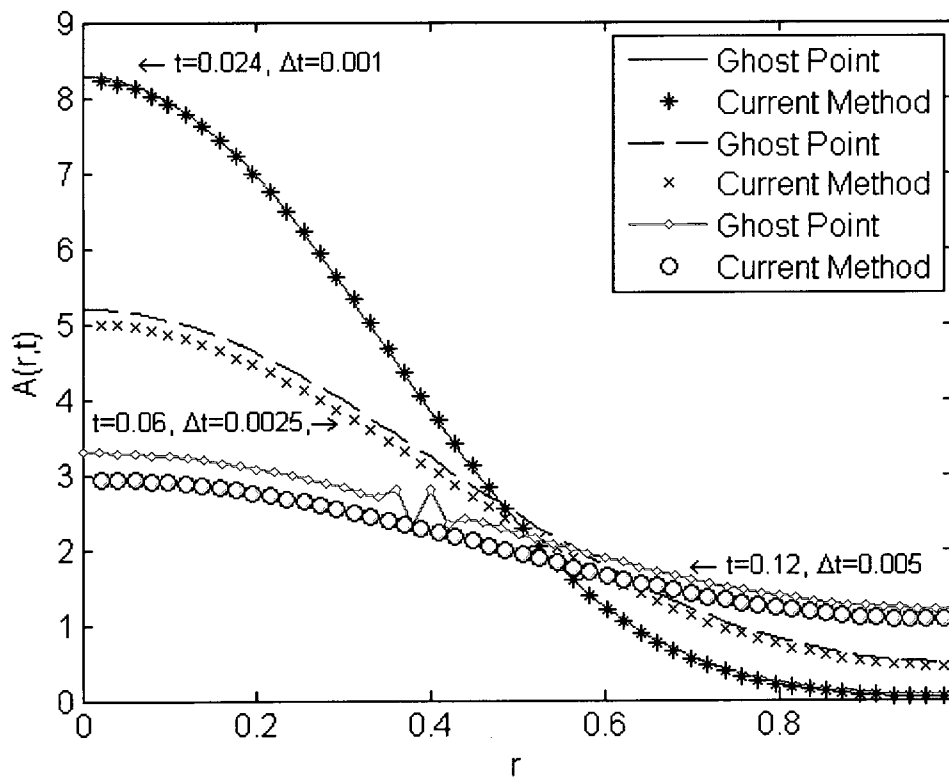
Figure 5.5 Comparison of our present method and the ghost point method solutions
at the various time and time increments Δt = 0.001, 0.0025, 0.005,
M = N= 51 and Δr = 0.02.

It should be pointed out that the ghost point scheme cannot be generalized to multidimensional diffusion equation cases such as:

$$\frac{\partial A(r,\phi,t)}{\partial t} = \frac{D_A}{r}\frac{\partial}{\partial r}\left(r\frac{\partial A(r,\phi,t)}{\partial r}\right) + \frac{D_\phi}{r^2}\frac{\partial^2 A(r,\phi,t)}{\partial \phi^2},$$ (5.10)

Where $0 < r < R, 0 \leq \phi \leq 2\pi$.

Because $\lim_{r\to 0}\left[\frac{D_\phi}{r^2}\frac{\partial^2 A}{\partial \phi^2}\right]$ is difficult to find and, hence, we cannot obtain a numerical scheme like Equation (5.10) at r = 0 . On the other hand, our present scheme can be easily generalized to the multi-dimensional diffusion equation cases because we avoid the approximation at r = 0.

5.2 1D Diffusion in Neuromuscular Junction

Finally, we employ our present scheme to solve a practical diffusion problem in neuromuscular junction where the Neumann boundary is applied at the center, and the Dirichlet boundary is assumed in the other end as shown in Figure 5.6.
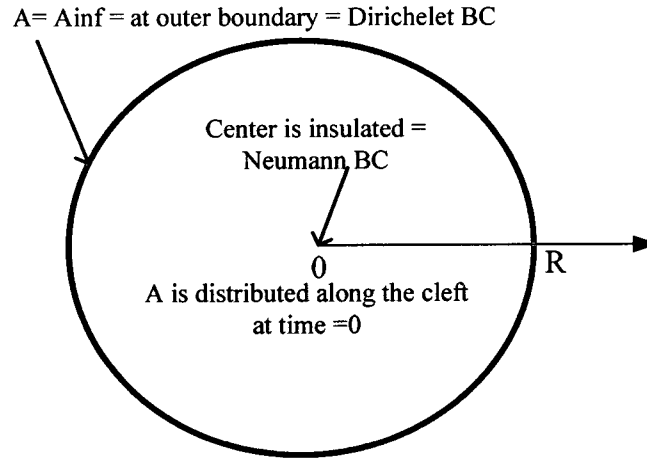
Figure 5.6. Neuromuscular model schematic.

An initial distribution of Acetylcholine is assumed across the cleft at t = 0. Figure 5.7 shows 1D axially symmetric neuromuscular junction model, where the standard diffusion equation in cylindrical coordinate system is given by:

$$\frac{\partial A(r,t)}{\partial t} = \frac{D_A}{r}\frac{\partial}{\partial r}\left(r\frac{\partial A(r,t)}{\partial r}\right), 0 < r < R, \qquad t > 0, \tag{5.11}$$

and the associated initial and boundary conditions are:

$$A(r,0) = 1 - r^2 \tag{5.12}$$

$$\frac{\partial A(0,t)}{\partial r} = 0 \quad , \quad A(R,t) = 0 \tag{5.13}$$
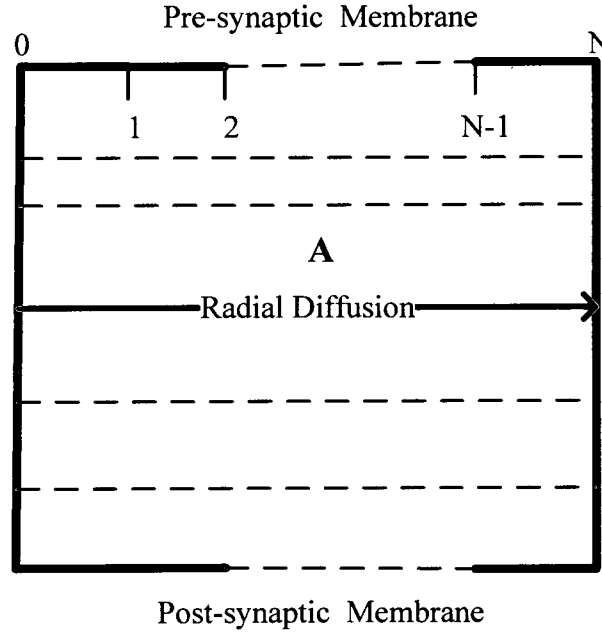
Figure 5.7. Neuromuscular junction model.

The above diffusion problem can be solved by using our present scheme. Since A(R, t) = 0 is not a Neumann boundary condition, we choose $\theta_2 = 1.0$ and use only Equations (4.24) and (4.25) with $2 \leq i \leq N$ in our scheme. It is noted that an analytical solution to the two-dimensional diffusion in cylindrical coordinates is given in [63],

where the transient diffusion in a circular cylinder is analyzed using an infinite series of Bessel functions, and the analytical solution is obtained by computing the series coefficients based on numerical integration and then summing the series solution for various r values with enough terms being used in the series to assure adequate satisfaction of the initial and boundary conditions. The model parameters for the analytical solution with physical significance are chosen to be the width of the cleft $= 0.5 \times 10^{-5}$ cm, the radius of the cleft $= 5.5 \times 10^{-5}$ cm, and the diffusion coefficient for Acetylcholine $= 2.0 \times 10^{-6}$ cm^2/ms [64]-[69].

Our numerical solution is seen to be in good agreement with the analytical solution. Both solutions for different time periods are illustrated in Figure 5.8, and they show that the concentration distribution of acetylcholine along the radius is less than 2% of its initial value in the cleft after 3 ms. These results are also supported by earlier experimental investigations and simulations [10], [26], [35], [39], [40] which demonstrate that under conditions of normal diffusion-reaction or pure diffusion, the acetylcholine entering the NMJ during a signal event will typically be cleared from the NMJ in an elapsed time on the order of 5 ms.
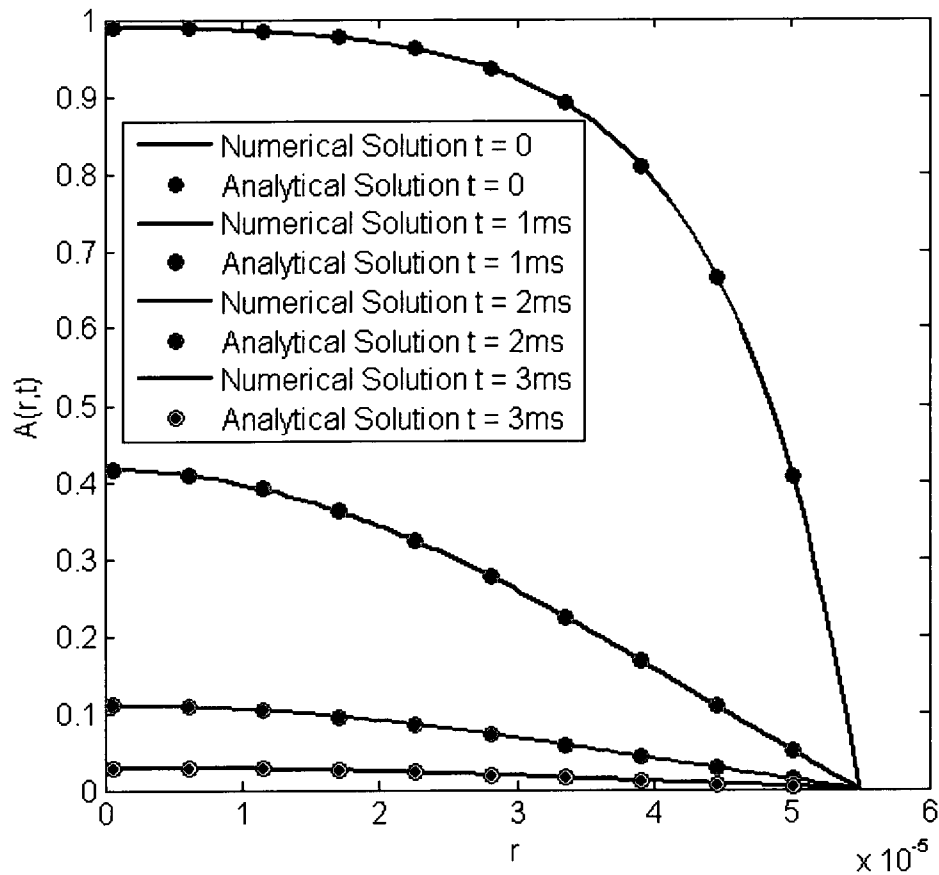
Figure 5.8. Acetylcholine diffusion in the neuromuscular junction.

5.3 3D Reaction-Diffusion Model Results and Discussion

To verify our model and numerical method, a complete description of the processes in the neuromuscular junction was developed, except for the reactions of acetylcholinesterase enzyme. This exclusion is equivalent to the behavior of the NMJ when the enzyme is totally inhibited and non-functional. This exclusion allows the comparison of our results with the results of other investigations which had simulated diffusion and reaction under completely inhibited enzyme conditions.

The behavior of the cholinergic receptors, particularly their open conformational state, is the foundation of descriptions of NMJ activity. Virtually all functional models of

the NMJ focus on relating the receptor conformational state to the other properties of interest [39]-[57]. A good test of the integrity of a model is how well the state of the receptors can be directly or indirectly coupled to a measurable property.

The amount of current generated during the time course of an action potential by a neuron is a property which can be measured directly. It has been demonstrated that the magnitude of current during an NMJ action potential is directly proportional to the number of cholinegeric receptors which are in the conducting state [66] as expressed by:

$$I_{ep}(t) = \gamma_R \, E \, N_{Av} \, V_R \, A_2 R^{open}(t), \tag{5.14}$$

where $I_{ep}(t)$ is the end-plate current, E is the potential across the end-plate, γ_R is the conductance of a single receptor channel, $A_2 R^{open}(t)$ is the concentration of receptors in the open state, N_{Av} is Avogadro's number and V_R is the volume occupied by the embedded receptors in the computation model. An accurate model should precisely predict the number of open receptors with time which are converted into current profile using Equation (5.14). Therefore, in order to test the validity of a neural synapse model, the simulated current should be compared with the experimentally measured values during an action potential. Rosenberry [65] provided an explicit graph of the experimentally measured magnitude of current as a function of time at the post synaptic NMJ membrane, with totally inactive enzyme. This invaluable data is utilized as reference to compare and determine the accuracy of ours and others' models.

Figure 5.9 shows the end-plate current simulated by the present model, the Friboulet model [67], and the Naka model [68] as compared with the experimentally measured current obtained in [65]. This current is taken as reference for the subsequent comparison. The simulated current data of each model, $I_{ep}(t)$, was calculated with

Equation (5.14) using the simulated number of open receptors, $\gamma_R \, E \, N_{Av} \, V_R \, A_2 R^{open}(t)$, $E = 70$ mV [65], and $\gamma_R = 42$ pS [22]-[24]. The conductance of a single channel and the membrane potential were assumed to be constant during the time course of the action potential. It can be seen from Figure 5.9 that the result obtained based on the present model is very close to the experimental data.
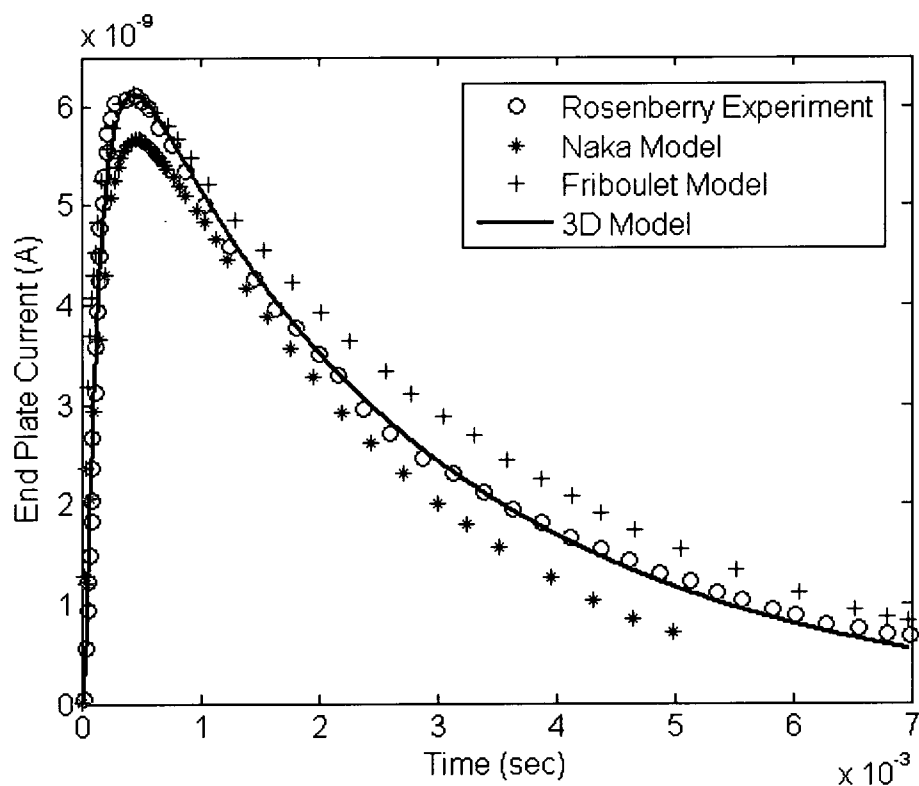
Figure 5.9. Experimentally measured Rosenberry current data compared with simulated current of Naka, Friboulet and 3D Model.

Figure 5.10 depicts the time course of the number of open receptors in the NMJ during an action potential with completely inhibited enzyme. The reference number of

open receptors is derived from the experimental current data in [65] and is based on the

Equation (5.15),

$$N_{Av}` V_R A_2 R^{open}(t) = \frac{I_{ep}(t)}{\gamma_R E},$$ (5.15)

while the simulated receptor data is graphed directly. From Figure 5.10, one may see that

the Friboulet simulation predicts that in the absence of enzyme hydrolysis the number of

open receptors in the NMJ peaks at approximately2100, and exhibits exponential decay

for a period of at least 6 ms. However, our results peak at the experimentally derived

reference value with a negligible error and depict a slower rise time than those of

Friboulet [67].
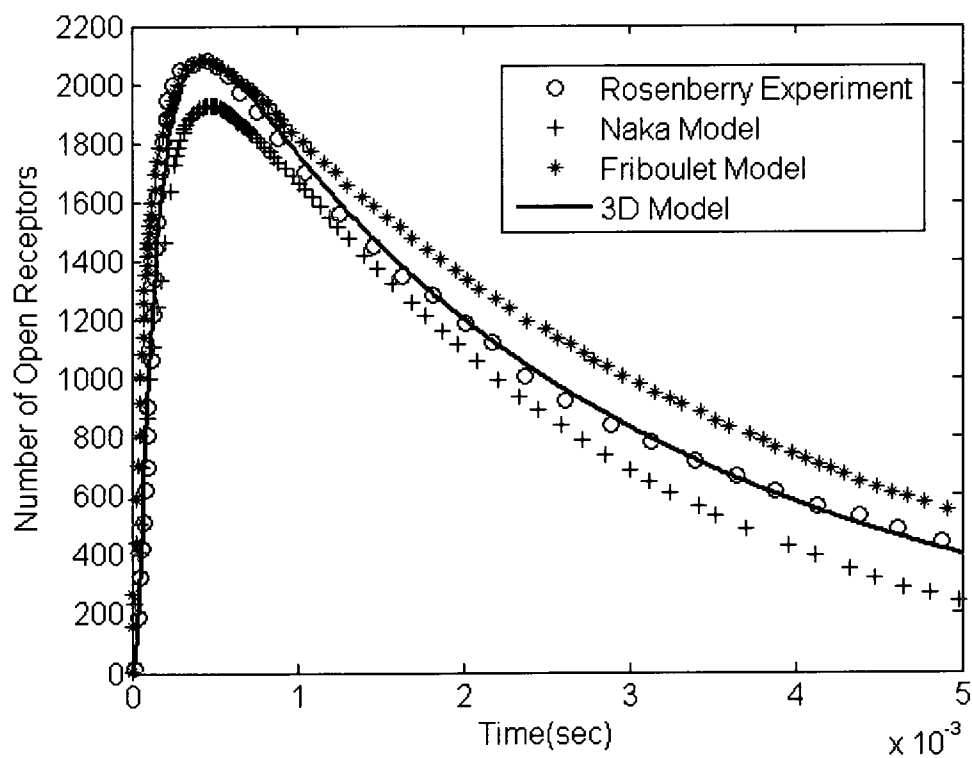
Figure 5.10   Open receptors derived from experimental current compared with computed simulated open receptor of Naka, Friboulet and 3D.

The Friboulet model's decay rate is significantly slower than ours. The Naka model and our model have equitable rise times. Naka model's decay phase is significantly faster than ours. His simulation predicts a peak open receptor number of about 1900 which is lower than the measured value. Our 3D model accurately overlaps with experimentally measured curve and captures the true dynamics of transport-reaction of the NMJ.

Figure 5.11 examines the influence of the width of the NMJ on the kinetics of receptor opening during the release of acetylcholine. When the width is simulated as wider than normal, one would expect an increased diffusional loss of acetylcholine which manifests as an overall decrease in the number of open receptors with time. When the width is less than normal, a decrease in diffusional loss is expected, leading to an overall increase in the number open receptors with time. The simulated kinetic results match the expectations at widths of 0.025 μm, 0.05 μm (normal width), and 0.1 μm, indicating our model is behaving correctly in this regime.
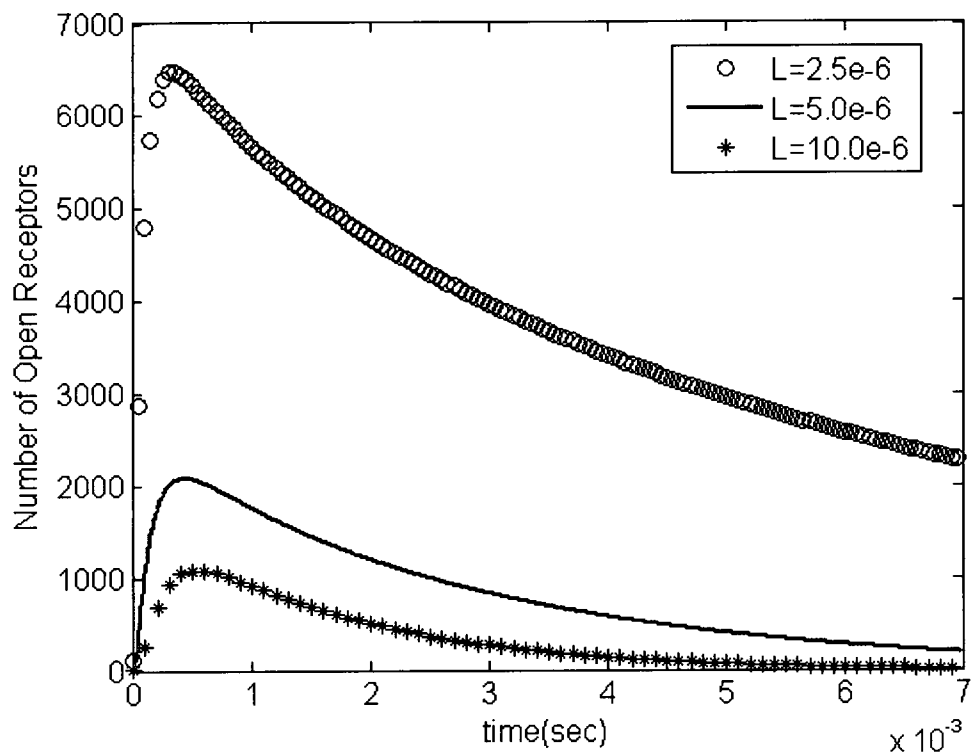
Figure 5.11 Sensitivity of open receptor dynamics to the transverse dimension.

Figures 5.12 through 5.14 depict the influence of the diffusion constant for each coordinate on the open receptor kinetics. In each graph, two of the diffusion constants are held constant while the remaining is perturbed above and below its normal value. Figures 5.12 through 5.14 show that the receptor kinetics is affected when the radial diffusion and transverse diffusion constants are varied, and the kinetics are not affected by varying the angular diffusion constant. Figure 5.12 shows the sensitivity of open receptor dynamics to different radial diffusivities. The concentration decay period increases with increasing radius as expected.
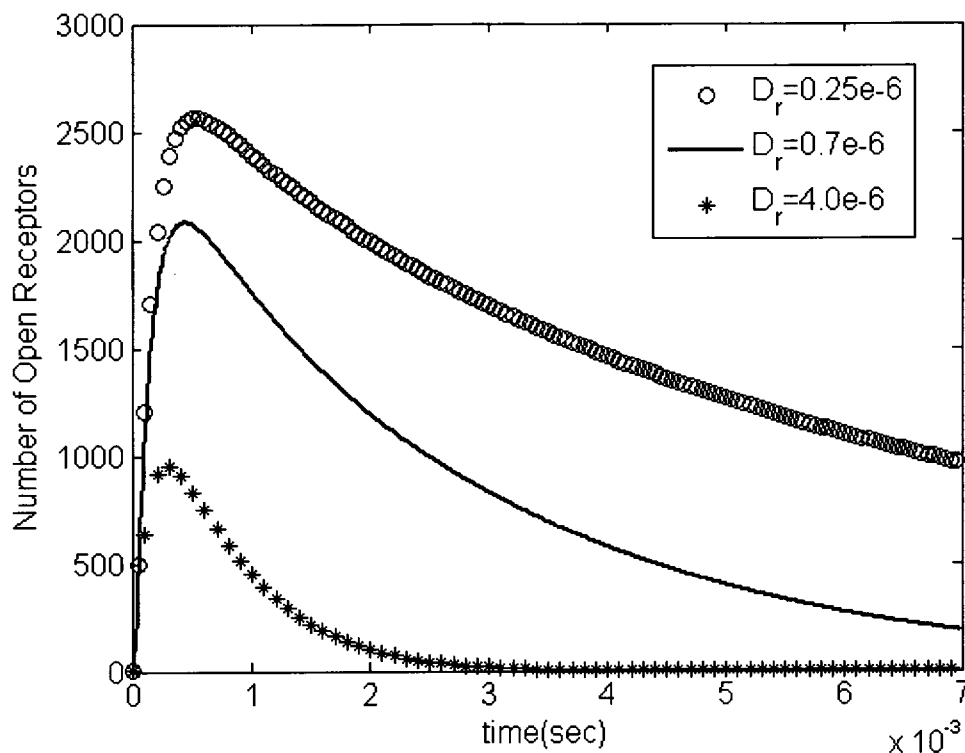
Figure 5.12 Sensitivity of open receptor dynamics to different radial diffusivities (D_r). The values of angular (D_φ) and transverse diffusivities (D_z) are 0.7×10^{-6} cm^2/s.

Anisotropy describes a region with different properties at different locations. Direct measurements of Ach concentration in space and time in the NMJ are difficult to obtain. Ach diffusion inside the NMJ has been determined indirectly through measurment of external NMJ properties and mathematical models [26],[39],[40],[57],[65]-[68]. The investigators vary different combinations of parameters, initial conditions, and boundary conditions; then compare the results of the simulation with measured experimental results. Simulations which generate results that fit experiments are candidates which might represent actual conditions in the NMJ.

The NMJ models of Magleby, Wathey, and Friboulet were well mixed or one dimensional, and so were not suitable to simulate the possibility of anisotropic diffusion affecting the course of an end-plate current. The two dimensional model of Naka and Shiba was one of the first investigations to systematically test the sensitivity of the end-plate current behavior to diffusion of Ach in the radial and transverse directions. They varied the magnitude range of the transverse and radial diffusion constants (D_z and D_r, respectively) and analyzed their effects on the maximum number of open receptors, the time to reach the maximum number of open receptors, and the rate of decay from maximum open receptors. Their simulation indicated that radial Ach diffusion has a larger effect on receptor states (and end-plate current) than transverse diffusion. A simulated D_r value of $\sim 1.0 \times 10^{-6}$ cm^2s^{-1} reproduced the characteristic behavior of the transmission process with no significant deviations with D_z greater than 2.0×10^{-6} cm^2s^{-1}. This functional sensitivity to diffusion in different directions suggests anisotropy is a factor inside the NMJ.

This analysis suggests our model can predict anisotropic effects in the radial and transverse directions, as demonstrated in the Naka model [68]. One would not expect any indications of anisotropic angular diffusion associated with an angularly symmetric initial distribution of acetylcholine, and Figure 5.13 supports this expectation. However, if we have non-symmetric angular distribution of the initial Ach concentration we may observe the appearance of angular concentration gradient. The other scenario where we may see the similar angular gradients is if the model is constructed with different diffusive properties in different regions (sectors) of the cleft.
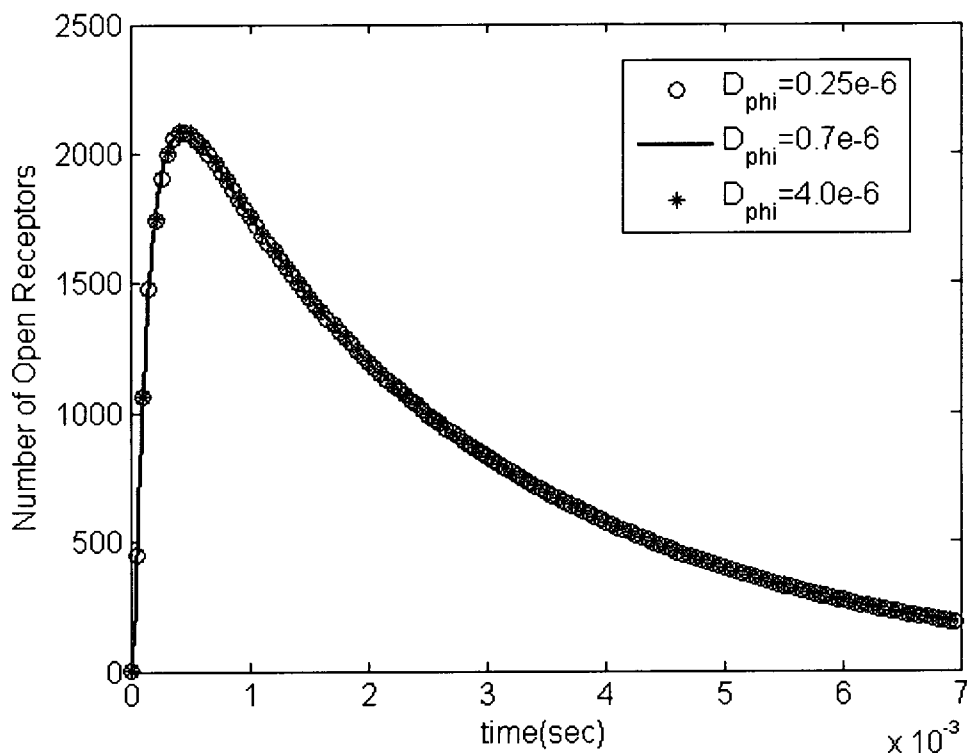
Figure 5.13 Sensitivity of open receptor dynamics to different angular diffusivities (D_φ). The values of radial (D_r) and transverse diffusivities (D_z) are 0.7×10^{-6} cm^2/s.

Figure 5.14 shows the sensitivity of open receptor dynamics to different transverse diffusivities. The maximum number of open receptors increases with increasing transverse diffusivities because relatively more Ach reaches the receptors which are located directly across (transversely) the pre-synaptic membrane. The maximum number of open receptors decreases with decreasing transverse diffusivities because relatively less Ach reaches the receptors, but Ach is still diffusing radially out of the cleft with the same rate.
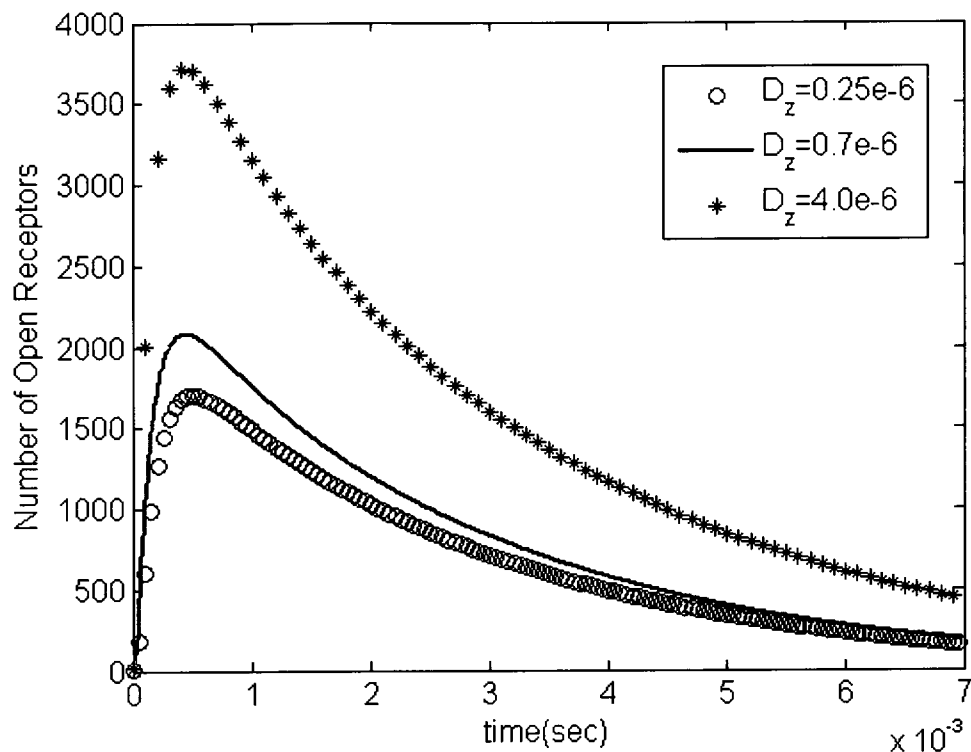
Figure 5.14 Sensitivity of open receptor dynamics to different transverse diffusivities (D_z). The values of angular (D_φ) and radial diffusivities (D_r) are 0.7×10^{-6} cm^2/s.

Figure 5.15 shows how the time course of open receptors changes when the acetylcholine vesicle is initially diffused from different sector locations in the cleft. These locations represent asymmetric initial distributions of acetylcholine molecules at the presynaptic membrane. Freeze fracture assays [3] have shown that acetylcholine can enter the NMJ at different locations on the presynaptic membrane, and the locations represented in the legend of Figure 5.15 simulate these events. The number of receptors opened by acetylcholine decreases as acetylcholine is emitted closer to the edge of the NMJ. This behavior is expected because more acetylcholine is lost to diffusion before it reacts with receptors when emitted close to the edge. The effects of simultaneously

emitting acetylcholine at different locations on the NMJ processes will be investigated in the future.
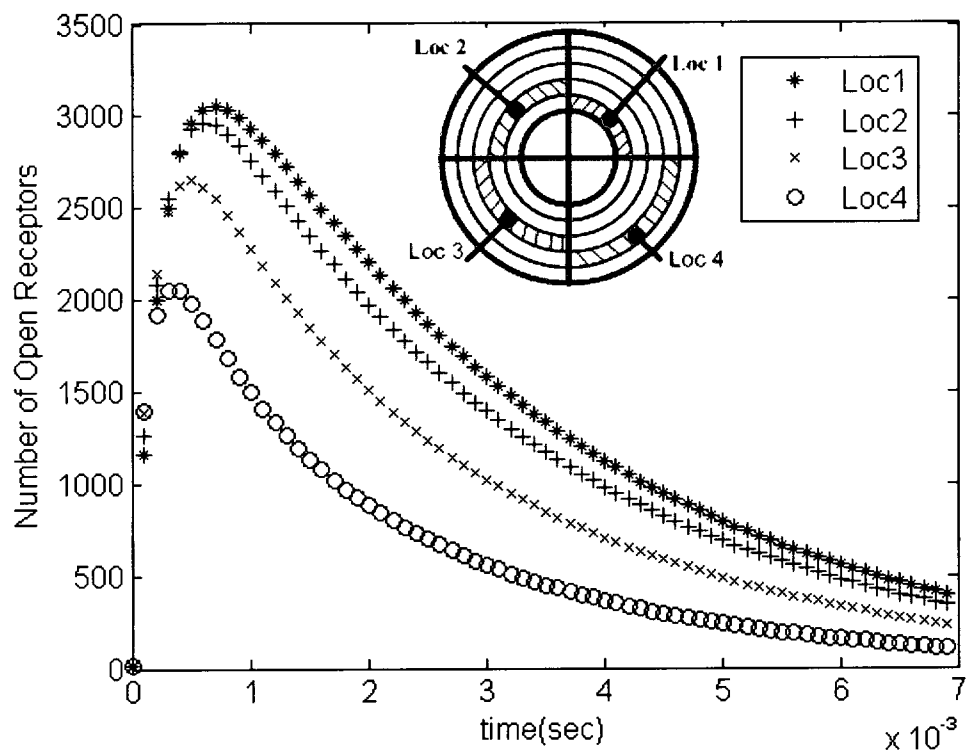
Figure 5.15 Sensitivity of open receptor dynamics to asymmetric Ach injection in different sectors.

CHAPTER 6

CONCLUSION AND FUTURE WORK

6.1 Conclusion

We have presented a novel finite difference scheme for solving a 1D diffusion equation with the Neumann boundary condition in cylindrical coordinates, which can be applied to neuromuscular junction problems. The new finite difference scheme is unconditionally stable, is second-order accurate, and efficiently computes solutions for the Neumann boundary near the zero coordinate. It has been tested against equations with a known analytical solution, and the results matched well with the analytic solution [63]. Also, it has been tested with equations that model real systems which have been simulated by other investigators, and the results match the simulated solutions of those published works in [65]-[68]. When parameters and dimensions which represent those of the real neuromuscular junction are used in our simulation, the results are supported by data collected from published experiments [10], [65]. Numerical results obtained here are relevant to physical reality and manage to capture a relevant portrayal of the actual process. Finally, our present scheme can be easily generalized to the multi-dimensional diffusion-reaction cases.

We have proposed a full 3D model of acetylcholine and acetylcholine receptor dynamics in the neuromuscular junction under conditions of inactivated enzyme.

An improved Crank-Nicolson finite difference scheme is presented for solving the 3D model with Neumann boundary condition in cylindrical coordinates. In particular, a new, stable and accurate finite difference scheme is developed for the Neumann boundary condition. The simulation analysis agrees well with experimental measurements of end-plate current, and it duplicates the open receptor results of earlier investigations. Sensitivity of the open receptor dynamics to the changes in the diffusion parameters has been studied. We present the first simulation of asymmetric emission of acetylcholine in the synaptic cleft and an analysis of the subsequent effects on open receptor population as a function of time. Results show that the population of open receptors decreases as acetylcholine is emitted closer to the edge of the NMJ.

Our 3D model is more accurate compared to Friboulet's 1D and Naka's 2D models under the conditions of completely inactivated enzyme. Our model tracks the experimental decay rate more closely than Friboulet and Naka. Friboulet's model underestimated the decay phase of the measured curve, while Naka overestimated. The Friboulet model and our simulation estimated the same peak value but Naka's model predicted a peak lower than the experimentally measured data. Our 3D model accurately overlaps with the experimental curve and simulates behavior which is closer to the true dynamics of transport-reaction in the NMJ.

6.2 Future Work

Future investigations will focus in-depth study of anisotropic diffusion in the cleft and asymmetric distribution of vesicles in the pre-synaptic membrane. Several anisotropic diffusion studies are suggested. These studies include simultaneous acetylcholine emissions at different locations on the presynaptic membrane and staggered

acetylcholine emissions. The established experimental technique of freeze fracture microscopy [3], [84], would provide a framework against which to compare simulation results, and the simulated detail resolved by the number of disks, annuli, and sectors would, in principle, be limited only by the available computing power.

It will also be possible to test this new numerical scheme with active enzyme in the NMJ. The addition of the acetylcholinesterase reactions to the cleft chemistry model would allow further comparisons with earlier simulations and experiments concerning NMJ processes from other investigations [55],[57].

The rise of terrorism has created an interest in the physiological consequences when humans are exposed to neurotoxins, especially nerve gases developed for military use, most of which are acetylcholinesterase inhibitors [85]-[93]. The process of acetylcholinesterase inhibition has been extensively studied. However, the science of regenerating the inhibited enzyme back to a functional state is advancing, and therapeutic protocols which address acetylcholinesterase inhibition exist. The *in vitro* kinetic models of this therapy are well established [94]-[99], but an effective therapy for living systems will require investigation of models that reflect a structure closer to that of the living systems. A model of the regeneration kinetics of acetylcholinesterase in the cleft using the model and numerical methods elucidated in this research is a step closer to that goal.

APPENDIX

SOURCE CODE IN FORTRAN OF THE NUMERICAL

METHOD

```fortran
C   1D    Code
C   Declaration of variables
C   and data structures
      DIMENSION u1(0:100001),
     & u2(0:100001),unew(0:100001
      DIMENSION r(0:100001),
     & rh(0:100001),s(1:100000)
      DIMENSION d(1:100001),
     & arph(0:100001),v(0:100001)
      DIMENSION a(1:100001),
     & b(1:100001),c(1:100001)
      DOUBLE PRECISION u1,u2,
     & c1,c2,da,rL,unew
      DOUBLE PRECISION a,b,c,d,
     & r,rh,beta,theta,arph,v,dt,dr
      DOUBLE PRECISION L_cleft,
     & pi,
C   Assignment of constants
      N=100
      nT=1;
      dt=1e-4
      sigma=0.001
      pi=3.14159265358979323846
      rL=5.5E-5
      L_cleft =0.55e-5
      da=2.0D-9
      theta=(3.0+sqrt(105.0))/12.0
      dr=rL/(N+theta-1.0)
      beta=dt/(dr*dr)
      w=1.0
      DO i=1,N
      r(i)=(i-1)*dr+theta*dr
      rh(i)=(i-0.5)*dr+theta*dr
      ENDDO
      rab=r(1)*theta/(rh(1)*(0.5*theta+1.0/3.0))
      c1=da*beta*rab*rh(1)
      c2=da*beta
C   initial condition
      DO i=1,N-1
       u1(i)=(1-r(i)*r(i))
      ENDDO
      u1(N)=0.0
      u2(N)=0.0

C   Begin time iteration
      nn=0
C   Begin Thomas Algorithm
      c(1)=(1.0+w)*c1
      a(1)=2.0*r(1)+(1.0+w)*c1
      b(1)=0.0
  1   d(1)=(2.0*r(1)-(1.0-
     & w)*c1)*u1(1)+(1.0-w)*c1*u1(2)
      DO i=2,N-1
      b(i)=(1.0+w)*c2*rh(i-1)
      a(i)=2.0*r(i)+(1.0+w)*c2*
     & (rh(i-1)+rh(i))
      c(i)=(1.0+w)*c2*rh(i)
      d(i)=(1.0-w)*c2*rh(i-1)*u1
     & (i-1)+(2.0*r(i)-(1.0-w)*c2*rh(i-1)
     & -(1.0-w)*c2*rh(i))*u1(i)
     & +(1.0-w)*c2*rh(i)*u1(i+1)
      ENDDO
      c(N-1)=0.0
      d(N-1)=d(N-1)+(1.0-w)*c2*
     & rh(N-1)*u2(N)
      arph(0)=0.0
      DO i=1,N-1
      arph(i)=c(i)/(a(i)-b(i)*arph(i-1))
      ENDDO
      v(0)=0.0
      DO i=1,N-1
      v(i)=(d(i)+b(i)*v(i-1))/(a(i)-b(i)*
     & arph(i-1))
      ENDDO
      unew(N)=0.0
      DO i=1,N-1
      m=N-i
      unew(m)=arph(m)*unew(m+1)+v(m)
      ENDDO
      DO i=1,N-1
      u2(i)=unew(i)
      ENDDO
C   Next time iteration
      nn=nn+1
      PRINT *,nn
      IF(nn.EQ.nT)GOTO 4
      DO i=1,N-1
      u1(i)=u2(i)
      ENDDO
      GOTO 1
C   Output
  4   OPEN(unit=6,file='result1.dat')
      DO i=1,N
       write(6,1000) r(i),u2(i)
      ENDDO
 1000   FORMAT(f18.10, e18.10)
      END
```

```fortran
C   Main Program "3D Reaction
&   Diffusion"
    DIMENSION u1(0:201,-1:201,1:201)
    DIMENSION u2(0:201,-1:201,1:201)
    DIMENSION u3(0:201,-1:201,1:201)
    DIMENSION u4(0:201,-1:201,1:201)
    DIMENSION u5(0:201,-1:201,1:201)
    DIMENSION u1ave(0:201,
&   -1:201,1:201)
    DIMENSION u2ave(0:201,
&   -1:201,1:201)
    DIMENSION u3ave(0:201,
&   -1:201,1:201)
    DIMENSION u4ave(0:201,
&   -1:201,1:201)
    DIMENSION u5ave(0:201,
&   -1:201,1:201)
    DIMENSION u0(0:201)
    DIMENSION constant1(0:201,
&   -1:201,1:201)

    DIMENSION constant2(0:201,
&   -1:201,1:201)
    DIMENSION constant3(0:201,
&   -1:201,1:201)

    DIMENSION u1n1(0:201,
&   -1:201,1:201),u1n2(0:201,-1:201,1:201)
    DIMENSION u1next(0:201,
&   -1:201,1:201)
    DIMENSION u2next(0:201,
&   -1:201,1:201)
    DIMENSION u3next(0:201,
&   -1:201,1:201)
    DIMENSION u4next(0:201,
&   -1:201,1:201)
    DIMENSION u5next(0:201,
&   -1:201,1:201)
    DIMENSION error(0:201,-1:201,1:201)
    DIMENSION r(0:201),rh(0:201),theta
&   (-1:201),z(1:201)
    DIMENSION areasec(0:201,
&   -1:201,1:201)
    DIMENSION volumesec(0:201,
&   -1:201,1:201)
    DOUBLE PRECISION
&   u1,u2,u3,rL,unew,u1n1,u1n2,u4,u5
    DOUBLE PRECISION
&   u1next,u2next,u3next,u4next,u5next
    DOUBLE PRECISION
&   r,rh,beta1,beta2,beta3,dt,dr,dtheta,dz
    DOUBLE PRECISION a,b,aa,bb
    DOUBLE PRECISION
&   theta1,theta2,pi,u20,constant1,constant2
    DOUBLE PRECISION constant3
    DOUBLE PRECISION dar,datheta,daz
    DOUBLE PRECISION
&   ckr12,ckr21,errormax,error,rth,c1,c2
    DOUBLE PRECISION
&   ckr34,ckr43,ckr56,ckr65
    DOUBLE PRECISION
&   rk1s1,rk1s2,rk1s3,rk1s4
    DOUBLE PRECISION
&   rk2s1,rk2s2,rk2s3,rk2s4
    DOUBLE PRECISION
&   rk3s1,rk3s2,rk3s3,rk3s4
    DOUBLE PRECISION
&   rk4s1,rk4s2,rk4s3,rk4s4
    DOUBLE PRECISION CHC1,sum1
    DOUBLE PRECISION
&   ts1,ts2,ts3,ts4,ts5,sumu1,sumu2,sumu3
    DOUBLE PRECISION sumu4,sumu5
    DOUBLE PRECISION
&   areasec,volumesec,psu1,
&   psu2,psu3,psu4,psu5
    DOUBLE PRECISION
&   u1ave,u2ave,u3ave,
&   u4ave,u5ave,u1initial
    integer iout
    parameter(iout=1000)
    character*255 myfilename
    number=0
C   Time Loop Start
    DO  ifn=1,3        ! filenameindex
    number= number+1
    IF  (ifn .EQ. 1) THEN
    dar=0.7e-6
    ENDIF
    IF  (ifn .EQ. 2) THEN
    dar=3.5e-7
    ENDIF
    IF  (ifn .EQ. 3) THEN
    dar=4.0e-7
    ENDIF
    DO k =  1,Kz
    DO j =  0, Jtheta
    DO i =  0, Ir
    u1(i,j,k)=0.0
    u2(i,j,k)=0.0
    u3(i,j,k)=0.0
    u4(i,j,k)=0.0
    u5(i,j,k)=0.0
    u1ave(i,j,k)=0.0
    u2ave(i,j,k)=0.0
    u3ave(i,j,k)=0.0
    u4ave(i,j,k)=0.0
    u5ave(i,j,k)=0.0
    constant1(i,j,k)=0.0
    constant2(i,j,k)=0.0
    constant3(i,j,k)=0.0
    u1n1(i,j,k)=0.0
    u1n2(i,j,k)=0.0
```

```
      u1next(i,j,k)=0.0
      u2next(i,j,k)=0.0
      u3next(i,j,k)=0.0
      u4next(i,j,k)=0.0
      u5next(i,j,k)=0.0
      ENDDO
      ENDDO
      ENDDO


      nT = 700000
C     Chemical Reaction
C     u1 is A,    u2 is R  u3 is AR
C     Time  increament
      dt=1e-8
C     Number of rings
      Ir= 25
C     Number of  sectors
      Jtheta=25
C     Number of  Disks
      Kz=25
C     pi value
      pi=3.14159265358979323846
C     Diffusion co-efficient along r
      datheta=dar
      daz=dar
      u1initial=1.55e-2
      u20=1.6725e-002
C     /(mole/litre) second
      ckr56=2.0e4
C     /second
C     ckr65=5.0e3
      ckr65=5.0e3
C     /(mole/litre) second
      ckr12=3.0e7
C     /second
      ckr21=1.0e4
C     /(mole/litre) second
      ckr34=ckr12
C     /second
      ckr43=ckr21
C     Diffusion co-efficient along r
C     datheta=2.0e-6
C     Diffusion co-efficient along r
C     daz=2.0e-6
C     Radious of the cleft   cm
      rL=5.0e-5
C     Thickness of cleft    cm
      rth=5.0e-6
C     radial increament
      dr=rL/Ir
C     angular increament
      dtheta=2.0*pi/Jtheta
C     transverse increament
      a=1.0
      b=0.5+sqrt(3.0)/3.0
```

```
      aa=a/b
      bb=a/b
      theta1=sqrt(3.0)/3.0
      theta2=sqrt(3.0)/3.0
      dz=rth/(Kz-1.0+theta1+theta2)
      beta1= dt/(dr*dr)
      beta2= dt/(dtheta*dtheta)
      beta3= dt/(dz*dz)
C     Axial  vector
      DO  i = 0, Ir
      r(i) = i*dr
      ENDDO
      DO  i = 1, Ir
      rh(i)=(i-1)*dr+0.5*dr
      ENDDO
C     Angular  Vector
      DO  j = 0, Jtheta
      theta(j) = j*dtheta
      ENDDO
C     Transverse  Vector
      DO  k = 1, Kz
      z(k) = theta1*dz+(k-1)*dz
      ENDDO
C     u1  initial  condition
      DO  k = 1,1
      DO  j = 0, Jtheta-1
      DO  i = 1, Ir-1
      u1(i,j,k) =u1initial      !0.8875e-2
      ENDDO
      ENDDO
      ENDDO
      DO  k = Kz,Kz
      DO  j = 0, Jtheta-1
      DO  i = 0, Ir
      u2(i,j,k) = u20
      ENDDO
      ENDDO
      ENDDO
C     u3  initial  condition
      DO  k = 1,Kz
      DO  j = 0, Jtheta-1
      DO  i = 0, Ir
      u3(i,j,k) = 0.0
      ENDDO
      ENDDO
      ENDDO

C     Step 1
C     Value at the outermost ring is known = 0
      DO  k = 1,Kz
      DO  j = 0,Jtheta-1
      u1(Ir,j,k) = 0.0
      ENDDO
      ENDDO
      DO  k = 1,Kz
      DO  i = 1, Ir-1
```

```
        u1(i,-1,k)= u1(i,Jtheta-1,k)
        u1(i,Jtheta,k)=u1(i,0,k)
        ENDDO
        ENDDO
        DO k = 1,Kz
        DO i = 1, Ir
        u2(i,-1,k)= u1(i,Jtheta-1,k)
        u2(i,Jtheta,k)=u1(i,0,k)
        ENDDO
        ENDDO
        DO k = 1,Kz
        DO i = 1, Ir
        u3(i,-1,k)= u1(i,Jtheta-1,k)
        u3(i,Jtheta,k)=u1(i,0,k)
        ENDDO
        ENDDO
        nn=0
11      DO k = 1,Kz
        DO j = -1,Jtheta
        DO i = 1,Ir
        u1n1(i,j,k) = u1(i,j,k)

        ENDDO
        ENDDO
        ENDDO
C       Zero Point Solution
        DO k = 1,Kz
        sum1=0.0
        DO j = 0, Jtheta-1
        sum1=(sum1+u1(1,j,k))
        ENDDO
        u0(k)=sum1/Jtheta
        ENDDO
        It =0
        DO k = 1,Kz
        DO j = 0, Jtheta-1
        u1n1(0,j,k)=u0(k)
        u1(0,j,k) =u0(k)
        ENDDO
        ENDDO
C   1   RK loop
1       DO k = 1,Kz
        DO j = -1, Jtheta
        DO i = 0, Ir
C       -------------------
        rk1s1= dt*
     &  ((-2.0*ckr12*(u1n1(i,j,k)
     &  +u1(i,j,k))/2.0)*u2(i,j,k) +
     &  ckr21*( u3(i,j,k)))

        rk1s2= dt*
     &  (( 2.0*ckr12*(u1n1(i,j,k)
     &  +u1(i,j,k))/2.0)*u2(i,j,k)
     &  - ckr21*( u3(i,j,k))
     &  - ckr34*((u1n1(i,j,k)+
     &  u1(i,j,k))/2.0)*u3(i,j,k)
```

```
     &  + 2.0*ckr43*u4(i,j,k) )
        rk1s3= dt*(ckr34*((u1n1(i,j,k)
     &  +u1(i,j,k))/2.0)*u3(i,j,k)
     &  - 2.0*ckr43*u4(i,j,k)
     &  - ckr56*u4(i,j,k)+ ckr65*u5(i,j,k) )
        rk1s4= dt*(ckr56*u4(i,j,k)
     &  -ckr65*u5(i,j,k) )
        rk2s1= dt*((-2.0*ckr12*
     &  (u1n1(i,j,k)+u1(i,j,k))
     &  /2.0)*(u2(i,j,k) +rk1s1/2.0)
     &  + ckr21*(u3(i,j,k)+rk1s1/2.0))
        rk2s2= dt*((2.0*ckr12*
     &  (u1n1(i,j,k)+u1(i,j,k))
     &  /2.0)*(u2(i,j,k) +rk1s2/2.0)
     &  - ckr21*(u3(i,j,k)+rk1s2/2.0)
     &  - ckr34*((u1n1(i,j,k)+u1(i,j,k))
     &  /2.0)*(u3(i,j,k)+rk1s2/2.0)
     &  + 2.0*ckr43*(u4(i,j,k)+rk1s2/2.0))
        rk2s3= dt*(ckr34*((u1n1(i,j,k)
     &  +u1(i,j,k))/2.0)*(u3(i,j,k) +rk1s2/2.0)
     &  - 2.0*ckr43*(u4(i,j,k)+rk1s2
     &  /2.0) - ckr56*(u4(i,j,k)+rk1s2/2.0)
     &  + ckr65*(u5(i,j,k)+rk1s2/2.0) )
        rk2s4= dt*(ckr56*(u4(i,j,k)+rk1s2
     &  /2.0) -ckr65*(u5(i,j,k)+rk1s2/2.0) )
        rk3s1=dt*((2.0*ckr12*(u1n1(i,j,k)
     &  +u1(i,j,k))/2.0)*(u2(i,j,k) +rk2s1/2.0)
     &  + ckr21*(u3(i,j,k)+rk2s1/2.0))
        rk3s2=dt*((2.0*ckr12*(u1n1(i,j,k)+u1(i,j,k))
     &  /2.0) *(u2(i,j,k) +rk2s2/2.0)
     &  - ckr21*(u3(i,j,k)+rk2s2/2.0)
     &  - ckr34*((u1n1(i,j,k)+u1(i,j,k))/2.0)*
     &  (u3(i,j,k)+rk2s2/2.0)
     &  + 2.0*ckr43*(u4(i,j,k)+rk2s2/2.0) )
        rk3s3= dt*(ckr34*((u1n1(i,j,k)
     &  +u1(i,j,k))/2.0)*(u3(i,j,k) +rk2s3/2.0)
     &  - 2.0*ckr43*(u4(i,j,k)+rk2s3/2.0)
     &  - ckr56*(u4(i,j,k)+rk2s3/2.0)
     &  + ckr65*(u5(i,j,k)+rk2s3/2.0) )
        rk3s4= dt*(ckr56*(u4(i,j,k)+rk2s4
     &  /2.0) -ckr65*(u5(i,j,k)+rk2s4/2.0) )
        rk4s1= dt*((-2.0*ckr12*(u1n1(i,j,k)+
     &  u1(i,j,k))/2.0)*(u2(i,j,k)
     &  +rk3s1) + ckr21*(u3(i,j,k)+rk3s1))
        rk4s2= dt*((2.0*ckr12*
     &  (u1n1(i,j,k)+u1(i,j,k))/2.0)
     &  *(u2(i,j,k)+rk3s2)
     &  - ckr21*(u3(i,j,k)+rk3s2)
     &  - ckr34*((u1n1(i,j,k)+u1(i,j,k))
     &  /2.0)*(u3(i,j,k)+rk3s2)
     &  + 2.0*ckr43*(u4(i,j,k)+rk3s2))
        rk4s3= dt*(ckr34*((u1n1(i,j,k)
     &  +u1(i,j,k))/2.0)*(u3(i,j,k) +rk3s3)
     &  - 2.0*ckr43*(u4(i,j,k)+rk3s3)
     &  - ckr56*(u4(i,j,k)+rk3s3)
     &  + ckr65*(u5(i,j,k)+rk3s3) )
```

```
        rk4s4= dt*(ckr56*(u4(i,j,k)+rk3s4)
     &  -ckr65*(u5(i,j,k)+rk3s4) )
        u2next(i,j,k)=u2(i,j,k)+(rk1s1+2.0*rk2s1
     &  +2.0*rk3s1+rk4s1)/6.0
        u3next(i,j,k)=u3(i,j,k)+(rk1s2+2.0*rk2s2
     &  +2.0*rk3s2+rk4s2)/6.0
        u4next(i,j,k)=u4(i,j,k)+(rk1s3+2.0*rk2s3
     &  +2.0*rk3s3+rk4s3)/6.0
        u5next(i,j,k)=u5(i,j,k)+(rk1s4+2.0*rk2s4
     &  +2.0*rk3s4+rk4s4)/6.0
        ENDDO
        ENDDO
        ENDDO
        DO k = 1,Kz
        DO j = -1, Jtheta
        DO i = 0, Ir
        constant1(i,j,k)= ( u2next(i,j,k)
     &  + u2(i,j,k) )/2.0
        ENDDO
        ENDDO
        ENDDO
        DO k = 1,Kz
        DO j = -1, Jtheta
        DO i = 0, Ir
        constant2(i,j,k)= ( u3next(i,j,k)
     &  + u3(i,j,k) )/2.0
        ENDDO
        ENDDO
        ENDDO
        DO k = 1,Kz
        DO j = -1, Jtheta
        DO i = 0, Ir
        constant3(i,j,k)= ( u4next(i,j,k)
     &  + u4(i,j,k) )/2.0
        ENDDO
        ENDDO
        ENDDO
        k=1
        DO j = 0, Jtheta-1
        DO i = 1, Ir-1
        CHC1= (2.0*r(i)+beta1*dar*(rh(i+1)+rh(i)))
     &  + 2.0*beta2*datheta/r(i)+beta3*r(i)
     &  *daz*aa
     &  + 2.0*dt*r(i)*ckr12*constant1(i,j,k)
     &  + 1.0*dt*r(i)*ckr34*constant2(i,j,k)
        uln2(i,j,k)=( beta1*dar*rh(i+1)*uln1
     &  (i+1,j,k&)+beta1*dar*rh(i)*uln1(i-1,j,k)
     &  +beta2*datheta/r(i)*(uln1(i,j+1,k)
     &  +uln1(i,j-1,k))+aa*beta3*r(i)*daz
     &  *uln1(i,j,2)
     &  +beta1*dar*(rh(i+1)*(ul(i+1,j,k)
     &  -ul(i,j,k))-rh(i)*(ul(i,j,k)-ul(i-1,j,k)))
     &  +beta2*datheta/r(i)*(ul(i,j+1,k)
     &  -2.0*ul(i,j,k)+ul(i,j-1,k))
     &  +aa*(beta3*daz*r(i))*(ul(i,j,2)
     &  -ul(i,j,k)) -2.0*dt*r(i)*ckr12*

     &  constant1(i,j,k)*ul(i,j,k)
     &  +2.0*dt*r(i)*ckr21*constant2(i,j,k)
     &  -1.0*dt*r(i)*ckr34*constant2(i,j,k)
     &  *ul(i,j,k)
     &  +4.0*dt*r(i)*ckr43*constant3(i,j,k)
     &  +2.0*r(i)*ul(i,j,k))*1/CHC1
        ENDDO
        ENDDO
        k=Kz
        DO j = 0, Jtheta-1
        DO i = 1, Ir-1
        CHC1= (2.0*r(i)+beta1*dar*(rh(i+1)
     &  +rh(i)))
     &  + 2.0*beta2*datheta/r(i)+1.0*beta3*r(i)
     &  *daz*bb + 2.0*dt*r(i)*ckr12*constant1
     &  (i,j,k)+1.0*dt*r(i)*ckr34*constant2(i,j,k)
        uln2(i,j,k)=(beta1*dar*rh(i+1)*uln1
     &  (i+1,j,k)+beta1*dar*rh(i)*uln1(i-1,j,k)
     &  +beta2*datheta/r(i)*(uln1(i,j+1,k)
     &  +uln1(i,j-1,k))+bb*beta3*r(i)*daz
     &  *uln1(i,j,k-1)
     &  + beta1*dar*(rh(i+1)*(ul(i+1,j,k)
     &  -ul(i,j,k)) -rh(i)*(ul(i,j,k)-ul(i-1,j,k)))
     &  +beta2*datheta/r(i)*(ul(i,j+1,k)
     &  -2.0*ul(i,j,k)+ul(i,j-1,k))
     &  -bb*beta3*daz*r(i)*(ul(i,j,k)
     &  -ul(i,j,k-1))
     &  -2.0*dt*r(i)*ckr12*constant1(i,j,k)
     &  *ul(i,j,k)+2.0*dt*r(i)*ckr21
     &  *constant2(i,j,k)
     &  -1.0*dt*r(i)*ckr34*constant2(i,j,k)
     &  *ul(i,j,k)+4.0*dt*r(i)*ckr43
     &  *constant3(i,j,k)
     &  +2.0*r(i)*ul(i,j,k) ) *1/CHC1
        ENDDO
        ENDDO
        DO k = 2,Kz-1
        DO j = 0, Jtheta-1
        DO i = 1, Ir-1
        CHC1= (2.0*r(i)+beta1*dar*(rh(i+1)
     &  +rh(i)))
     &  + 2.0*beta2*datheta/r(i)+2.0*beta3
     &  *r(i)*daz + 2.0*dt*r(i)*ckr12
     &  *constant1(i,j,k)
     &  + 1.0*dt*r(i)*ckr34*constant2(i,j,k)
        uln2(i,j,k)=( beta1*dar*rh(i+1)
     &  *uln1(i+1,j,k) +beta1*dar*rh(i)
     &  *uln1(i-1,j,k)
     &  +beta2*datheta/r(i)*(uln1(i,j+1,k)
     &  +uln1(i,j-1,k))
     &  +beta3*r(i)*daz*(uln1(i,j,k+1)+
     &  uln1(i,j,k-1)) + beta1*dar*(rh(i+1)
     &  *(ul(i+1,j,k)-ul(i,j,k))
     &  -rh(i)*(ul(i,j,k)-ul(i-1,j,k)))
     &  +beta2*datheta/r(i)
     &  *(ul(i,j+1,k)-2.0*ul(i,j,k)+ul(i,j-1,k))
```

```
&      +beta3*daz*r(i)
&      *(u1(i,j,k+1)-2.0*u1(i,j,k)+u1(i,j,k-1))
&      -2.0*dt*r(i)*ckr12*constant1(i,j,k)
&      *u1(i,j,k) +2.0*dt*r(i)*ckr21
&      *constant2(i,j,k)
&      -1.0*dt*r(i)*ckr34*constant2(i,j,k)
&      *u1(i,j,k) +4.0*dt*r(i)*ckr43
&      *constant3(i,j,k)
&      +2.0*r(i)*u1(i,j,k)  ) *1/CHC1
       ENDDO
       ENDDO
       ENDDO
       DO  k = 1,Kz
       DO  i = 1, Ir-1
       uln2(i,-1,k)= uln2(i,Jtheta-1,k)
       uln2(i,Jtheta,k)=uln2(i,0,k)
       ENDDO
       ENDDO
       DO  k = 1,Kz
       sum1=0.0
       DO  j = 0, Jtheta-1
       sum1=(sum1+uln2(1,j,k))
       ENDDO
       u0(k)=sum1/Jtheta
       ENDDO
       DO  k = 1,Kz
       DO  j = 0, Jtheta-1
       uln2(0,j,k)=u0(k)

       ENDDO
       ENDDO
C      Find maximum error
       DO  k = 1,Kz
       DO  j = 0, Jtheta-1
       DO  i = 1, Ir-1
       error(i,j,k)=abs(uln2(i,j,k)-uln1(i,j,k))
       ENDDO
       ENDDO
       ENDDO
       errormax=0.00000001
        DO  i = 1, Ir-1
        DO  j = 0, Jtheta-1
        DO  k = 1,Kz
        IF   (error(i,j,k) .GT. errormax) then
           errormax = error(i,j,k)
       ENDIF
       ENDDO
       ENDDO
       ENDDO
       IF  (errormax .LT. 1.0e-6) GOTO 2
       DO  k = 1,Kz
       DO  j = -1, Jtheta
       DO  i = 1, Ir-1

       uln1(i,j,k)=uln2(i,j,k)
       ENDDO
```

```
       ENDDO
       ENDDO
       It=It+1
       GOTO 1
 2     nn=nn+1
       DO  k = 1,Kz
       DO  j = -1, Jtheta
       DO  i = 1, Ir-1
       u1(i,j,k)=uln2(i,j,k)
       ENDDO
       ENDDO
       ENDDO
       DO  k = 1,Kz
       DO  j = -1, Jtheta
       DO  i = 0, Ir
       u2(i,j,k) = u2next(i,j,k)
       u3(i,j,k) = u3next(i,j,k)
       u4(i,j,k) = u4next(i,j,k)
       u5(i,j,k) = u5next(i,j,k)
       ENDDO
       ENDDO
       ENDDO
       PRINT *,nn

C      Avarage for u1  start
       DO  k=1,Kz
       DO  i=1,Ir
       DO  j=0,Jtheta-1
       IF (i .EQ. 1) THEN
       IF ((j .GE. 0 ) .AND. (j .LT. Jtheta-1 ))
&      THEN
       areasec(i,j,k)=(1.0/2.0)*dtheta*dr*dr
       volumesec(i,j,k)=(1.0/2.0)*dtheta*dr*dr*dz
C      u2(i,Jtheta,k)=u2(i,0,k)
       u1ave(i,j,k) = ((u1(0,j,k) + u1(i,j,k)
&      + u1(i,j+1,k))/3.0) *areasec(i,j,k)*dz
       ENDIF
       IF (j .EQ. Jtheta-1 ) THEN
       areasec(i,j,k)=(1.0/2.0)*dtheta*dr*dr
       volumesec(i,j,k)=(1.0/2.0)*dtheta*dr*dr*dz
       u1ave(i,j,k) = ((u1(0,j,k) + u1(i,j,k)
&      + u1(i,0,k))/3.0) *areasec(i,j,k) *dz
       ENDIF
       ENDIF
       IF (i .GT. 1) THEN
       IF ((j .GE. 0 ) .AND. (j .LT. Jtheta-1 ))
&      THEN
       areasec(i,j,k)=(1.0/2.0)*dtheta*dr*dr*(2
&      *i-1)
       volumesec(i,j,k)=(1.0/2.0)*dtheta*dr*dr*
&      (2*i-1)*dz
       u1ave(i,j,k) = ((u1(i-1,j,k) + u1
&      (i-1,j+1,k) + u1(i,j,k)+ u1(i,j+1,k))
&      /4.0) *areasec(i,j,k)*dz
       ENDIF
```

```fortran
         IF (j .EQ. Jtheta-1 ) THEN
         areasec(i,j,k)=(1.0/2.0)*dtheta*dr*dr*
     &   (2*i-1)
         volumesec(i,j,k)=(1.0/2.0)*dtheta*dr*dr*
     &   (2*i-1)*dz
         u1ave(i,j,k) = ((u1(i-1,j,k) + u1
     &   (i-1,0,k)+ u1(i,j,k)+ u1(i,0,k))/4.0)
     &   *areasec(i,j,k) *dz
         ENDIF
         ENDIF
         ENDDO
         ENDDO
         ENDDO
C    Avarage for u1  End
C    U1   End   Here !!!!!!!!!!!!
C    Time avarage for u2,u3,u4,u5  start
C    -------------------------------
         DO  k=Kz,Kz
         DO  i=1,Ir
         DO  j=0,Jtheta-1
         IF (i .EQ. 1) THEN
         IF ((j .GE. 0 ) .AND. (j .LT. Jtheta-1 ))
     &   THEN
         areasec(i,j,k)=(1.0/2.0)*dtheta*dr*dr
         volumesec(i,j,k)=(1.0/2.0)*dtheta*dr*dr*dz
         u2ave(i,j,k) = ((u2(0,j,k) + u2(i,j,k)
     &   + u2(i,j+1,k))/3.0) *areasec(i,j,k)
     &   *dz*1.0
         u3ave(i,j,k) = ((u3(0,j,k) + u3(i,j,k)
     &   + u3(i,j+1,k))/3.0)
     &   *areasec(i,j,k)*dz*1.0
         u4ave(i,j,k) = ((u4(0,j,k)
     &   + u4(i,j,k) + u4(i,j+1,k))/3.0)
     &   *areasec(i,j,k) *dz*1.0
         u5ave(i,j,k) = ((u5(0,j,k) + u5(i,j,k)
     &   + u5(i,j+1,k))/3.0) *areasec(i,j,k)
     &   *dz*1.0
         ENDIF
         IF (j .EQ. Jtheta-1 ) THEN
         areasec(i,j,k)=(1.0/2.0)*dtheta*dr*dr
         volumesec(i,j,k)=(1.0/2.0)*dtheta*dr*dr*dz
         u2ave(i,j,k) = ((u2(0,j,k) + u2(i,j,k)
     &   + u2(i,0,k))/3.0) *areasec(i,j,k) *dz*1.0
         u3ave(i,j,k) = ((u3(0,j,k) + u3(i,j,k)
     &   + u3(i,j+1,k))/3.0)
     &   *areasec(i,j,k)*dz*1.0
         u4ave(i,j,k) = ((u4(0,j,k) + u4(i,j,k)
     &   + u4(i,j+1,k))/3.0)*areasec(i,j,k)*dz*1.0
         u5ave(i,j,k) = ((u5(0,j,k) + u5(i,j,k)
     &   + u5(i,j+1,k))/3.0)*areasec(i,j,k)*dz*1.0
         ENDIF
         ENDIF
         IF (i .GT. 1) THEN
         IF ((j .GE. 0 ) .AND. (j .LT. Jtheta-1 ))
     &   THEN
         areasec(i,j,k)=(1.0/2.0)*dtheta*dr*dr*

         (2*i-1)
         volumesec(i,j,k)=(1.0/2.0)*dtheta*dr*dr*
     &   (2*i-1)*dz
         u2ave(i,j,k) = ((u2(i-1,j,k) + u2
     &   (i-1,j+1,k) + u2(i,j,k)+ u2(i,j+1,k))
     &   /4.0) *areasec(i,j,k)
     &   *dz*1.0
         u3ave(i,j,k) = ((u3(i-1,j,k) + u3
     &   (i-1,j+1,k) + u3(i,j,k)+ u3(i,j+1,k))
     &   /4.0) *areasec(i,j,k)
     &   *dz*1.0
         u4ave(i,j,k) = ((u4(i-1,j,k) + u4
     &   (i-1,j+1,k) + u4(i,j,k)+ u4(i,j+1,k))
     &   /4.0) *areasec(i,j,k)
     &   *dz*1.0
         u5ave(i,j,k) = ((u5(i-1,j,k) + u5
     &   (i-1,j+1,k) + u5(i,j,k)+ u5(i,j+1,k))
     &   /4.0) *areasec(i,j,k)
     &   *dz*1.0
         ENDIF
         IF (j .EQ. Jtheta-1 ) THEN
         areasec(i,j,k)=(1.0/2.0)*dtheta*dr*dr*
     &   (2*i-1)
         volumesec(i,j,k)=(1.0/2.0)*dtheta*dr*dr*
     &   (2*i-1)*dz
         u2ave(i,j,k) = ((u2(i-1,j,k) + u2(i-1,0,k)
     &   + u2(i,j,k)+ u2(i,0,k))/4.0)
     &   *areasec(i,j,k)*dz*1.0
         u3ave(i,j,k) = ((u3(i-1,j,k) + u3
     &   (i-1,j+1,k) + u3(i,j,k)+
     &   u3(i,j+1,k))/4.0)*areasec(i,j,k)
     &   *dz*1.0
         u4ave(i,j,k) = ((u4(i-1,j,k) + u4
     &   (i-1,j+1,k) + u4(i,j,k)+ u4(i,j+1,k))
     &   /4.0) *areasec(i,j,k)
     &   *dz*1.0
         u5ave(i,j,k) = ((u5(i-1,j,k) + u5
     &   (i-1,j+1,k)+ u5(i,j,k)+ u5(i,j+1,k))
     &   /4.0) *areasec(i,j,k)
     &   *dz*1.0
         ENDIF
         ENDIF
         ENDDO
         ENDDO
         ENDDO
C    Time avarage for u2  End
C    Volume  start here   Volume start
         DO  k=1,Kz
         DO  i=1,Ir
         DO  j=0,Jtheta-1
         IF (i .EQ. 1) THEN
         IF ((j .GE. 0 ) .AND. (j .LT. Jtheta-1 ))
     &   THEN
         areasec(i,j,k)=(1.0/2.0)*dtheta*dr*dr
         volumesec(i,j,k)=(1.0/2.0)*dtheta*dr*dr*dz
         ENDIF
```

```
         IF (j .EQ. Jtheta-1 ) THEN
         areasec(i,j,k)=(1.0/2.0)*dtheta*dr*dr
         volumesec(i,j,k)=(1.0/2.0)*dtheta*dr*dr*dz
         ENDIF
         ENDIF
         IF (i .GT. 1) THEN
         IF ((j .GE. 0 ) .AND. (j .LT. Jtheta-1 ))
    &    THEN
         areasec(i,j,k)=(1.0/2.0)*dtheta*dr*dr*
    &    (2*i-1)
         volumesec(i,j,k)=(1.0/2.0)*dtheta*dr*dr*
    &    (2*i-1)*dz
         ENDIF
         IF (j .EQ. Jtheta-1 ) THEN
         areasec(i,j,k)=(1.0/2.0)*dtheta*dr*dr*
    &    (2*i-1)
         volumesec(i,j,k)=(1.0/2.0)*dtheta*dr*dr*
    &    (2*i-1)*dz
         ENDIF
         ENDIF
         ENDDO
         ENDDO
         ENDDO
C    ---------------------------
C    Volume  End
         if (mod(nn,iout).eq.0) then
         sumu1=0.0
         sumu2=0.0
         sumu3=0.0
         sumu4=0.0
         sumu5=0.0
         cvol =0.0
         DO  k=1,Kz
         DO  i=1,Ir
         DO  j=0,Jtheta-1
         sumu1=u1ave(i,j,k)+sumu1
         cvol=volumesec(i,j,k)+cvol
         ENDDO
         ENDDO
         ENDDO

         DO  k=Kz,Kz
         DO  i=1,Ir
         DO  j=0,Jtheta-1
         sumu2=u2ave(i,j,k)+sumu2
         sumu3=u3ave(i,j,k)+sumu3
         sumu4=u4ave(i,j,k)+sumu4
         sumu5=u5ave(i,j,k)+sumu5
         ENDDO
         ENDDO
         ENDDO
C    open (file='test1.dat', unit=number)
         write(myfilename,100) number
100      format('file_',i3.3,'.dat')
         open (file=myfilename, unit=number)

         write(number,1000) dt*nn,sumu1,
    &    sumu2,sumu3,sumu4,sumu5,
    &    sumu1*6.02e23*1.0e-
    &    3,sumu2*6.02e23*1.0e-
    &    3,sumu3*6.02e23*1.0e-3,
    &    sumu4*6.02e23*1.0e-
    &    3,sumu5*6.02e23*1.0e-3,
    &    psu1,psu2,psu3,psu4,psu5
1000     FORMAT(e18.10,e18.10,e18.10,e18.10,
    &    e18.10,e18.10,
    &    e18.10,e18.10,e18.10,
    &    e18.10,e18.10,
    &    e18.10,e18.10,e18.10,e18.10,e18.10)
C    IF(nn.EQ.nT)GOTO 4
         endif

         IF(nn.EQ.nT) CLOSE(number)
         IF(nn.EQ.nT) GOTO 4

         GOTO 11
C    Time Loop END
4        ENDDO

C    Program END  Statement
         END
```

REFERENCES

[1]   Aidley, D., *The Physiology of Excitable Cells*, 4th Ed., New York: Cambridge University Press, 1998, pp. 107-128.

[2]   Kandel, E., *Principles of Neuroscience*, 4th Ed., New York: McGraw-Hill, 2000, pp. 258-268

[3]   Matthews, G., *Cellular Physiology of Nerve and Muscle,* 2nd Ed., Boston: Blackwell Scientific Publications, 1991, pp. 113-134.

[4]   Junge, D., *Nerve and Muscle Excitation*, Sunderland: Sinauer Associates Inc., 1992, pp. 7-22.

[5]   Purves, D., *Neuroscience*, 4th Ed., Sunderland: Sinauer Associates Inc., 2007, pp. 69-161.

[6]   Levitan, I., *The Neuron: Cell and molecular biology*, New York: Oxford University Press, 1997, pp. 47-195.

[7]   Weiss, T., *Cellular Biophysics*, Cambridge: The MIT Press, 1996, pp. 351-455.

[8]   Johnston, D., and Mao-Sin Wu, Samuel, *Foundations of Cellular Neurophysiology*, Cambridge: The MIT Press, 1995, pp. 287-422.

[9]   Miledi, R., Molenaar, P. C., and Polak, R. L., "Acetylcholinesterase activity in intact and homogenized skeletal muscle of the frog," *Journal of Physiology*, vol. 349, pp. 663-686, 1984.

[10]   Hartzell, H. C., and Kuffler, S. W., "Post-synaptic potentiation: interaction between quanta of acetylcholine at the skeletal neuromuscular synapse," *Journal of Physiology*, vol. 251, pp. 427-463, 1975.

[11]   Margolis, H., *Patterns, Thinking, and Cognition: A theory of judgment*, Chicago: University Of Chicago Press, 1990, pp. 1-339.

[12]   Davies, E., "Intercellular and intracellular signals and their transduction via the plasma me," *Seminars in Cell Biology*, vol. 4, pp. 139-147, 1993.

[13]   Bialek, W., and Setayeshgar, S., "Physical limits to biochemical signaling," *Proceedings of the National Academy of Sciences*, vol. 102, pp. 10040-10045, 2005.

[14]   Fowler, A. C., *Mathematical Models in the Applied Sciences*, Cambridge: Cambridge University Press, 1997, pp. 10-424.

[15]   Basmadjian, D., *The Art of Modeling in Science and Engineering*, Boca Raton: Chapman & Hall, 1999, pp. 1-509.

[16]   Jerome, J. W., Ed., *Modeling and Computation for Applications in Mathematics, Science, and Engineering*, New York: Oxford University Press, 1998, pp 1-232.

[17]   Murray, J. D., *Mathematical Biology*, New York: Springer-Verlag, 1989, pp 200-736.

[18]   Konopka, A., *Systems Biology*, Boca Raton: CRC Press, 2007, pp. 1-256.

[19]   Truskey, G. A., *Transport Phenomena in Biological Systems*, Prentice Hall, 2004, pp. 346-398.

[20]   Lester, H., "The response to acetylcholine," *Scientific American*, vol. 236, no. 2, pp. 106-117, 1977.

[21] Beers, W. H., and Reich, E., "Structure and activity of acetylcholine," *Nature*, vol. 228, pp. 917-921, 1970.

[22] Barry, P., and Lynch, J., "Ligand-gated channels," *IEEE Transactions on Nanobioscience*, vol. 4, pp. 70-80, 2005.

[23] Mathie, A. and Cull-Candy, S. G., "Conductance and kinetic properties of single nicotinic acetylcholine receptor channels in rat sympathetic neurons," *Journal of Physiology*, vol. 439, pp. 717-750, 1991.

[24] Jackson, M. B., "Perfection of a synaptic receptor: kinetics and energetic of the acetycholine receptor," *Proceedings of the National Academy of Sciences*, vol. 86, pp. 2199-2203, 1989.

[25] Hess, G., and Andrews, J., "Functional acetylcholine receptor-electroplax membrane microsacs: Purification and characterization," *Proceedings of the National Academy of Sciences*, vol. 74, pp. 482-486, 1977.

[26] Katz, B., and Miledi, R., "The binding of acetylcholine to receptors and its removal from the synaptic cleft," *Journal of Physiology*, vol. 231, pp. 549-574, 1973.

[27] Dudai, Y., "Molecular structures of acetylcholinesterase from electric organ tissue of the electric eel," *Proceedings of the National Academy of Sciences*, vol. 70, pp. 2473-2476, 1973.

[28] Cooper, J.R., *The Biochemical Basis of Neuropharmacology*, Oxford: Oxford University Press, 1996.

[29]   Rosenberry, T. L., "Purification of acetylcholinesterase by affinity chromatography and determination of active site stoichiometry," *Journal of Biological Chemistry*, vol. 247, pp. 1555-1565, 1972.

[30]   Krohn, K., "Interpreting enzyme and receptor kinetics: keeping it simple, but not too simple," *Nuclear Medicine and Biology*, vol. 30, pp. 819-826, 2003.

[31]   Grunhagen, H., Iwatsubo, M., and Changeux, J., "Fast Kinetic studies on the interaction of cholinergic agonists with membrane-bound acetylcholine receptor from *Torpedo maramorta* as revealed by quinacrine fluorescence," *European Journal of Biochemistry*, vol. 80, pp. 225-242, 1977.

[32]   Cornish-Bowden, A., *Fundamentals of Enzyme Kinetics*, Portland: Portland Press, 2004, pp. 1-343.

[33]   Schulz, G. E., *Principles of Protein Structure*, New York: Springer-Verlag, 1979, pp. 45-336.

[34]   Koshland, D., "Application of a theory of enzyme specificity to protein synthesis," *Proceedings of the National Academy of Sciences*, vol. 44, pp. 98-104, 1958.

[35]   Magleby, K. L., Terrar, D. A., "Factors affecting the time course of decay of end-plate currents: A possible cooperative action of acetylcholine on receptors at the neuromuscular junction," *Journal of Physiology*, vol. 244, pp. 467-495, 1975.

[36]   Chang, R., *Chemistry*, 6th Ed., New York: McGraw-Hill, 1998, pp. 1-1133.

[37]   McQuarrie, D., *General Chemistry*, New York: W. H. Freeman and Company, 1984, pp. 1-690.

[38]   McQuarrie, D., *Physical Chemistry: A molecular approach*, Sausalito: University Science Books, 1997, pp. 1-1360.

[39]   Kordas, M., "An attempt at an analysis of the factors determining the time course of the end-plate current," *Journal of Physiology*, vol. 224, pp. 333-348, 1972.

[40]   Magleby, K. L., Terrar, D. A., "Factors affecting the time course of decay of end-plate currents: A possible cooperative action of acetylcholine on receptors at the neuromuscular junction," *Journal of Physiology*, vol. 244, pp. 467-495, 1975.

[41]   Anderson, C. R., and Stevens, C. F., "Voltage clamp analysis of acetylcholine produced end-plate current fluctuations at frog neuromuscular junction," *Journal of Physiology*, vol. 235, pp. 655-691, 1973.

[42]   Magleby, K., and Stevens, C., "The effect of voltage on the time course of end-plate currents," vol. 223, *Journal of Physiology*, pp. 151-171, 1972.

[43]   Faber, D., "Intrinsic quantal variability due to stochastic properties of receptor-transmitter interactions," *Science*, vol. 258, pp. 1494-1498, 1992.

[44]   Katz, B., "The statistical nature of the acetylcholine potential and its molecular components," *Journal of Physiology*, vol. 224, pp. 665-699, 1972.

[45]   Madsen, B. W., Edeson, R. O., Lam, H. S., and Milne, R. K., "Numerical simulation of miniature endplate currents," *Neuroscience Letters*, vol. 48, pp. 67-74, 1984.

[46]   Schild, J. H., Clark, J. W., Canavier, C. C., Kunze, D. L., and Andresen, M. C., "Afferent synaptic drive of rat medial nucleus tractus solitarius neurons: dynamic simulation of graded vesicular mobilization, release, and non-NMDA receptor kinetics," *Journal of Neurophysiology*, vol. 74, no. 4, pp. 1529-1548, 1995.

[47]   Kleinle, J., "Transmitter concentration profiles in the synaptic cleft: an analytical model of release and diffusion," *Biophysical Journal*, vol. 71, pp. 2413-2426, 1996.

[48]   Bartol, T., "Monte Carlo simulation of miniature endplate current generation in the vertebrate neuromuscular junction," *Biophysical Journal*, vol. 59, pp. 1290-1307, 1991.

[49]   Giniatullin, L. S., "Modeling endplate currents: dependence on quantum secretion probability and decay of miniature current," *European Biophysics Journal*, vol. 23, pp. 443-446, 1995.

[50]   Vieth, W. and Ciftci, T., "Transport models of the neurotransmitter-receptor interaction," *Annals of the New York Academy of Sciences*, vol. 369, pp. 99-111, 1981.

[51]   Vieth, W. and Chotani, G., "Diffusional/kinetic analysis of the neurotransmission process at the nerve-muscle junction," *Annals of the New York Academy of Sciences*, vol. 413, pp. 114-132, 1983.

[52]   Naka, T. and Sakamoto, N., "Simulation analysis of the effects of simultaneous release of quanta of acetylcholine on the endplate current at the neuromuscular junction," *Mathematics and Computers in Simulation*, vol. 59, pp. 87-94, 2002.

[53]   Vijayendran, R., "A computational reaction-diffusion model for the analysis of transport-limited kinetics," *Analytical Chemistry*, vol. 71, pp. 5405-5412, 1999.

[54]   Van der Kloot, W., and Cohen, I. S., "End-plate potentials in a model muscle fiber," *Biophysical Journal*, vol. 45, pp. 905-912, 1984.

[55] Stojan, J., "Analysis of progress curves in an acetylcholinesterase reaction: a numerical integration treatment," *Journal of Chemical Information and Modeling*, vol. 37, pp. 1025-1027, 1997.

[56] Land, B., Harris,W. V., Salpeter, E. E., and Salpeter, M. M., "Diffusion and binding constants for acetylcholine derived from the falling phase of miniature endplate currents," *Proceeding of the National Academy of Sciences*, vol. 81, pp. 1594-1598, March, 1984.

[57] Kordas, M., "On the role of junctional cholinesterase in determining the time course of the endplate current," *Journal of Physiology*, vol. 270, pp. 133-150, 1977.

[58] Grindrod, P., *The Theory and Applications of Reaction-Diffusion Equations: Patterns and Waves*, London: Clarendon Press, 1996, pp. 123-256.

[59] Schnell, S. and Turner, T. E., "Reaction kinetics in intracellular environments with macromolecular crowding: simulations and rate laws," *Progress in Biophysics & Molecular Biology*, vol. 85, pp. 235-260, 2004.

[60] Morton, K. and Mayers, D., *Numerical Solution of Partial Differential Equations*, New York: Cambridge University Press, 1994, pp. 1-239.

[61] Schiesser, W. E., *The Numerical Method of Lines: Integration of partial differential equations*, San Diego: Academic Press, 1991, pp. 1-326.

[62] Thomas, J. W., *Numerical Partial Differential Equations: Finite difference methods*, New York: Springer-Verlag, 1995, pp. 1-460.

[63] Wilson, H., *Advanced Mathematics and Mechanics Applications Using MATLAB*, 2nd Ed., London: Chapman and Hall, 1997, pp. 1-696.

[64]   Magleby, K., and Stevens, C., "A quantitative description of endplate currents,"
       Journal of Physiology, vol. 223, pp. 173-197, 1972.

[65]   Rosenberry, T. L., "Quantitative simulation of endplate currents at neuromuscular
       junctions based on the reaction of acetylcholine with acetycholine receptor and
       acetylcholinesterase," *Biophysical Journal*, vol. 26, pp. 263-290, 1979.

[66]   Wathey, J. C. and Nass, M. M., "Numerical reconstruction of the quantal event at
       nicotinic synapses," *Biophysical Journal*, vol. 27, pp. 145-164, 1979.

[67]   Friboulet, A. and Thomas, D., "Reaction-diffusion coupling in a structured
       system: application to the quantitative simulation of endplate currents," *Journal of
       Theoretical Biology*, vol. 160, pp. 441-455, 1993.

[68]   Naka, T. and Shiba, K., "A two-dimensional compartment model for the reaction-
       diffusion system of acetylcholine in the synaptic cleft at the neuromuscular
       junction," *BioSystems*, vol. 41, pp. 17-27, 1997.

[69]   Cheng, Y., Suen, J., Radic, Z., Bond, S., Holst, M., and McCammon, J.,
       "Continuum simulations of acetylcholine diffusion with reaction-determined
       boundaries in neuromuscular junction models," *Biophysical Chemistry*, vol. 127,
       pp. 129-139, 2007.

[70]   Tai, K., Bond, S., MacMillan, H., Baker, N., Holst, M., and McCammon, J.,
       "Finite element simulations of acetylcholine diffusion in neuromuscular junctions,"
       Biophysical Journal, vol. 84, pp. 2234-2241, 2003.

[71]   Smart, J., and McCammon, J., "Analysis of synaptic transmission in the
       neuromuscular junction using a continuum finite element model," *Biophysical
       Journal*, vol. 75, pp. 1679-1688, 1998.

[72] Kuzenetsov, A. V. and Hooman, K., "Modeling traffic jams in intracellular transport in axons," *International Journal of Heat and Mass Transfer*, vol. 51, pp. 5695-5699, 2008.

[73] Crank, J., *The Mathematics of Diffusion*, Clarendon Press, Oxford, 1975, pp. 1-424.

[74] Carslaw, H. S., *Conduction of Heat in Solids*, 2nd Ed., Oxford University Press, London, 1959, pp. 1-520.

[75] Evans, L. C., *Partial Differential Equations*, Providence: American Mathematical Society, 1998, pp. 1-749.

[76] Moaveni, S., *Finite Element Analysis*, New Jersey: Prentice-Hall Inc., 1999, pp. 1-880.

[77] Pregla, R., "General formulas for the method of lines in cylindrical coordinates," *IEEE Transactions on Microwave Theory and Techniques*, vol. 43, pp. 1617-1620, 1995.

[78] Spevak, M. and Grasser, T., "Discretization of macroscopic transport equations on non-cartesian coordinate systems," *IEEE Transactions on Computer Aided Designs of Integrated Circuits and Systems*, vol. 26, pp. 1408-1416, 2007.

[79] Dooner, D. B., "Equilibrium and diffusion equations using cylindriodal coordinates," *Proceedings of the Institution of Mechanical Engineers, Part C: Journal of Mechanical Engineering Science*, vol. 216, pp. 61-72, 2002.

[80] Morinishi, Y., Vasiyev, O., and Ogi, T., "Fully conservative finite difference scheme in cylindrical coordinates for incompressible flow simulations," *Journal of Computational Physics*, vol. 197, pp. 686-710, 2004.

[81]   Chu, P., and Fan, C., "A three point combined compact difference scheme,"

        Journal of Computational Physics, vol. 140, pp. 370-399, 1998.

[82]   Zhao, J., Dai, W., and Niu, T., "Fourth-order compact schemes of a heat

        conduction problem with Neumann boundary conditions," *Numerical Methods for*

        Partial Differential Equations, vol. 23, pp. 949-959, 2007.

[83]   Zhao, J., Dai, W., and Zhang, S., "4th-order compact schemes for solving

        multidimensional heat conduction problems with Neumann boundary conditions,"

        Numerical Methods for Partial Differential Equations, vol. 24, pp. 165-178, 2008.

[84]   Severs, N. J., "Freeze fracture electron microscopy," *Nature Protocols*, vol. 2, pp.

        547-576, 2007.

[85]   Forsberg, A., and Puu, G., "Kinetics of inhibition of acetylcholinesterase from the

        electric eel by some organophosphates and carbamates," *European Journal of*

        Biochemistry, vol. 140, pp. 153-156, 1984.

[86]   Walker, B., "Current concepts: organophosphate toxicity," *Inhalation Toxicology*,

        vol. 14, pp. 975-990, 2002.

[87]   Krupesh, N., "Organophosphorus poisioning - still a challenging proposition,"

        Indian Journal of Anesthesia, vol. 46, no. 1, pp. 40-43, 2002.

[88]   Prevention and treatment of Chemical Warfare Agents, *The Medical Letter*, vol.

        44, No. 1121, pp. 1-3, 2002.

[89]   Sidell, F. R., and Borak, J., "Chemical warfare agents: II. Nerve agents," *Annals*

        of Emergency Medicine, vol. 21, pp. 865-871, 1992.

[90] Polhuijs, M., and Langenberg, J. P., "New method for retrospective detection of exposure to organophosphorus anticholinesterases: application to alleged sarin victims of Japanese terrorists," *Toxicology and Applied Pharmacology*, vol. 146, pp. 156-161, 1997.

[91] Gage, P. W., and McBurney, R., "Effects of membrane potential, temperature, and neostigmine on the conductance change caused by a quantum of acetylcholine at the toad neuromuscular junction," *Journal of Physiology*, vol. 244, pp. 385-407, 1975.

[92] Carr, R. L., and Chambers, H., "Modelling the interactions of mixtures of organophosphorus insecticides with cholinesterase," *Electronic Journal of Differential Equations*, Conference 10, pp. 89-99, 2003.

[93] Rosenfeld, C., and Sultatos, L., "Concentration dependent kinetics of acetylcholinesterase inhibition by the organophosphate paraxon," *Toxicological Sciences*, vol. 90, no. 2, pp. 460-469, 2006.

[94] Worek, F., Szinicz, L., Eyer P., and Thiermann H., "Evaluation of oxime efficacy in nerve agent poisoning: development of a kinetic-based dynamic model," *Toxicology and Applied Pharmacology*, vol. 209, pp. 193-202, 2005.

[95] Aurbek, N., Wetherell, J., Pearce, P., Mann, T., and Thiermann, H., "Analysis of inhibition, reactivation, and aging kinetics of highly toxic organophosphorus compounds with human and pig acetylcholinesterase," *Toxicology*, vol. 224, pp. 91-99, 2006.

[96]   Worek, F., and Thiermann, H., "Kinetic analysis of interactions between human acetylcholinesterase, structurally different organophosphorus compounds and oximes," *Biochemical Pharmacology*, vol. 68, pp. 2237-2248, 2004.

[97]   Aurbek, N., and Thiermann, H., "Application of kinetic-based computer modeling to evaluate the efficacy of HI 6 in percutaneous VX poisoning," *Toxicology*, vol. 224, pp. 74-80, 2006.

[98]   Fossier, P., and Baux, G., "Direct and indirect effects of an organophosphorus acetylcholinesterase inhibitor and of an oxime on a neuro-neuronal synapse," *Pflügers Archive*, vol. 396, pp. 15-22, 1983

[99]   Kuča, K., "Reactivation of organophosphate inhibited acetylcholinesterase activity by α,β-bis-(4-hydroxyiminomethylpyridinium) alkanes *in vitro*," *Journal of Applied Biomedicine*, vol. 1, pp. 207-211, 2003.